ABSTRACT

Title of Document: PROBABILISTIC PHYSICS OF FAILURE ASSESSMENT OF THERMOMECHANICAL FATIGUE IN HIGH-I/O AREA-ARRAY INTERCONNECTS

Shaughn Michael Roettele, Master's Science in Mechanical Engineering, 2009

Directed By: Professor Abhijit Dasgupta, Department of Mechanical Engineering

Thermal cycling durability of plastic ball grid array (PBGA) interconnects is known to decrease as I/O count increases. This is due, in part, to mechanistic effects; such as increasing thermal expansion mismatches between component and PWB, due to increasing package sizes. Failure prediction due to these mechanistic effects is a deterministic process and is based on the load level found in the critical joint (joint with the most severe loading). However, due to probabilistic effects, for example manufacturing variabilities, premature failure may result in one of several joints in the neighborhood of the critical one. Failure probability increases as the number of joints in this critical region increases. Thus, observed failure rates are due to a convolution of deterministic and probabilistic effects. In effect, for large BGAs, deterministic predictions may overestimate interconnect durability. This thesis uses thermal cycling experiments and detailed mechanistic modeling to present a

methodology for adjusting deterministic predictions of solder joint failure with a suitable probabilistic correction factor.

PROBABILISTIC PHYSICS OF FAILURE ASSESSMENT OF THERMOMECHANICAL FATIGUE IN HIGH-I/O AREA-ARRAY INTERCONNECTS

By

Shaughn Michael Roettele

Thesis submitted to the Faculty of the Graduate School of the
University of Maryland, College Park, in partial fulfillment
of the requirements for the degree of
Master of Science in
Mechanical Engineering
2009

Advisory Committee:
Professor Abhijit Dasgupta, Chair
Professor Donald Barker
Associate Professor Peter Sandborn

© Copyright by
Shaughn Michael Roettele
2009

Acknowledgements

I would like to thank Dr. Dasgupta for his time, patience and depth of understanding in both engineering and for the human condition. I will miss working with him; but not enough to pursue a doctorate. I would also like to thank my thesis committee members, Dr. Barker and Dr. Sandborn, for their time and input. Additionally, my degree and greater understanding of engineering principles would not have been possible without the CALCE center; and it's wonderful faculty, research scientists, staff, and of course my fellow peers. I would also like to thank Tommi Reinikaininen and Germano Freitas from Instituto Nokia de Technologia (InDT) for encouraging CALCE to pursue the problem presented in this thesis, and for helping me out when I was road-blocked.

My time at UMD and CALCE in particular would not nearly have been as enjoyable if it had not been for Dr. Dasgupta's wonderful lab group, and our unofficial 2nd advisor Dr. Moustafa Al-Bassyiouni. His input and willingness to lend an ear or idea has kept us all going. Additionally, I could not have finished this thesis without the help of Dan Farley whose expertise in all things "computerable" has saved me form years worth of frustration; Gayatri Cuddalorepatta for her ability to endure my bitching and moaning; Stuart Douglas for selflessly helping me out with the dirty work of cross-sectioning specimens; and everyone else in lab 0102 who has had to listen to my terrible jokes.

Most importantly, I would like to thank my family for being there when I wasn't. In particular, my curious and crazy son Maxwell and my incredible wife Edra for everything she has done for me since the day I met her way back in the summer of

love, 1998. She encouraged me to return to school after a long hiatus and was willing to leave DC for the depressing MD suburbs so I could get in-state tuition. She helped me with my studies when there was time, and always had good coffee brewing. During all of my many long, late-night writing sessions she carried more than her fair share in taking care of our son and our home. I will always be grateful for her kindness and love.

Table of contents

Acknowledgements ii
Table of contents iv
List of tables v
List of figures vii
1 Introduction 1
1.1 Problem Statement and Objectives 1
1.2 Background and Motivation 3
1.3 Overview of Approach 5
2 Thermomechanical Durability Experiments 7
2.1 Introduction 7
2.2 Design of Experiment 10
2.2.1 Specimen Design 11
2.2.2 Test Design 14
2.2.3 Failure Monitoring 15
2.3 Test Results 16
2.3.1 Basics of the Weibull Distribution 16
2.3.2 Examination of First Solder Joint Failure 23
2.4 Failure Analysis 27
2.5 Summary and Conclusions of Test 28
3 Analysis of Test Results 30
3.1 Overview 30
3.2 Scaling for Mechanistic Effects 34
3.2.1 Finite Element Analysis 34
3.2.2 Energy-Partitioning Damage Model 40
3.2.3 Mechanistically Scaled Test Data 45
3.3 Effect of Number of Joints 46
3.3.1 Scaled Weibull Parameters 48
3.4 Grouping of Daisy-chain Nets: Simulation of Increasing Critical Region 51
3.4.1 Grouping of Mechanistically Scaled Thermal Cycling Test Data 52
3.4.2 Series Reliability Model 53
3.4.3 Results: PPoF Correction Factor for Mechanistic Durability Predictions 54
3.5 Summary and Conclusions 60
4 Summary 62
4.1 Conclusions & Discussions 62
4.2 Contributions of Thesis 64
4.3 Limitations and Suggestion for Future Work 65
4.3.1 Effect of Assembly Quality 65
4.3.2 Daisy-Chain Design 65
4.3.3 Thermal Cycling Test Limitations 66
4.3.4 FEA Approximations 67
4.3.5 Determination of Package Critical Region 67
5 Appendices 69
6 References 28

List of tables

Table 2-1: Comparison of Weibull parameter estimates for the 3-P distribution using both the MLE and RRX methods. The total number of samples per daisy-chain net was 53. The number of survivors per D-C net at the conclusion of testing, as well as the number of probable ground wire failures are shown in columns four and five respectively. Nets seven and two have negative failure free periods when using the MLE method. 18

Table 2-2: Comparison of Weibull 2-P estimates using both the MLE and RRX methods. 18

Table 2-3: Comparison of 3-P Weibull estimates for the adjusted failure data. The failure data for daisy-chain nets 7 and 2 were adjusted for additional probable wire failures. The RRX method was found to be better than the MLE method for estimating the statistical parameters of the adjusted test data. For example, Net 2 has a shape parameter estimate of 0.5 using MLE estimators. 22

Table 2-4: Package level reliability estimates based on first failures per component. Weibull parameters were found for the 2-P and 3-P distribution using both RRX and MLE methods... 27

Table 3-1: relevant package dimensions in milimeters... 35

Table 3-2: linear elastic material properties used in FEA model.............................. 37

Table 3-3: solder constitutive properties used in FEA modeling [13] and [15] 38

Table 3-4: Energy-partitioning constants W_{po}, c and d were obtained from Zhang et al. [14]; W_{co} was recalibrated using thermal cycling test data from this study. .. 42

Table 3-5: comparison of mechanistic predicted damage for the 12 daisy-chain test nets. The cycles to failure (N_f), and damage ratios for each net are also shown. 43

Table 3-6: rank regression estimated Weibull parameters for mechanistically scaled test data. Mechanistic scaling factors were applied to the cycles to failure from test data. Scaling of test data was done to simulate equivalent damage levels for all 12 daisy-chain nets. As expected, the shape parameter (β) does not scale with damage level, but the location (γ) and scale (η) parameters have shifted by the mechanistic scaling factor... 46

Table 3-7: comparison of mechanistically and probabilistically scaled Weibull parameters for the 12 daisy-chain test nets. The parameter values represent the characteristics of a single solder joint per net... 49

Table 3-8: comparison of Weibull parameter estimates for mechanistically scaled and grouped test net data. The thermal cycling test results for each daisy-chain net

were grouped in order of decreasing DNP to simulate increasing component size as the number of equivalently loaded joints in the critical region increases. 52

Table 3-9: comparison of series reliability estimated Weibull parameters for grouped daisy-chain Weibull reliability distributions. The grouped Weibull parameter estimates were calculated using graphical methods. The correlation coefficients (ρ) for the fitted data are also presented.. 54

List of figures

Figure 1-1: cross-section of a typical wire-bonded plastic ball grid array (PBGA) package [1].. 3

Figure 1-2: flow chart of necessary steps to calculate probabilistic correction factor for mechanistic predictions of interconnect durability for high-I/O PBGAs. 5

Figure 2-1: Schematic of dummy PBGA1156 test vehicle daisy-chain design and package internal I/O connections. The black "dog-bone" shapes represent internal daisy-chains. The color bands represent board-level interconnect daisy-chains. The test vehicle was divided into 12 independent daisy-chains, each shown in a distinct color. 12

Figure 2-2: Schematic of board level trace layout. The package internal "dog-bones" are shown in green. Board level traces are shown in red. The green blocks represent board-level copper pads. The board design was such that no vias or buried traces were necessary to complete the daisy-chain layout. 12

Figure 2-3: Close-up of a quarter of the package test vehicle daisy-chain pattern. In the diagram, the die is outlined with a dashed black line. Each test net is identified by a distinct color. The goal was to ensure that all the solder joints in each test net had approximately the same DNP.. 13

Figure 2-4: A sample of the test boards. Each board had six PBGA1156 components mounted on one side. High temperature wire was soldered to the copper pads on the board surface. These were used to monitor the 12 daisy-chain nets per component.. 14

Figure 2-5: Average thermal cycle profile of the test chamber (solid black line) is compared to the IPC9701 TC-4 profile (dashed red line). The test chamber temperature profile was measured by 12 thermocouples placed strategically in the chamber. The chamber temperature variations by location were found to be minimal. The cold ramp is seen to diverge from the IPC spec, due to the fact that the chamber ran on refrigeration only and did not use LN2............................... 15

Figure 2-6: Comparison of Weibull 3-P properties for all 12 daisy-chain test nets using both MLE and RRX methods. MLE estimated parameters are shown in grey, and RRX estimated parameters are shown in orange. Both methods yielded comparable parameter values, except for Net 7 and Net 2 which had poor fits. . 19

Figure 2-7: plot of Weibull cdfs for daisy-chain Net 7 and Net 2 using both the MLE and RRX estimates. The RRX estimates are seen to fit the test data for these two nets better than the MLE estimates... 20

Figure 2-8: bi-modal mixed-Weibull cdf of daisy-chain Net 7. The presence of a second population can be seen as a kink in the cdf at approximately 1,000 cycles. These data points are probably due to wire failures, not interconnect failures. .. 21

Figure 2-9: RRX estimate of the 3-P Weibull cdf for daisy-chain Net 2. The first four data points evidently do not fit the estimated cdf. These points are probable wire failures, not interconnect failures.. 21

Figure 2-10: comparison of Weibull parameters for adjusted test data using both MLE and RRX methods. Parameter estimates using both methods produce similar results per daisy-chain net except for Net 2. MLE methods estimate a shape parameter of 0.5. This is indicative of early failure for a population. However, the test data for this net contained a large number of survivors. 22

Figure 2-11: 3-P Weibull MLE estimated cdf for daisy-chain Net 2. Parameter estimates using MLE provide a poor fit, resulting in clearly erroneous estimates such as a shape parameter of 0.5, which is usually a sign of infant mortality. 23

Figure 2-12: 3-P Weibull cdfs for daisy-chain nets 7 and 2. The data sets for these nets have been appropriately adjusted for probable wire failures. The RRX estimated Weibull distribuitons for both test nets fit the test data quite well. 23

Figure 2-13: Histogram showing the location of first failures; the number of components failed is plotted by daisy-chain net ID. Net 10 has the most first failures, in 29 components out of 53. For reference, Net 12 is at the package outer corner and Net 3 is at the die outer corner. Decreasing net numbering corresponds to decreasing DNP. 25

Figure 2-14: comparison of observed cycles to first failure with Weibull predicted values. Daisy-chain Nets 7, 5 and 3 had no first failures per daisy-chain per component, therefore only predicted values are reported for these nets.................... 26

Figure 2-15: optical micrograph of a cross-sectioned PBGA interconnect. A large crack, circled in blue, can be seen at the solder neck. 28

Figure 2-16: optical micrograph of a cross-sectioned PBGA interconnect. The solder neck has almost completely cracked through. Also, a large void can be seen in the bottom right corner of the joint.. 28

Figure 3-1: schematic of a cross-section of the package geometry. 35

Figure 3-2: schematic of package foot-print, including all relevant dimensions [13]. 36

Figure 3-3: oblique view of FEA model showing the package mounted on the PWB. The package molding compound is shown in red, the substrate is shown in cyan..... 36

Figure 3-4: underside view of the meshed package. The 17x17 array of solder joints can be seen in dull gray color. The die is visible in the pictures as the dark purple region below the molding compound. 36

Figure 3-5: temperature profile used for temperature cycling of FEA model. The profile was based on the average thermocouple readings from the thermal chamber.......... 39

Figure 3-6: contour plots of von Mises stress at the end of the hot dwell for the third temperature cycle for select solder joints located at the package corner. The solder joints with the maximum stress in Nets 11 and 10 are labeled for reference. The package corner joint, located in Net 12, experienced the highest stress, strain and work density levels of all joints in the package 40

Figure 3-7: contour plots of von Mises strain at the end of the hot dwell for the third temperature cycle for select solder joints located at the package corner. The solder joints with the maximum Mises strain for Nets 12, 11 and 10 are shown. 40

Figure 3-8: highlight of the element layers used for volume averaged work density calculations. The E-P model constants were calculated based on 10% of the solder volume. For this model, 10% of the solder volume is shown in the upper right-hand corner of the figure, and it had three out-of-plane layers and 44 elements. 42

Figure 3-9: contour plots of creep work density for 10% volumetric slices of four solder joints located at the package corner. The joints with the maximum creep work densities for Nets 12 and 11 are highlighted. 44

Figure 3-10: comparsion of damage ratios for various values of W_{co}. Damage ratios are relatively insensitive to the value of the energy-partitioning constant. 44

Figure 3-11: comparison of mechanistic scaling factors for thermal cycling test data. Mechanistic scaling factors were calculated using 3-D FEA and energy-partitioning. Scaling factors are the damage ratios for each net based on the maximum damage levels found in all 12 daisy-chain nets. 45

Figure 3-12: comparison of probabilistic scaling factors per daisy-chain net. Large scale factors for Nets 9-7 are attributed to the high-I/O counts (>100) found in these nets; while in Net 2 the scale factor is large because of the extremely low shape factor (1.1). The probabilistic scaling factor adjusts the Weibull scale parameter of a group of identically loaded joints to provide the scale parameter of a single solder joint in the set. Theoretically, neither the location parameter, nor the shape parameter is affected by the number of joints in the daisy-chain. 47

Figure 3-13: comparsion of characteristic life estimates scaled to account for the number of solder joints per daisy-chain net. Essentially, these estimates imply that each solder joint per net has the given characteristic life. 48

Figure 3-14: comparison of characteristic life (θ_j) estimates for a each solder joint per daisy-chain net, scaled for mechanistic and probabilistic differences per net..... 50

Figure 3-15: comparison of mechanistic scaling factors. The FEA/energy-partitioning (E-P) method is shown based on maximum damage ratios. The probabilistically implied mechanistic scaling factor (θ_{j12}/ θ_{jnet}), shown in orange, is the result of subtracting probabilistic effects (difference in number joints per net) from the unscaled test data. The package corner is located in Net 12, and the die-corner shadow is located in Net 3. 51

Figure 3-16: comparison of Weibull shape parameter estimates for grouped nets mechanistically scaled to the maximum damage ratios. This data set had the greatest difference in parameter values between the test data and the series model. The grouped test data shows that was a large spread in the CTFs for the grouping of data sets 12-9 and 12-8. However, the spread in β values for the test data, 1.5 to 2.5, is relatively small. 55

Figure 3-17: comparsion of characteristic life estimates for the mechanistically scaled, to the maximum damage ratio, grouped daisy-chain nets. The grouped test data agrees well with the series reliability model. Additionally, the characteristic life is seen to saturate as the number of I/O in the critical region increases due to increasing size of the component. 56

Figure 3-18: comparison of Weibull scale parameter estimates for the mechanistically scaled and grouped test data sets. The data scaled to maximum damage ratios are shown in red circles, the series reliability model estimates are shown in open-face black squares. A power-law was fitted to the test data, and is shown by a black dashed line. Combination of this result with the durability test results of this study (620 thermal cycles to failure) suggest that the manufacturing quality of the tested PBGA1156 is such that it has approx 24 joints in the critical region (6 per quadrant) 57

Figure 3-19: probabilistic correction factor for mechanistic predictions of solder characteristic life. Correction factors based on maximum damage ratios for mechanistic scaling of the grouped daisy-chain test data are presented. For large critical region I/O counts in a quadrant of the package (>30) the results suggest that mechanistic predictions could over-predict characteristic life by as much as an order of magnitude. The critical region I/O count per quadrant is the number of highest stressed solder joints at identical load levels for one quadrant of the package. 58

Figure 3-20: comparison of probabilistic de-rating factors for mechanistic predictions of solder damage. The family of curves shown in black dashed lines represents series summations of equivalently stressed solder joints having identical Weibull distributions, with shape parameters β. The parameter α is the ratio of failure-free period to the characteristic life of a single solder joint in each series. The red solid line represents the probabilistic correction factor obtained from mechanistically scaled and grouped test data. The grouped solder joints had equivalent load levels, but dissimilar Weibull parameters. 60

1 Introduction

The trend in modern electronics is towards smaller, lighter, cost-efficient, high-performance portable products; for example, personal digital assistants (PDAs), pagers, MP3 players, touch-pad cellular phones, etc. One way to reduce product size it to incorporate more device functionality into a component, thus reducing board real-estate and overall cost and minimizing circuit path length. Area-array component architectures are one of several ways to minimize real-estate. However, increasing functionality is constantly driving up the size and I/O counts of such packages. Such increase in complexity and decrease in size and cost naturally present reliability challenges. This thesis explores methodologies for improving reliability estimates of plastic ball grid array (PBGA) components, a common area-array architecture.

1.1 Problem Statement and Objectives

A prevelant reliability concern for PBGA assemblies is solder fatigue under cyclic temperature excursions caused by environmental changes or by power cycling. The thermal cycling durability of PBGA interconnects is believed to decrease as the component I/O count increases. Part of the decrease is due to higher stresses, since the package size usually increases too, resulting in a corresponding increase in thermal expansion mismatches between the component and the PWB. This is the mechanistic contribution to the drop in the durability and can be assessed with deterministic failure models, based on either maximum strain range or maximum work density in the most critical joint. The most critical joint from this deterministic perspective is usually determined by a combination of the DNP (distance from neutral point) and the mismatch in the effective CTE of the component, the solder pads and the PWB. Thus, the critical

joint is usually the one at the outer corner of either the die foot-print or the package foot-print, depending on the details of the package architecture. Such deterministic models are commonly used by assembly designers to assess interconnect durability and they are based on the mechanistic effects.

Unfortunately, such deterministic models fail to account for probabilistic effects that also contribute to interconnect failure, for example, manufacturing variabilities such as microstructural variations, inconsistent joint geometries, nonuniformities in interfacial intermetallic layers, and void distributions; all of which can be collectively considered as a "defect density" for each joint.

The actual observed failure distributions and the failure sites are due to a convolution of both the deterministic (mechanistic) effects as well as the probabilistic effects discussed above. Thus, the first joint to fail may be one of several joints in the package. Collectively, these joints comprise a critical (highest stressed) region for package reliability. Furthermore, as package-I/O count increases, the number of joints in the critical region increases. As a consequence, failure probability increases. In essence, for high-I/O PBGAs the mechanistic prediction therefore produces a non-conservative estimate of component characteristic life because it fails to account for crucial probabilistic effects. Therefore, to produce a more realistic estimate of package durability the mechanistic estimate must be adjusted for to account for probabilistic effects.

The objective of this thesis is to provide a methodology for incorporating a probabilistic physics of failure (PPoF) approach that considers both mechanistic and probabilistic effects in interconnect durability assessment for high I/O BGAs subjected to thermo-mechanical cycling. In particular the focus is on establishing methodologies to

generate probabilistic correction factors that can be used to correct mechanistic durability estimates for high I/O PBGAs. The approach is validated with thermal cycling experiments.

1.2 Background and Motivation

Area-array components can have I/O counts ranging from less than 100 up to the mid-thousands; contained on a relatively small footprint. A common grid array component style is the plastic ball grid array (PBGA). This package type generally has an integrated circuit (IC) silicon chip connected to an organic multi-layer substrate. The chip is usually covered by a protective overmold. The electrical, thermal and structural connections of the package are done through solder balls arranged in a grid array on the underside of the substrate. A schematic of a wire-bonded PBGA is shown in Figure 1-1.

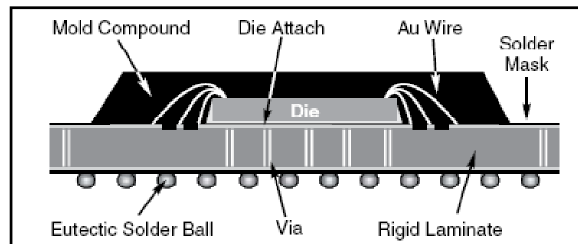

Figure 1-1: cross-section of a typical wire-bonded plastic ball grid array (PBGA) package [1]

During temperature swings, the package deforms due to thermal expansion mismatch between the printed wiring board (PWB) and the component, generating complex stress states and permanent cyclic fatigue damage in the solder joints. The damage initiates as distributed micro-cracks and microvoids; propagating and coalescing into macro-cracks with further cycling. Eventually, the macro-cracks develop enough energy, to cause the solder joint to sever from the board or the component, depending on the solder geometry.

The first joint to fail in high-I/O packages may not be the highest stressed joint, because of probabilistic effects. A method to identify these probabilistic effects for interconnect failure is to selectively partition a component into multiple daisy-chain nets. In this fashion the failure site is resolved to specific regions of the package. Thus, it is possible to pinpoint the cycles to failure for particular component regions subjected to a given stress level. This strategy of partitioning of a test component into multiple daisy-chain nets to target interconnect failure has been reported before in the literature [5], [6], [7]. In the previous studies, the authors did not consider probabilistic effects in the failure of their test data. The goal of the current study is to experimentally quantify the probabilities of first failure at different locations in a large I/O PBGA, and to quantify the relative contribution of mechanistic and probabilistic effects on failure predictions.

In the literature, Darveaux et al. [2] and Clech et al. [4] showed that assembly fatigue failure distributions must be correlated to distributions of interconnect fatigue life distributions. In other words, reliability estimates based on a single solder joint or a small group of solder joints will tend to overpredict the package durability, especially in high I/O component. Therefore, it is necessary to adjust package durability predictions to account for the number of solder joints in the system that are at approximately the same load level. Clech, et al. [4] showed the relationship of component parameters to solder parameters for the Weibull 3-P distribution. Darveaux et al. [2] suggest that for BGAs with many solder joints that the component be partitioned into subsets of identically loaded joints when determining the component level characteristic life. A more extensive review of these papers is presented in Section 2.1.

1.3 Overview of Approach

A flow chart of the approach presented in this thesis is shown in Figure 1-2. A high-I/O test specimen is partitioned into independent daisy-chain nets to isolate solder failure sites. The sample population of test components is thermal cycled to failure. Statistical analysis is performed on the test data. Mechanistic modeling is performed using a combination of FEA and energy-partitioning to develop a reliability estimate of the test component. The thermal cycling test data is scaled for mechanistic effects to account different load levels per daisy-chain net. The test data is then grouped in order of decreasing DNP to simulate increasing component size. The scaled test data is compared to a series reliability model. Finally, develop a correction factor to mechanistic predictions of interconnect durability to account for probabilistic effects.

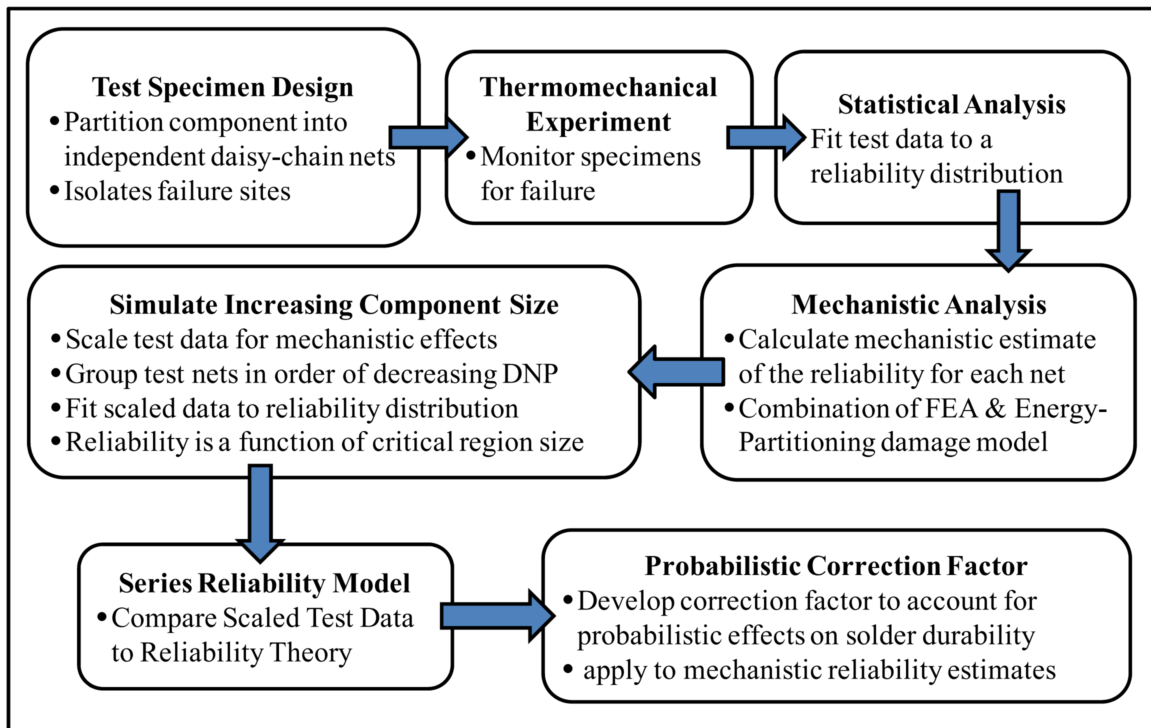

Figure 1-2: flow chart of necessary steps to calculate probabilistic correction factor for mechanistic predictions of interconnect durability for high-I/O PBGAs.

Chapter 2 of this thesis details an experimental study of the cyclic thermo-mechanical reliability of a high-I/O PBGA; steps 1-3 in Figure 1-2. The test vehicle was specially daisy-chained into 12 distinct test nets to track the failure progression of the interconnects as a function of the number of temperature cycles. The daisy-chain design, test set-up and failure monitoring are presented in detail. The reliability of each daisy-chained net is assessed using the 3-parameter Weibull distribution.

Chapter 3, outlines the PPoF approach; steps 4-7 in Figure 1-2. The test data from Chapter 2 are scaled for mechanistic differences between the daisy-chains using non-linear 3-D finite element analysis and an energy-partitioning damage model. The scaled data mimics the expected reliability statistics of the 12 nets under a common reference stress state. The failure data are then grouped in order of decreasing DNP to simulate increasing number of I/O in the critical region as component size increases. The grouped results are found to agree well with a simple series reliability model. The test results are then used to formulate a probabilistic de-rating factor that can be used to adjust mechanistic predictions of thermo-mechanical durability of package interconnects.

2 Thermomechanical Durability Experiments

In this chapter an experimental study is presented to quantify probabilistic effects of manufacturing variabilities on the durability of high I/O PBGA interconnects subjected to temperature cycling. A test methodology was developed whereby a single PBGA component type was systematically partitioned into multiple daisy-chain nets in order to track the location of the first interconnect failure in the test specimen. A population of 53 test components was subjected to temperature cycling, and Weibull analysis was performed on the test results. The data reveals that the site of first failure in the sample population was not necessarily in the solder joint that experienced the highest load, and indicates that probabilistic effects need to be considered when predicting the durability of high I/O PBGAs. Detailed results are available in Appendix A.

2.1 Introduction

The thermal cycling durability of plastic ball grid array (PBGA) interconnects is believed to decrease as the component I/O count increases. Part of the decrease is due to higher stresses, since the package size usually increases too, resulting in a corresponding increase in the thermal expansion mismatch between the component and the PWB. This mechanistic contribution to the drop in the durability can be assessed with a combination of deterministic stress analysis and failure models. Typical failure models are based on cyclic inelastic strain-range or work density (see for example, Darveaux et al. [2]), or on partitioned versions of the strain-range and work density models (see for example, Dasgupta et al. [3]), in the most critical joint. The most critical joint from this deterministic perspective is usually determined by a combination of the DNP (distance from neutral point) and the package architecture. Thus, the critical joint is usually the one

at the outer corner of either the die foot-print or the package foot-print. These deterministic models account for all the mechanistic effects.

Unfortunately, these deterministic models fail to account for probabilistic effects that also contribute to interconnect failure. For example, the manufacturing process may introduce factors such as microstructural variations (especially in SAC joints), inconsistencies in joint geometries, non-uniformities in interfacial intermetallic layers, and void distributions; all of which can perturb the failure probabilities for each joint.

The actual observed failure distributions and the failure sites are due to a convolution of both the deterministic (mechanistic) effects as well as the probabilistic effects listed above. Thus the first solder joint to fail may be one of several joints within a critical, highly-stressed region in the package. As package-I/O count increases, the number of joints in the critical region increases. Consequently, the failure probability under a given loading history will increase with increasing number of joints, due to these probabilistic factors, even if the damage levels due to mechanistic effects could be held constant. Consequently, for large I/O PBGAs, mechanistic predictions will produce a non-conservative estimate of component life because they fail to account for crucial probabilistic effects.

The idea that first joint failure may not occur at the highest stressed joint due to probabilistic effects is not a new proposition; Darveaux et al. [2] and Clech et al. [4] both discuss this in detail. Qualitatively this issue can be easily proved by destructive failure analysis techniques such as “dye and pry” and cross-sectioning. It is a simple matter of thermal cycling a batch of daisy-chained components and performing failure analysis on each component as soon as a failure is detected. However, there have been no studies in

the literature to quantify the severity of the probabilistic effects because that requires a separation of the relative magnitudes of the deterministic (mechanistic) and probabilistic effects.

A method to identify probabilistic effects for interconnect failure is to selectively partition a component into multiple daisy-chain nets. In this fashion the failure site is resolved to specific regions of the package. Thus, it is possible to pinpoint the cycles to failure for particular component regions subjected to a given stress level. Partitioning of a test component into multiple daisy-chain nets to target interconnect failure has been done before, examples of this procedure can be found in the literature. Perkins and Sitaraman [5] performed vibration durability experiments on high lead (10Sn90Pb) 1089 I/O ceramic column grid array (CCGA) components. The test vehicle was partitioned into a total of ten daisy-chains, with nine of the ten daisy-chains containing joints with approximately the same DNP, and the 10th net containing the remaining joints.

Meulinas and Dunford [6] conducted a thermomechanical reliability study of SnPb and Pb-free solders for a specially daisy-chained 256 I/O perimeter-array BGA. The authors daisy-chained all the joints in the package onto one test net. Then, they had additional traces with exposed test pads connected to the main net; which isolated the array into groups of two or three joints. In this way, they were able to locate approximately which joint(s) failed in the event of a component failure.

Manock and Moy [7] presented a study on the thermomechanical reliability of 63Sn27Pb solder for a 244 I/O quad flat pack (QFP) component. The QFP test vehicle was divided into eight daisy-chains per component, two daisy-chains per component side. Partitioning the QFP effectively increased their test sample size by a factor of eight,

assuming that the failure of each octant per component was independent. They conducted thermal cycling of the test population up to 13,840 cycles. The test data was then examined using Weibull analysis to quantify the solder durability.

In the previous studies, the authors did not consider probabilistic effects in the failure of their test data. Perkins and Sitaraman [5] did track failure progression in the component in relation to the package DNP. However, the effect of the number of joints in each daisy-chain on the probability of failure was not considered. Meulinas and Dunford [6] isolated the failure of a component down to one of a few joints, and Manock and Moy [7] used their partitioned test vehicle to virtually increase their sample size. However due to the relatively small package I/O counts found in both [6] and [7], the failure location exhibited very little randomness in their data.

The goal of this chapter is to experimentally quantify the probabilities of first failure at different locations in a large I/O PBGA. The results will be used in chapter 3 to quantify the relative contribution of mechanistic and probabilistic effects on failure predictions.

2.2 Design of Experiment

A specially daisy-chained, high-I/O count PBGA was subjected to cyclic thermomechanical durability testing. The test vehicle was an 1156 I/O PBGA containing a dummy die. The component daisy-chain design was such that the test component was selectively partitioned into 12 independent test nets. Each test net was designed such that all joints encompassed in the net had approximately similar DNPs. The sample size for this study was 53 test components. The sample population was subjected to a harsh -55°C to 125°C temperature cycle. The test nets were continuously monitored *in-situ*. Thermal

cycling was stopped after approximately 90% of all the test nets had registered as failures (approximately 2,400 cycles).

2.2.1 Specimen Design

The goal of this study was to track the various locations that first solder joint failure could occur in large I/O PBGAs subjected to temperature cycling. In order to accomplish this task an 1156 I/O PBGA was chosen as the test vehicle. The package footprint measured 35mm x 35mm and had a full array of 95.5Sn4.0Ag0.5Cu (SAC405) solder balls on 1 mm pitch. The test components had rectangular dummy silicon dies measuring 8 mm x 10 mm, attached to bismaleimide triazine (BT) substrates. The test vehicle contained internally daisy-chained solder joints ("dog-bones") laid out in concentric rectangles of increasing size. A schematic of the dog-bone pattern is shown in Figure 2-1. By selectively grouping these dog-bones through board level copper traces, it was possible to partition the component into 12 independent daisy-chains (see Figure 2-2). In the test vehicle daisy-chain schematic, each color band represents a single daisy-chain net, and corresponding quadrants are connected in series.

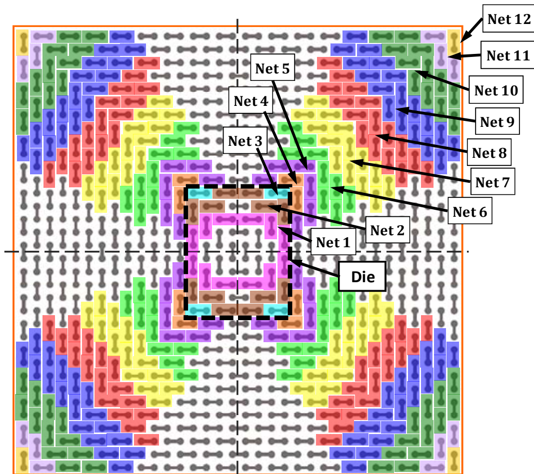

Figure 2-1: Schematic of dummy PBGA1156 test vehicle daisy-chain design and package internal I/O connections. The black "dog-bone" shapes represent internal daisy-chains. The color bands represent board-level interconnect daisy-chains. The test vehicle was divided into 12 independent daisy-chains, each shown in a distinct color.

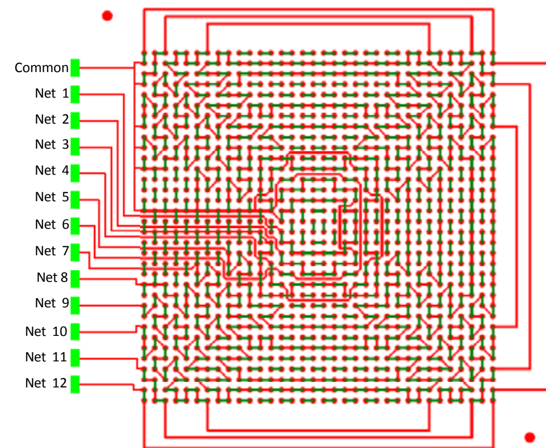

Figure 2-2: Schematic of board level trace layout. The package internal "dog-bones" are shown in green. Board level traces are shown in red. The green blocks represent board-level copper pads. The board design was such that no vias or buried traces were necessary to complete the daisy-chain layout.

As discussed earlier, the daisy-chained nets were laid out in such a fashion that all solder joints in a net had approximately the same DNP. Therefore, during temperature cycling tests, all joints in a net will initially experience approximately the same load levels due to thermal expansion mismatch. However, with increasing thermal cycles the load sharing can change drastically as interconnect failures progress. Mechanistic factors dictate that failures of each net should be sequenced in descending order of stress levels. However, probabilistic factors can interrupt this sequence. Thus, the daisy-chained layout enables the tracking of the failure site progression for each component, and shows for the sample population to what extent the failure sites deviate from the sequence predicted by mechanistic factors. In other words, they demonstrate how strong the probabilistic factors are in high-I/O PBGA assemblies. The nets with highest stress levels are usually the nets at the outer corners of either the die foot-print (Net 3) or of the component foot-print (Net 12).

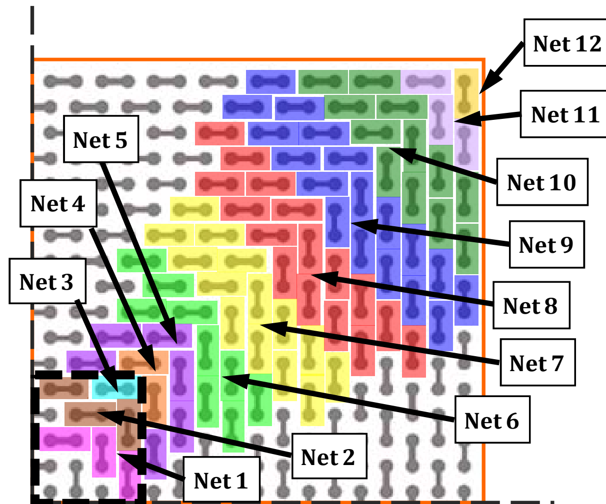

Figure 2-3: Close-up of a quarter of the package test vehicle daisy-chain pattern. In the diagram, the die is outlined with a dashed black line. Each test net is identified by a distinct color. The goal was to ensure that all the solder joints in each test net had approximately the same DNP.

Detailed PWB design for the test specimen was performed by the component supplier, in conformance with the daisy-chain pattern provided to them. The daisy-chain test nets were completed by using exclusively board level copper traces without the necessity of using vias and buried traces. This eliminated the likelihood of via or buried trace failures during thermal cycling. Board fabrication was carried out by an established commercial house with typical manufacturing quality and Pb-free experience. The board level finish was organic solder preservative (OSP), and the solder paste was SAC405. The finalized product resulted in test boards measuring 203mm x 140mm with a thickness of 1.6mm. Each board was populated with six components. High temperature wire was connected to the board test pads using Sn37Pb solder, for in-situ failure monitoring. A complete test board is shown in Figure 2-4.

Figure 2-4: A sample of the test boards. Each board had six PBGA1156 components mounted on one side. High temperature wire was soldered to the copper pads on the board surface. These were used to monitor the 12 daisy-chain nets per component.

2.2.2 Test Design

For this study, the sample population was subjected to accelerated temperature cycling in a commercial thermal chamber. The temperature profile chosen was IPC 9701 temperature cycle - 4 (TC4). This profile has a range of -55° C to +125° C; with a 20 minute ramp up, 12 minute hot dwell, 26 minute ramp down and a 14 minute cold dwell. The chamber profile was monitored with 12 thermocouples placed in strategic locations. Prior to testing, uniformity of the chamber temperature was verified throughout the temperature cycle. A comparison of the chamber profile compared to the IPC 9701 TC4 profile is shown in Figure 2-5. The chamber reached a peak temperature of +129°C, resulting in a slight overshoot of +125°C. Upon temperature stabilization, there was a hot dwell temperature of +125° C for eight minutes. The minimum chamber temperature was -58° C, with a cold dwell time of 12 minutes. For this experiment, the chamber was cooled by refrigeration only, without the use of any LN2. The chamber therefore could not maintain the cool-down ramp rate recommended by IPC and had to be programmed for some overshoot to optimize the profile.

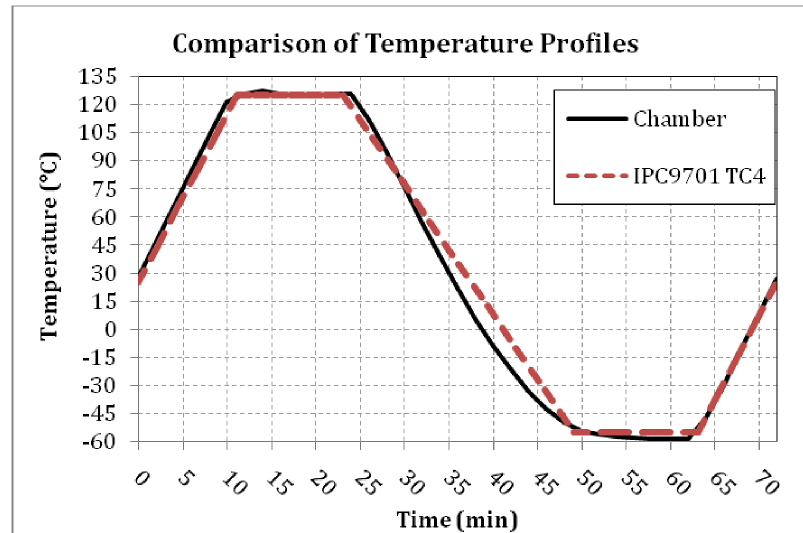

Figure 2-5: Average thermal cycle profile of the test chamber (solid black line) is compared to the IPC9701 TC-4 profile (dashed red line). The test chamber temperature profile was measured by 12 thermocouples placed strategically in the chamber. The chamber temperature variations by location were found to be minimal. The cold ramp is seen to diverge from the IPC spec, due to the fact that the chamber ran on refrigeration only and did not use LN2

2.2.3 Failure Monitoring

The resistance of each daisy-chain net in the test specimens was monitored *in-situ* using a commercial 640-channel Data Logger. Thus, the sample size was limited to 53 components with 12 nets each, resulting in a total of 636 channels. The sampling interval for *in-situ* resistance monitoring was two minutes. The resistance measurements were exported to a comma separated variable (csv) file. A MATLAB program was written to analyze these csv files for net failures. Interconnect failure generally results in high resistance spikes. Generally, as a solder crack occurs, the resistance value for the daisy-chain containing that joint will fluctuate as the crack opens and closes with fluctuations in the temperature cycle. Therefore, a net failure was defined as a resistance measurement greater than 20% of the base resistance for that net and occurring at least once per cycle for ten consecutive cycles. When a daisy-chain net failure occurred, the cycle to first

failure (CTF) was denoted as the first of the ten consecutive cycles. Thermal cycling was stopped after 2,415 cycles; and approximately 89% of the test nets had registered as failures. Any surviving channels were tagged as right censored (type-II) data; known good up to *X* cycles.

At the conclusion of thermal cycling test, the specimens were removed from the chamber and checked for wire failures. Failure analysis was conducted on 13 samples to determine the location of failure sites. Dye and pry analysis was conducted for 10 specimens. Cross-sectioning was performed on 3 samples. A detailed account of failure analysis is presented in Section 2.4.

2.3 Test Results

The test results were post-processed using a MATLAB code. Upon examination of the test results, 13 of the test components were deemed to have probable ground wire failures, because of simultaneous premature failure in at least two or more of the 12 D-C nets in each. All nets found to have probable ground wire failures were treated as type II censored data. Weibull distributions were found to fit the failure results from the thermal cycling experiment well. Therefore, a brief explanation of the Weibull distribution is presented in Section 2.3.1 and thermal cycling test results are discussed in Section 2.3.2.

2.3.1 Basics of the Weibull Distribution

A common failure distribution for the deterioration of a system with time or cycles, also called wear-out, is the Weibull distribution family. The Weibull distribution has two general forms; two parameter (2-P) and three parameter (3-P) distributions. The Weibull 3-P distribution has a cumulative density function (cdf) given by

$$F(N) = \begin{cases} 1 - \text{Exp}\left[-\left(\frac{\text{N}-\gamma}{\eta}\right)^{\beta}\right], N \geq \gamma \\ 0, N < \gamma \end{cases} \tag{1}$$

where F is the portion of failures at N thermal cycles, the location parameter γ is the failure-free operating period of the population, η is the scale parameter, and β is the shape parameter [8]. The characteristic life of the distribution is expressed as

$$\theta = \eta + \gamma; \tag{2}$$

representing the number of cycles until 63.2% of the population has failed. The Weibull 2-P distribution is the same as the 3-P except there is no failure-free operating period for the population. The 2-P cdf given by:

$$F(N) = 1 - \text{Exp}\left[-\left(\frac{\text{N}}{\eta}\right)^{\beta}\right], \ \ \text{N} > 0 \tag{3}$$

where η is equal to the characteristic life of the population.

Preliminary analysis of the thermal cycling test data for this study was performed using a commercial statistical program, Weibull++ [9]. The Weibull parameters for cycles to failure of each daisy-chain net were estimated using both the maximum likelihood estimation (MLE) method and rank regression (RRX) method. A comparison of the estimated parameters from both methods for both 3-parameter and 2-parameter distributions are presented in Table 2-1 and Table 2-2. The Weibull 3-P distribution was found to have a better fit to the test data than the 2-P distribution; consistent with the literature, Clech et al. [4] and Liu and Lewis [10]. Therefore Weibull 3-P was selected for further analysis of all test results.

Table 2-1: Comparison of Weibull parameter estimates for the 3-P distribution using both the MLE and RRX methods. The total number of samples per daisy-chain net was 53. The number of survivors per D-C net at the conclusion of testing, as well as the number of probable ground wire failures are shown in columns four and five respectively. Nets seven and two have negative failure free periods when using the MLE method.

D-C Net ID	D-C Net I/O Count	Number of Failures	Number of Survivors	Probable Wire Failures	MLE Estimated Parameters β	η	γ	θ	RRX Estimated Parameters β	η	γ	θ	ρ
12	8	51	1	1	2.6	1,500	70	1,570	2.5	1,570	10	1,580	0.992
11	24	52	2	0	2.3	1,100	150	1,250	2.3	1,160	110	1,270	0.980
10	96	53	0	0	1.8	690	130	820	2.0	740	90	830	0.989
9	144	51	0	2	2.0	970	140	1,110	1.8	1,000	120	1,120	0.989
8	128	46	4	3	1.5	1,080	580	1,660	1.5	1,180	520	1,700	0.992
7	112	30	14	9	6.2	4,670	-2,350	2,320	1.2	1,620	740	2,360	0.978
6	72	33	9	11	1.6	1,620	550	2,170	1.9	1,760	390	2,150	0.994
5	48	32	9	12	1.9	1,630	590	2,220	2.1	1,730	490	2,220	0.991
4	16	40	5	8	1.6	1,300	560	1,860	1.7	1,380	500	1,880	0.996
3	8	37	10	6	1.5	1,500	610	2,110	1.2	1,710	600	2,310	0.990
2	24	38	10	5	5.6	4,420	-2,400	2,020	1.3	1,610	400	2,010	0.983
1	24	35	11	7	2.5	2,090	170	2,260	2.5	2,280	40	2,320	0.993

Table 2-2: Comparison of Weibull 2-P estimates using both the MLE and RRX methods.

D-C Net ID	D-C Net I/O Count	Number of Failures	Number of Survivors	Probable Wire Failures	MLE Estimated β	η	RRX Estimated Parameters β	η	ρ
12	8	51	1	1	2.7	1,580	2.6	1,580	0.992
11	24	51	0	2	2.7	1,270	2.8	1,250	0.982
10	96	53	0	0	2.3	840	2.5	830	0.987
9	144	51	0	2	2.4	1,130	2.3	1,120	0.986
8	128	46	4	3	2.8	1,730	3.2	1,680	0.974
7	112	30	14	9	2.5	2,330	3.5	2,000	0.925
6	72	33	9	11	2.7	2,170	3.1	2,040	0.988
5	48	32	9	12	3.2	2,220	3.7	2,110	0.988
4	16	40	5	8	2.8	1,900	3.3	1,800	0.983
3	8	37	10	6	2.8	2,120	2.9	2,070	0.967
2	24	38	10	5	2.1	1,970	2.4	1,840	0.966
1	24	35	11	7	2.9	2,250	2.7	2,300	0.993

RRX methods were found to produce a better overall fit to the test data than MLE methods. Examples of this can be seen in Figure 2-6. For the most part, MLE and RRX methods produced similar parameter estimates. However, the MLE fits produced poor results for Net 7 and Net 2, resulting in negative failure-free periods and large shape parameters (approximately six). Typical solder shape parameters are range from 2-3, Clech et al. [4]. A negative failure free period would imply that the solder populations for these nets had failures before testing; indicative of manufacturing or handling issues. However, these data are part of the solder joints from a high I/O component. Therefore, the other test nets would have similar location parameters if there were manufacturing or

handling issues. Therefore, these test results suggest that the test data for Net 7 and Net 2 may contain probable wire failures that would require further data censoring.

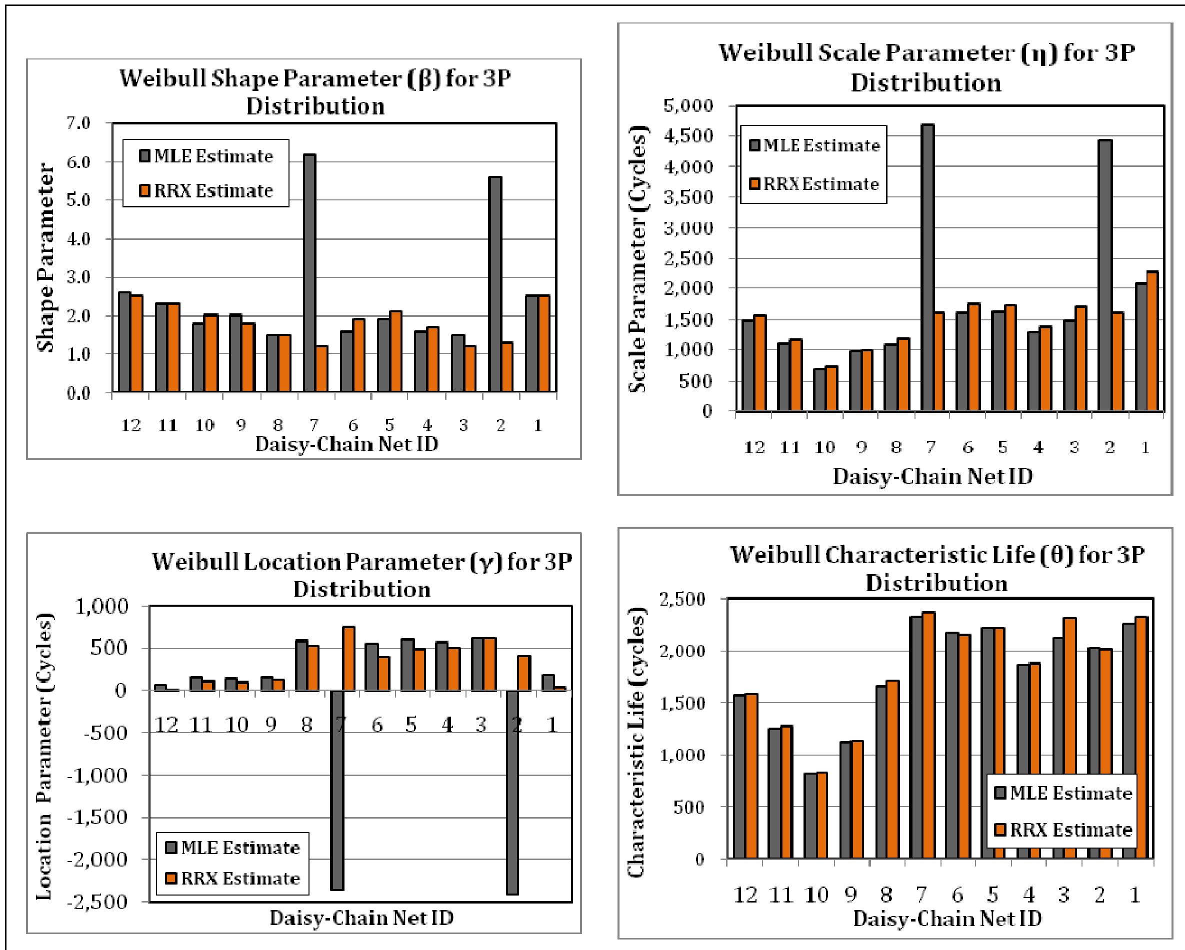

Figure 2-6: Comparison of Weibull 3-P properties for all 12 daisy-chain test nets using both MLE and RRX methods. MLE estimated parameters are shown in grey, and RRX estimated parameters are shown in orange. Both methods yielded comparable parameter values, except for Net 7 and Net 2 which had poor fits.

The Weibull 3-P cdfs for Net 7 and Net 2, plotted for both the MLE and RRX estimates in Figure 2-7, show that the RRX estimate is a better descriptor for the test data, for the majority of the data; while for the MLE estimates provide good fits only at the tails of the failure data. The poor MLE fit, resulting in negative failure-free periods for these nets, is indicative of the presence of probable mixed failure modes, such as wire failures.

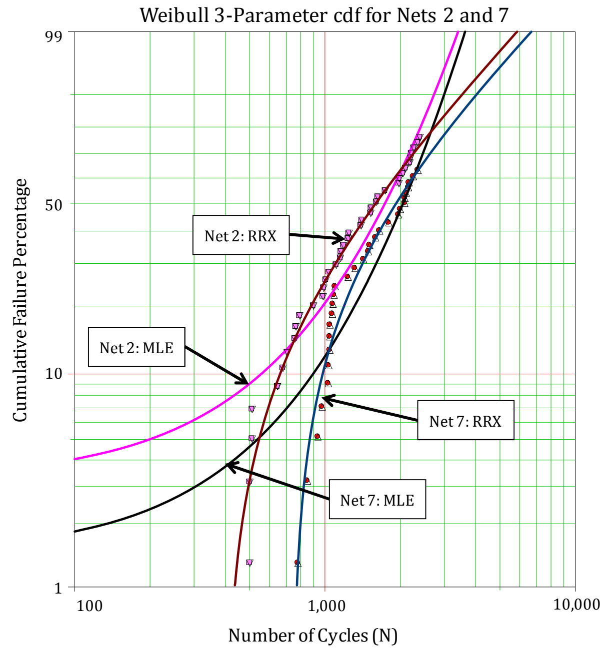

Figure 2-7: plot of Weibull cdfs for daisy-chain Net 7 and Net 2 using both the MLE and RRX estimates. The RRX estimates are seen to fit the test data for these two nets better than the MLE estimates.

Test data for daisy-chain Net 7 was examined using a mixed-Weibull two-population distribution. Mixed-Weibull analysis is a technique used to determine if there are multiple failure modes for a population. The cdf plot for the mixed-Weibull is shown in Figure 2-8. The distinct hump seen in the cdf at approximately 1,000 cycles is an indicator of two separate populations. This group of failure points is probably due to wire failures, rather than interconnect failures. These suspect data points were edited to be right censored data for this net. A similar analysis, performed for daisy-chain Net 2, did not suggest multiple populations. However, careful visual examination of the cdf plot (Figure 2-9) for the RRX 3-P distribution shows that the first four failures at the leading edge of the distribution should be on a separate Weibull curve with a very high slope. The reasons this was not detected by the mixed-Weibull analysis may have been due to

the very small number of data points in this secondary failure population. These data points may represent probable wire failures, and were edited to be right censored as well.

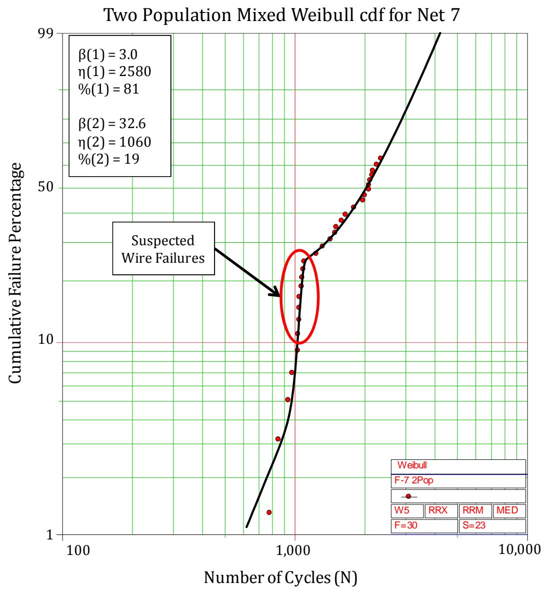

Figure 2-8: bi-modal mixed-Weibull cdf of daisy-chain Net 7. The presence of a second population can be seen as a kink in the cdf at approximately 1,000 cycles. These data points are probably due to wire failures, not interconnect failures.

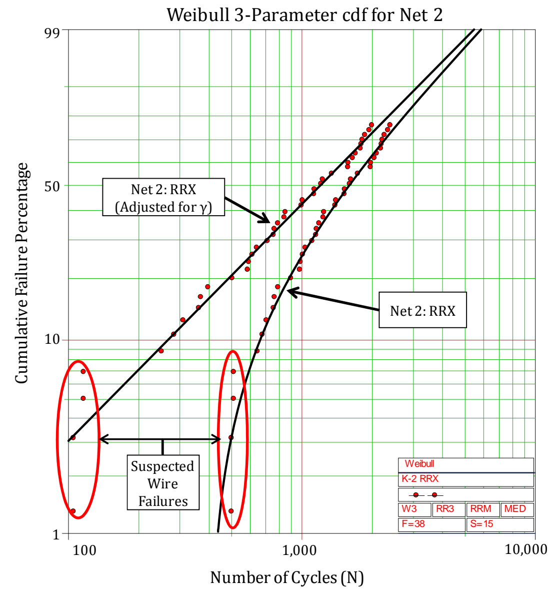

Figure 2-9: RRX estimate of the 3-P Weibull cdf for daisy-chain Net 2. The first four data points evidently do not fit the estimated cdf. These points are probable wire failures, not interconnect failures.

Only daisy-chain nets 7 and 2 were adjusted for additional wire failures. The other 11 daisy-chain nets either did not produce bimodal Weibull distributions or did not have visually obvious premature failure data points. The adjusted data sets for the sample population were re-examined using both MLE and RRX methods for the 3-P Weibull distribution. A comparison of parameter estimates is shown in Table 2-3.

Table 2-3: Comparison of 3-P Weibull estimates for the adjusted failure data. The failure data for daisy-chain nets 7 and 2 were adjusted for additional probable wire failures. The RRX method was found to be better than the MLE method for estimating the statistical parameters of the adjusted test data. For example, Net 2 has a shape parameter estimate of 0.5 using MLE estimators.

D-C Net ID	D-C Net I/O Count	Number of Failures	Number of Survivors	Probable Wire Failures	MLE Estimated Parameters				RRX Estimated Parameters				
					β	η	γ	θ	β	η	γ	θ	ρ
12	8	51	1	1	2.6	1,500	70	1,570	2.5	1,570	10	1,580	0.992
11	24	52	0	2	2.3	1,100	150	1,250	2.3	1,160	110	1,270	0.980
10	96	53	0	0	1.8	690	130	820	2.0	740	90	830	0.989
9	144	51	0	2	2.0	970	140	1,110	1.8	1,000	120	1,120	0.989
8	128	46	4	3	1.5	1,080	580	1,660	1.5	1,180	520	1,700	0.992
7	112	25	15	13	1.4	1,900	750	2,650	1.5	2,090	660	2,750	0.997
6	72	33	9	11	1.6	1,620	550	2,170	1.9	1,760	390	2,150	0.994
5	48	32	9	12	1.9	1,630	590	2,220	2.1	1,730	490	2,220	0.991
4	16	40	6	7	1.6	1,300	560	1,860	1.7	1,380	500	1,880	0.996
3	8	37	10	6	1.5	1,500	610	2,110	1.2	1,710	600	2,310	0.990
2	24	34	10	9	0.5	2,010	500	2,510	1.1	1,540	610	2,150	0.997
1	24	35	11	7	2.5	2,090	170	2,260	2.5	2,280	40	2,320	0.993

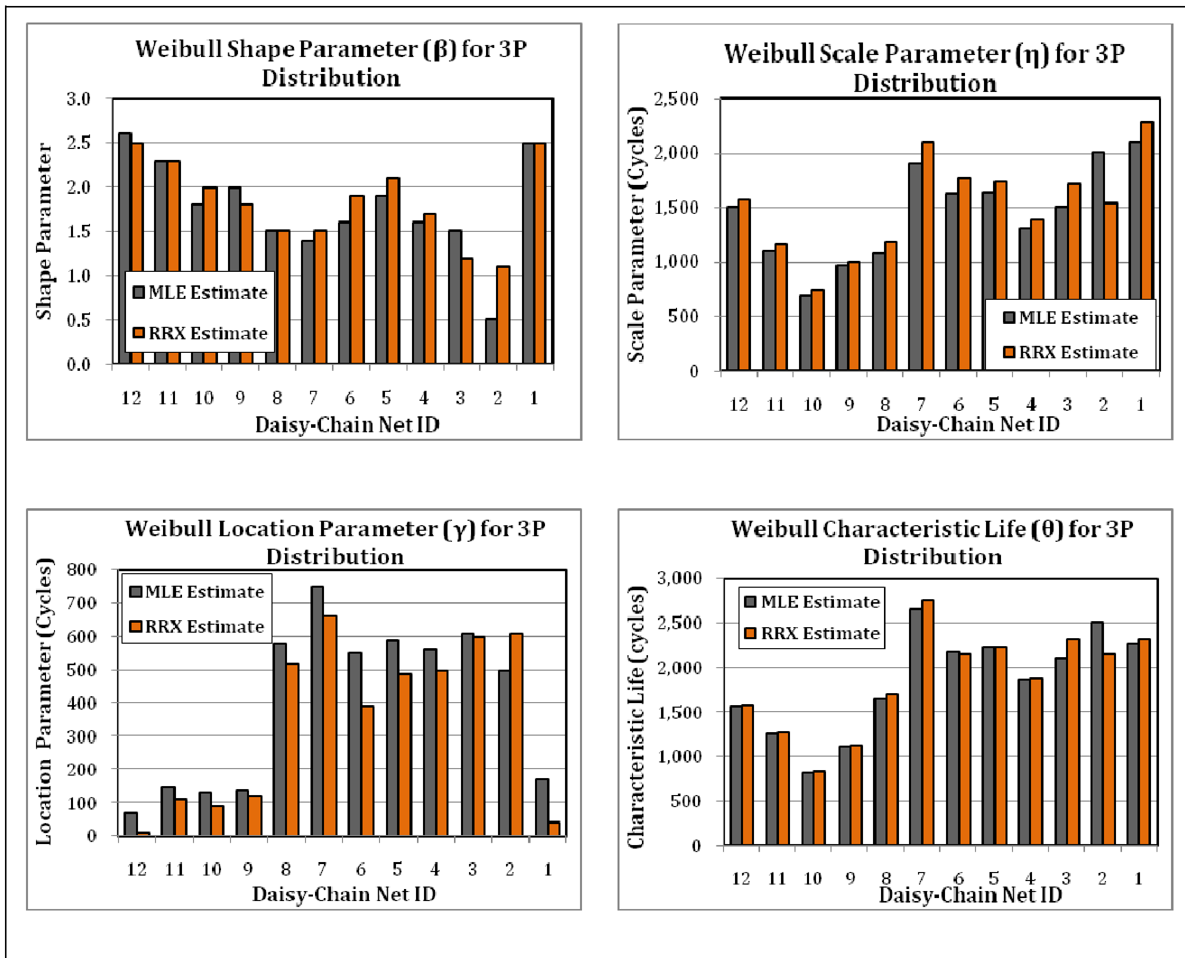

Figure 2-10: comparison of Weibull parameters for adjusted test data using both MLE and RRX methods. Parameter estimates using both methods produce similar results per daisy-chain net except for Net 2. MLE methods estimate a shape parameter of 0.5. This is indicative of early failure for a population. However, the test data for this net contained a large number of survivors.

After censoring nets 7 and 2 for probable wire failures, the RRX method was found to provide a better fit to the adjusted test data than MLE estimates for Net 2. This daisy-chain net had an estimated shape factor of 0.5 for the MLE method, indicating early failures ("infant mortality"). However, the test data does not support this. The MLE estimate of the cdf of Net 2 data after adjusting for probable wire failures (plotted in Figure 2-11) shows a very poor fit. In contrast, the RRX cdf estimates of nets 2 and 7 (after adjustment for probable wire failures), shown in Figure 2-12, clearly indicate a good fit.

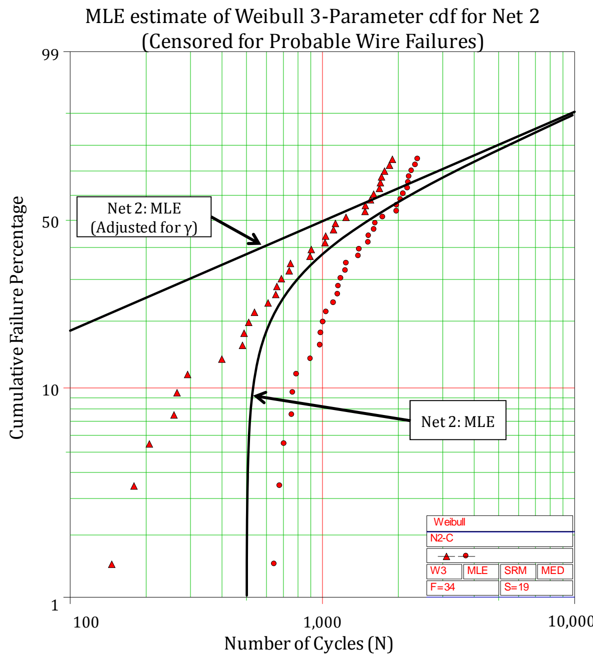

Figure 2-11: 3-P Weibull MLE estimated cdf for daisy-chain Net 2. Parameter estimates using MLE provide a poor fit, resulting in clearly erroneous estimates such as a shape parameter of 0.5, which is usually a sign of infant mortality.

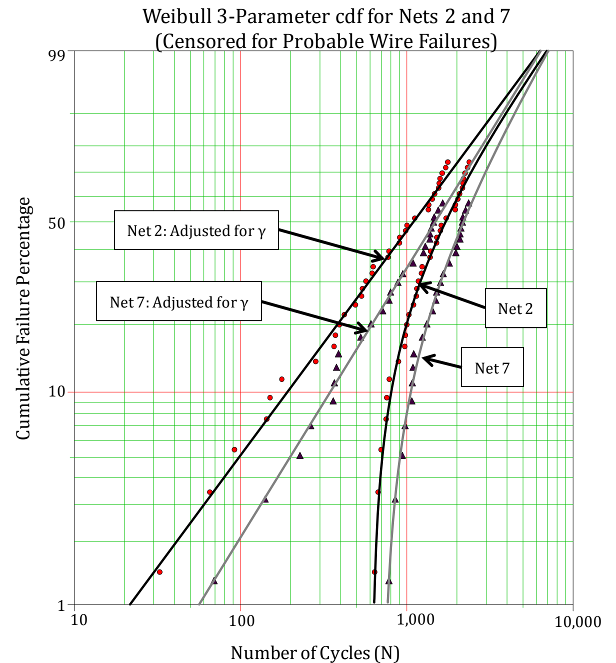

Figure 2-12: 3-P Weibull cdfs for daisy-chain nets 7 and 2. The data sets for these nets have been appropriately adjusted for probable wire failures. The RRX estimated Weibull distribuitons for both test nets fit the test data quite well.

2.3.2 Examination of First Solder Joint Failure

The thermal cycling test results of the test specimen provide insightful evidence on the location of first joint failure in the test components. Mechanistic models for solder

durability will usually predict the location of first failure to be either at the package corner, or under the die-shadow corner depending on the package architecture. The net location for most frequent occurrence of first joint failure in this study was not consistently at either of these locations. The test results showed random variability in which net failed first in any given component. A frequency plot of first failure per daisy-chain net is shown in Figure 2-13. The prevalence of first failures is clearly in Net 10, in a total of 29 out of the 53 components, rather than in the highest stressed nets (likely to be nets 3 or 12). The predominance of first failures in Net 10 indicates; a) that the large number of joints, 96, in this net increases the probability of failure, and b) that this location in the package experienced high load levels. Additionally, it can be seen in Figure 2-13 that Net 9 also had a large number of first failures (total of 11). This is not surprising given the large joint count, 144, for this net. Even though this net has more solder joints than Net 10, and hence more likelihood of failure, Net 9 had fewer 1st failures than Net 10.

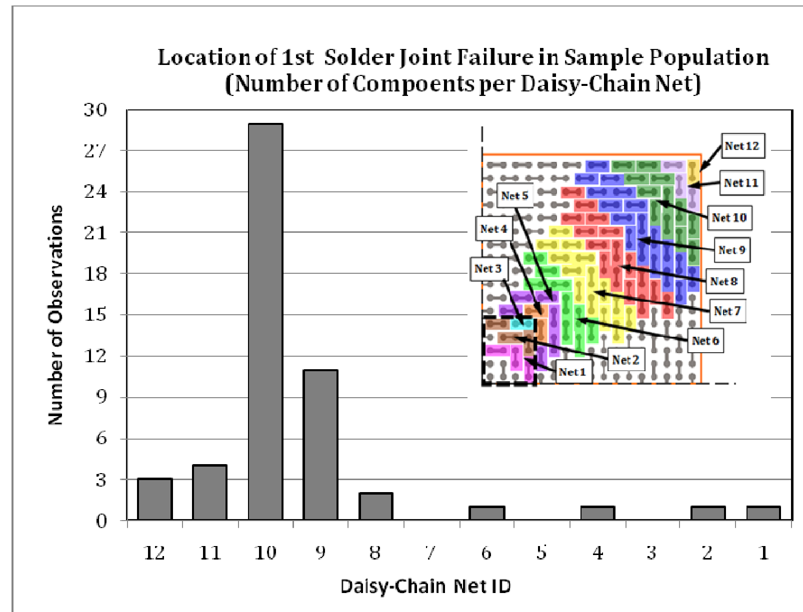

Figure 2-13: Histogram showing the location of first failures; the number of components failed is plotted by daisy-chain net ID. Net 10 has the most first failures, in 29 components out of 53. For reference, Net 12 is at the package outer corner and Net 3 is at the die outer corner. Decreasing net numbering corresponds to decreasing DNP.

Additionally, results showed the location for first interconnect failure of the population was predominantly located in middle region of the package. As discussed before, mechanistic models for solder durability will usually predict the location of first failure to be either at the package outer corner (Net 12), or under the die-shadow corner (Net 3). In the test population failures were found at the package corner, Net 12 had only three first failures, approximately 6% of the first failures. Nets near the die-shadow (Nets 4 and 2) collectively had 7.5% of all the reported first failures. However, of the 12 daisy-chain nets in the population, the majority of the locations for first joint failure per package in the population were located in Nets 10 and 9 (a total of 72% of the reported failures). Both of these nets should have had relatively benign stress levels during thermal cycling. Therefore, based on strictly mechanistic concepts, this region should not have first failure. These discrepancies therefore are likely to be due to probabilistic effects.

Weibull predictions of first failure per daisy-chain net can be calculated by rearranging the 3-P cdf. The cycles to failure is then,

$$N = \gamma + \eta * \left[-ln\left(1 - F(N)\right)\right]^{\frac{1}{\beta}} \tag{4}$$

The cumulative failure percentage, F(N), is found using median ranking. The following formula is the approximation method for median ranking [8];

$$\tilde{F}(N_i) = \frac{i - 0.3}{n + 0.4} \tag{5}$$

where i is the failure ranking and n is the sample size. The cumulative failure percentage for this sample is 1.22%. Results of the Weibull predictions of cycles to first failure are compared to the observed cycles to first failure in Figure 2-14. The observed values are described well with the values predicted by the Weibull statistics. Of the 12 daisy-chain nets, Nets 7, 5 and 3 had no first failures per component. Therefore, in Figure 2-14 there are no observed first failures plotted.

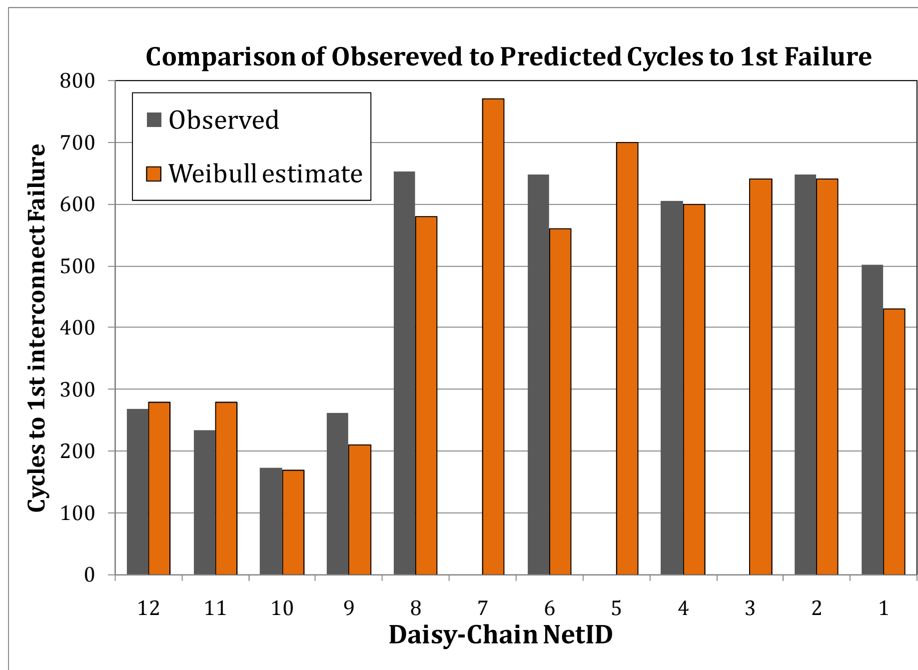

Figure 2-14: comparison of observed cycles to first failure with Weibull predicted values. Daisy-chain Nets 7, 5 and 3 had no first failures per daisy-chain per component, therefore only predicted values are reported for these nets.

The package level reliability was evaluated using 3-P Weibull analysis. Package level reliability is the unique set of 1st failures for the sample population. The Weibull parameters are shown in Table 2-4. Weibulll parameter estimates were made for both the 2-P and 3-P distributions, using both the RRX and MLE methods. Either RRX or MLE methods produce identical parameter estimates for the 2-P distribution. The failure free period estimated using MLE is more than twice as long as that predicted by RRX methods. However, the characteristic life is the same for either estimation method. Thus, the RRX estimates produce a more conservative estimate of the package life than MLE estimates at low failure percentages.

Table 2-4: Package level reliability estimates based on first failures per component. Weibull parameters were found for the 2-P and 3-P distribution using both RRX and MLE methods.

Package Level Reliability Estimates				
Parameter	3-P		2-P	
	RRX	MLE	RRX	MLE
β	2.6	2.4	2.9	2.9
η	580	530	630	630
γ	40	90	N/A	N/A
θ	620	620	630	630
ρ	0.995	N/A	0.994	N/A

2.4 Failure Analysis

Failure analysis was performed on 13 samples. The goal of failure analysis was to determine the location of solder failures. A total of ten samples were examined using the dye and pry, revealing that a majority of specimen failures were in the neck of solder joints located near the package perimeter. However, there were multiple joint failures found interspersed though-out the package. This is expected, given the probabilistic

distributions seen in the failure site location in the test data. These locations can be associated with probabilistic effects.

Specimen cross-sectioning was performed on three of the specimens. Polished specimens were examined using optical microscopy. The results revealed both partial and full cracks for interconnect failure. Of the three specimens, only solder neck cracks were observed. Examples of this are shown in Figure 2-15 and Figure 2-16. Additionally, solder voids were found in multiple joints. An example of this is shown in Figure 2-16.

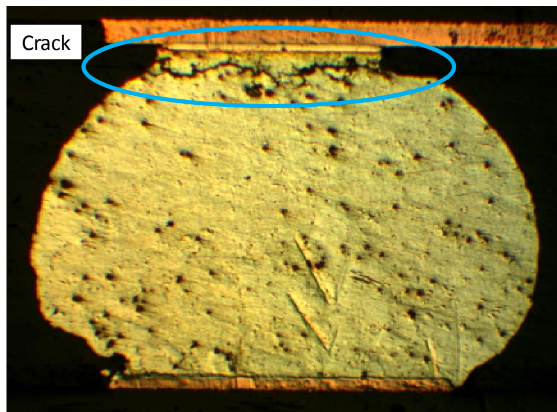

Figure 2-15: optical micrograph of a cross-sectioned PBGA interconnect. A large crack, circled in blue, can be seen at the solder neck.

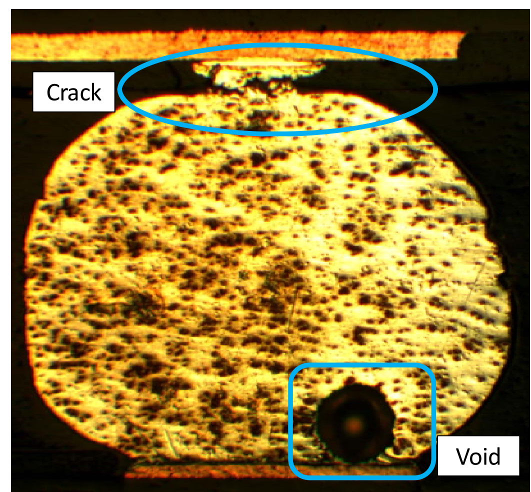

Figure 2-16: optical micrograph of a cross-sectioned PBGA interconnect. The solder neck has almost completely cracked through. Also, a large void can be seen in the bottom right corner of the joint

2.5 Summary and Conclusions of Test

In this chapter, thermal cycling durability experiments were performed on 1156 I/O PBGAs. The test specimens were specially daisy-chained into 12 distinct and independent test nets per component for systematically tracking the interconnect failure progress in the test population. A sample population of 53 test components was subjected to temperature cycling. Weibull analysis of the results revealed that the 3-P distribution

using RRX methods provided the best fit to the data for parameter estimation. Additionally, results showed that the location of first interconnect failure of the population was predominantly (for almost 72% of all reported failures) located in the middle region of the package in Nets 10 and 9; rather than at the package corner (Net 12) or die corner (Net 3).

3 Analysis of Test Results

In this study, the failure data for all 12 nets from the previous study are scaled for mechanistic effects to normalize all daisy-chain nets to the same reference damage level. The mechanistically scaled results for all nets are then systematically grouped in order of decreasing distance from neutral point (DNP) to simulate increasing number of joints in the critical region of the PBGA, as the component size increases. A "weakest link" series reliability model is used to further normalize the results to account for the fact that the number of joints is not the same in all the nets. The scaled series model is then used to predict the degradation of Weibull characteristic life with increasing number of solder joints. The series model results are found to compare well with the mechanistically scaled and grouped test results. The results show that degradation of durability due to probabilistic effects has a power-law dependence on the number of joints in the package critical region. The final output is a probabilistic de-rating factor that can be used to adjust mechanistic predictions of thermal cycling durability in high I/O PBGAs.

3.1 Overview

Studies in the literature (Darveaux et al. [2] and Clech et al. [4]), have shown that component fatigue life depends on the collective failure distribution of all the solder joints in the component. In other words, reliability estimates based on a single solder joint or a small group of solder joints tend to over-predict the package durability. Therefore, it is necessary to adjust package durability predictions to account for the number of solder joints in the system that are at approximately the same load level. Essentially, since failure of a single solder joint is failure of the component, the system is seen to be acting

in series. Using a traditional series-reliability model, the package reliability, R_c, can be estimated from the reliability of an individual solder joint, as;

$$R_c(N) = \prod_{j=1}^{k} R_i(N) = \prod_{j=1}^{k} 1 - F_j(N) \tag{6}$$

In (6), k is the total number of units in the system, and R_j is the reliability of each independent unit and F_j is the cumulative density function (cdf), sometimes called the unreliability, of each unit.

Darveaux [12] and Clech, et al. [4] used the Weibull 3-parameter (3-P) distribution to show the relationship between the failure distribution of a single solder joint (or group of similarly stressed joints) to the component failure distribution. The Weibull 3-P distribution has a cdf given by

$$\begin{aligned} \mathrm{F(N)} = 1 - \exp\left[-\left(\frac{\mathrm{N} - \gamma}{\eta}\right)^{\beta}\right];\ \mathrm{N} \geq \gamma \\ \mathrm{F(N)} = 0;\ \mathrm{N} < \gamma \end{aligned} \tag{7}$$

where N is the number of thermal cycles, the location parameter γ is the failure-free operating period of the population, η is the scale parameter, and β is the shape parameter. The characteristic life, θ, (the number of cycles until 63.2% of the population has failed) is the sum of the scale and location parameters. In [4], Clech, et al. showed that for the 3-P Weibull distribution, the component parameters are related to the subset parameters, by the simple relationships;

$$\begin{aligned} \beta_{component} &= \beta_{subset} = \beta \\ \gamma_{component} &= \gamma_{subset} = \gamma \\ \eta_{component} &= \frac{\eta_{subset}}{\mathrm{k}^{1/\beta}} \end{aligned} \tag{8}$$

given that each of the k units in the subset has the same Weibull distribution. The authors compared test data of a daisy-chained QFP partitioned into eight nets. Results showed that component Weibull parameter calculations using series reliability modeling of the octile Weibull parameters matched well with test data for the QFP on a component basis.

In [12], Darveaux proposed that reliability predictions for BGAs based on a single solder joint are erroneous; BGA reliability predictions must incorporate the component I/O count. The authors suggest dividing the component into sets of solder joints under identical loading. The reliability of a set of solder joints subjected to identical loading is then;

$$R_c(N) = exp\left[-k\left(\frac{N-\gamma_j}{\eta_j}\right)^{\beta_i}\right]. \quad (9)$$

The authors also suggest that for BGAs with many solder joints the component should be partitioned into subsets of similarly loaded joints. Then this result can be extended with a series model to the entire package, for each relevant stress level. However, Darveaux suggests that for high-I/O components the characteristic life predictions will be significantly reduced if all the joints are taken into account. Therefore, he proposes only grouping the worst case joints, either at the package corner or at the corner of the die-shadow, when calculating the package durability. Component durability predictions can then be de-rated by the simple formula;

$$\frac{\theta_c}{\theta_j} = \frac{1}{2}\left[1 + \left(\frac{1}{k}\right)^{\frac{1}{\beta}}\right]. \quad (10)$$

In (10); θ_c is the characteristic life of the component, θ_j is the characteristic life of the joint(s) with the highest cyclic work density, and k is the number of worst case solder

joints in the component. This formula is dependent on the failure-free period of each of the worst case solder joints being equal to half the characteristic life of the joint. Darveaux et al. [2] found this relationship from crack growth tests conducted on ceramic BGAs with Sn36Pb2Ag solder joints. Thus, this de-rating factor (10) may not be applicable for other geometries and solders.

Equation (10) can easily be generalized as follows:

$$\gamma = \alpha\theta j; \tag{11}$$

where, α can take some value other than 0.5. Thus, inserting (11) into (9) and rearranging terms yields the generalized package de-rating factor;

$$\frac{\theta_c}{\theta_j} = \alpha + (1-\alpha)\left(\frac{1}{k}\right)^{\frac{1}{\beta}}. \tag{12}$$

In this paper, the authors investigate the accuracy of this approach presented by Darveaux et al. [2], Darveaux [12] and Clech et al. [4] to quantify the effect that probabilistic factors have on durability predictions for high-I/O PBGAs. The test results from Chapter 2, are used to group the failure data of similarly loaded solder joints. The daisy-chain failure data are scaled for mechanistic effects to ensure that all test nets are effectively at the same reference load level and also for the fact that there are different numbers of solder joints in each net. The scaled test results for all nets are then systematically grouped in order of decreasing DNP to effectively mimic the effect of increasing number of joints in the critical region as the component size increases. Furthermore, a "weakest link" series reliability model is also used to predict the degradation of Weibull characteristic life with increasing number of solder joints. The series model results are found to compare well with the scaled and grouped test results. The results show that degradation of durability due to probabilistic effects has a power-

law dependence on the number of joints in the package critical region. The final output is a probabilistic de-rating factor that can be used to adjust mechanistic predictions of thermal cycling durability in high I/O PBGAs.

3.2 Scaling for Mechanistic Effects

In the thermal cycling test data, mechanistic differences between independent daisy-chain nets were not considered. In other words, the difference in the thermomechanical load and damage levels in different nets was not considered. These differences must be considered before the test data can be grouped. Essentially, to effectively group the failure data across different nets of solder joints, the grouped joints must be at approximately the same load levels. The grouping can be accomplished by scaling all test data to a common reference mechanistically predicted damage level, using a combination of nonlinear 3-D finite element analysis (FEA), and an energy-partitioning (E-P) fatigue damage model. This mechanistic modeling approach was used to determine the maximum cyclic damage in each daisy-chain net, and thus develop a mechanistic scaling factor for the test data from each net. The scaled failure results from all nets can be considered to be from a common damage accumulation rate.

3.2.1 Finite Element Analysis

Three dimensional (3-D) non-linear FEA was used to obtain the cyclic work density of the solder joints, necessary for energy-partitioning damage calculations. This study used a 3-D viscoplastic model with quarter-symmetry of the test component; incorporating a 17x17 solder joint array. The model was developed using ANSYS APDL. Relevant cross-sectional model geometry was based on averaged dimensions obtained

from component cross-sections. A schematic of the package architecture is shown in Figure 3-1, and the relevant package dimensions are found in Table 3-1. In the FEA model the printed wiring board (PWB) was given a length five times as long as the package length on a side. An oblique view of the meshed model is shown in Figure 3-3, and an underside view of the meshed package is shown in Figure 3-4. The meshed model consisted of 137,098 elements and total of 164,170 nodes.

Table 3-1: relevant package dimensions in milimeters

Height (mm)	
PWB (h1)	1.47
Bottom pad (h2)	0.02
Solder ball (h3)	0.48
Solder neck (h4)	0.03
Top pad (h5)	0.03
Substrate (h6)	0.51
Die attach (h7)	0.07
Die (h8)	0.51
Overmold (h9)	0.60
Diameter (mm)	
Bottom pad (d1)	0.45
Solder ball (d2)	0.62
Solder neck (d3)	0.32
Top pad (d4)	0.51

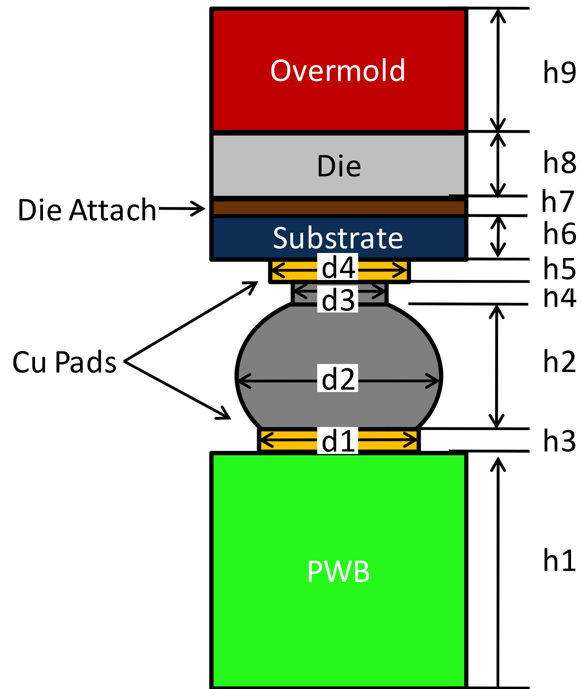

Figure 3-1: schematic of a cross-section of the package geometry.

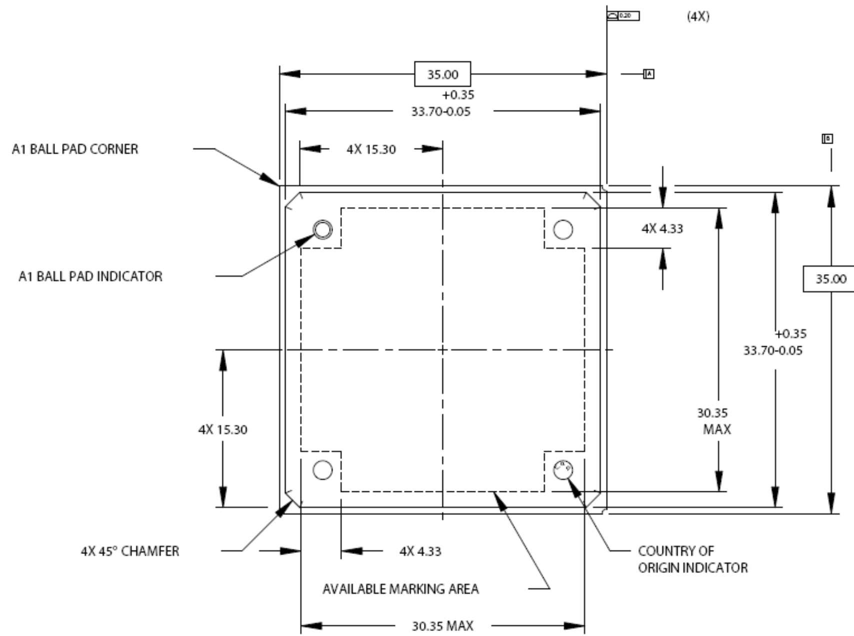

Figure 3-2: schematic of package foot-print, including all relevant dimensions [13].

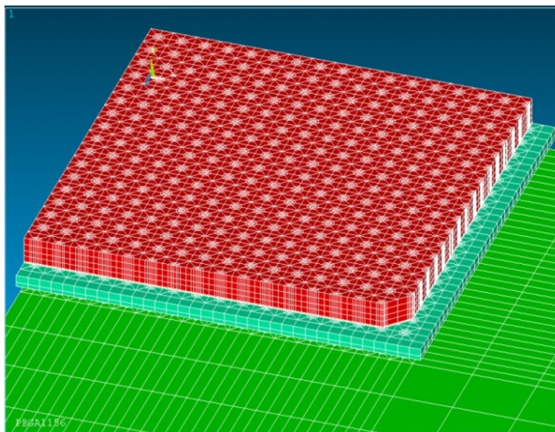

Figure 3-3: oblique view of FEA model showing the package mounted on the PWB. The package molding compound is shown in red, the substrate is shown in cyan.

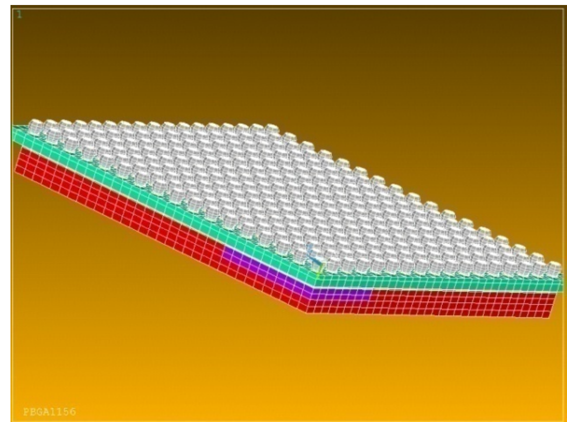

Figure 3-4: underside view of the meshed package. The 17x17 array of solder joints can be seen in dull gray color. The die is visible in the pictures as the dark purple region below the molding compound.

The material properties used for FEA modeling were taken from the literature, Zhang et al. [14] and Cuddalorepatta et al. [15]. All materials, except solder, were modeled as linear elastic. Model material properties, excluding solder, are shown in Table 3-2. The package substrate (BT) and the PWB (FR4) were modeled as transversely isotropic materials.

Table 3-2: linear elastic material properties used in FEA model

Material		E (GPa)	ν	α (ppm/°C)
FR4	In-plane	17.7	0.11	18
	Out-of-plane	7.7	0.28	60
Copper		12.9	0.35	19
BT	In-plane	20.0	0.11	15
	Out-of-plane	4.0	0.39	60
Silicon Die		19.0	0.28	2
Die Attach		1.2	0.42	110
Overmold		23.6	0.30	9

Solder was modeled using a partitioned constitutive relationship for elastic, plastic, and creep properties. Solder elastic and rate-independent plastic properties were measured from thermomechanical testing of Sn3.8Ag0.7Cu [13]. The solder Young's modulus (E) has a temperature dependent relationship as follows:

$$E = E_0 - E_1 * T(°C). \quad (13)$$

Solder plasticity was modeled using a rate-independent, temperature dependent power hardening relation of the form

$$\begin{gathered} \sigma = C_{pl}\left(\sqrt{3}\varepsilon_{pl}\right)^m \\ C_{pl} = C_{pl0} + C_{pl1} * T(°C). \\ m = m_0 + m_1 * T(°C) \end{gathered} \quad (14)$$

Only secondary (steady-state) creep was used for the solder creep constitutive relationship. Solder steady-state creep rate properties were measured from thermomechanical testing of Sn3.0Ag0.5Cu [15]. A Garafalo hyperbolic sine model (15) was used to represent the steady-state creep strain rate.

$$\dot{\varepsilon}_{cr} = A * [sinh(\lambda\sigma)]^n * exp\left(-\frac{\mathrm{Q}}{\mathrm{R*T(K)}}\right) \quad (15)$$

In (15); A, λ, and n are material constants, Q is the activation energy and R is Boltzman's constant. All solder material constants can be found in Table 3-3.

Table 3-3: solder constitutive properties used in FEA modeling [13] and [15]

Elastic:	E_0 (MPa)	18.6E+3	E_1 (MPa/°C)	-21	ν	0.35	α (ppm/°C)	26
Plastic:	C_{pl0} (MPa)	104	C_{pl1} (MPa/°C)	-0.31	m_0	2.90E-01	m_1 (1/°C)	-460.0E-6
Secondary Creep:	A	0.0271	λ (1/MPa)	0.369	n	1.05	Q (J/mol)	5.1E+3

Eight-node, brick elements were used in the FEA simulations. Planes of symmetry were given appropriate symmetry displacement boundary conditions. The node located at the model origin was constrained in all directions to prevent rigid body motion. The temperature was uniformly changed everywhere in the model. The applied temperature profile was taken as the average of the thermocouple readings from the temperature cycling experiments. The FEA temperature profile is shown in Figure 3-5. The model was subjected to three temperature cycles in order for the cyclic hysteresis values to reach steady-state.

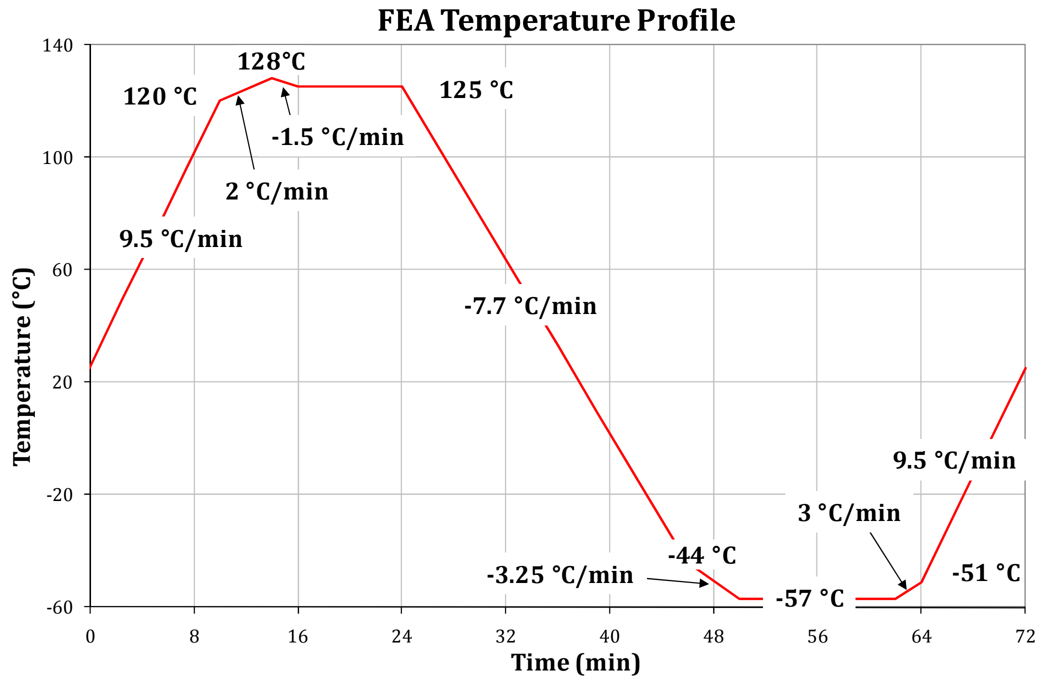

Figure 3-5: temperature profile used for temperature cycling of FEA model. The profile was based on the average thermocouple readings from the thermal chamber.

Contour plots of the von Mises stress and strain at the end of the third hot dwell are shown below for select joints in Nets 12 through10 located near the package corner. In Figure 3-6 von Mises stress contour plots are shown for a total of nine solder joints. The joints in Nets 10 and 11 with the maximum stress are highlighted. In Figure 3-7 von Mises strain contour plots are shown for the same solder set. The package corner joint, located in Net 12 was found to have the highest stress, strain and work densities for the model.

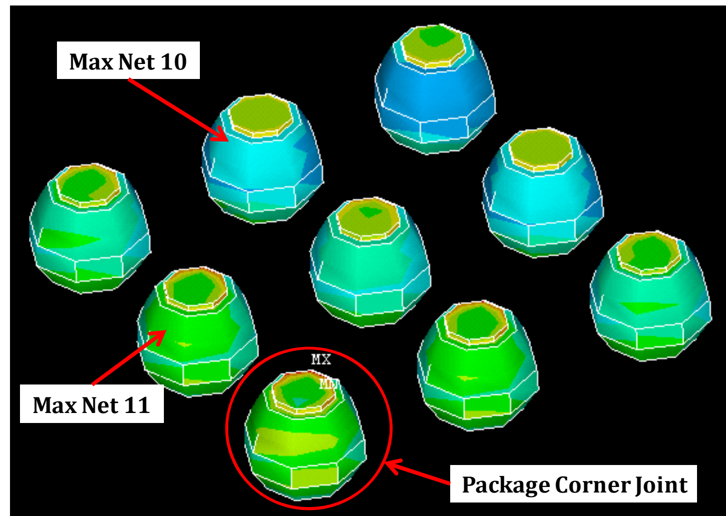

Figure 3-6: contour plots of von Mises stress at the end of the hot dwell for the third temperature cycle for select solder joints located at the package corner. The solder joints with the maximum stress in Nets 11 and 10 are labeled for reference. The package corner joint, located in Net 12, experienced the highest stress, strain and work density levels of all joints in the package

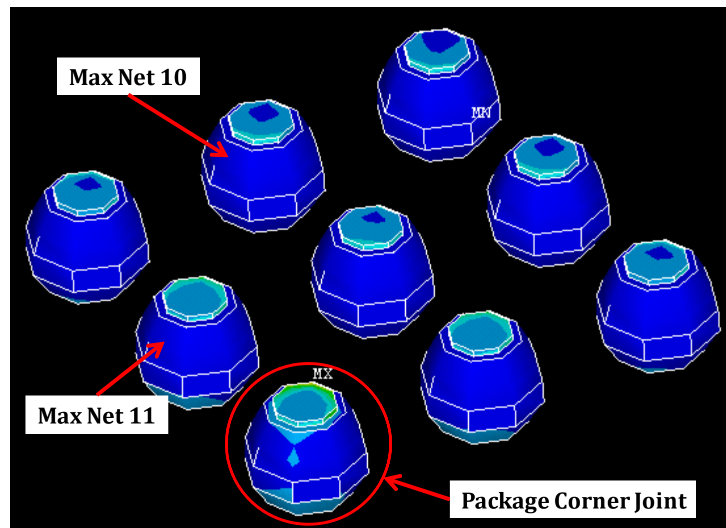

Figure 3-7: contour plots of von Mises strain at the end of the hot dwell for the third temperature cycle for select solder joints located at the package corner. The solder joints with the maximum Mises strain for Nets 12, 11 and 10 are shown.

3.2.2 Energy-Partitioning Damage Model

The interconnect cyclic fatigue damage was estimated from the FEA results using an energy-partitioning damage model, Dasgupta et al. [3]. This model uses partitioned plastic (W_p) and creep (W_c) work densities to predict the number of temperature cycles to

failure (N_f) for a solder joint. The cyclic elastic strain energy density can also be an important contributor to fatigue damage, but is usually negligibly small in temperature cycling. The governing equations, neglecting the elastic contributions, are:

$$Total\ Energy = W_p + W_c = W_{po}(N_{fp})^c + W_{co}(N_{fc})^d$$
$$Damage = \frac{1}{N_f} = \frac{1}{N_{fp}} + \frac{1}{N_{fc}} \tag{16}$$

where, W_{po} and W_{co} are the intercepts of the plot of plastic and creep work densities vs. cycles to failure, on a log-log scale. The exponents c and d are the corresponding slopes of these two plots. The terms N_{fp} and N_{fc} are the cycles to failure due to plastic and creep work, respectively. The energy-partitioning constants are material properties and are available in the literature for eutectic SAC396 solder. The fatigue properties of the SAC305 used in this study are expected to be very similar.

The test data generated in this study provide the opportunity to recalibrate some of these constants. Since the test data are available for only one test condition, it is possible to derive only W_{po} or W_{co} in this study. Of these two, it makes more sense to calibrate W_{co} since it has far more influence than W_{po} on thermal cycling durability. Consequently, W_{po}, c and d, used for this study are for SAC396 from the literature [14], and W_{co}, was recalculated using thermal cycling test data coupled with FEA simulation. Data for Net 12 was used as FEA simulations revealed that the joint with the highest work density was located at the package corner. The characteristic life for Net 12 encompassed eight solder joints in series. Therefore, series reliability was used to calculate the characteristic life of four solder joint in series. This would be equivalent to having test data for the four corner joints of the package. This corresponded to a characteristic life of 2,080 cycles.

The revised energy-partitioning constants are shown in Table 3-4. The recalibrated y-intercept, W_{co}, was found to be 1.28E+4. Zhang, et al. [14] calculated a W_{co} of 1.23E+4.

Table 3-4: Energy-partitioning constants W_{po}, c and d were obtained from Zhang et al. [14]; W_{co} was recalibrated using thermal cycling test data from this study.

Plasticity:	W_{po} (mJ/mm^3)	198	c	-0.8
Secondary Creep:	W_{co} (mJ/mm^3)	1.28E+04	d	-1.4

Following customary procedures, Zhange et al. [14], the plastic and creep work densities were averaged over 10% of the solder joint volume, in the immediate vicinity of the critical region of the joint of interest. This averaging helps to minimize the influence of the mesh density on the E-P fatigue constants, and hence, and on damage predictions. In the FEA model used in this study, the averaging region encompasses three out-of-plane element layers and a total of 44 elements, as shown in Figure 3-8. Solder damage was calculated for the solder joint with maximum DNP in each net. This enabled the estimation of maximum damage values per net.

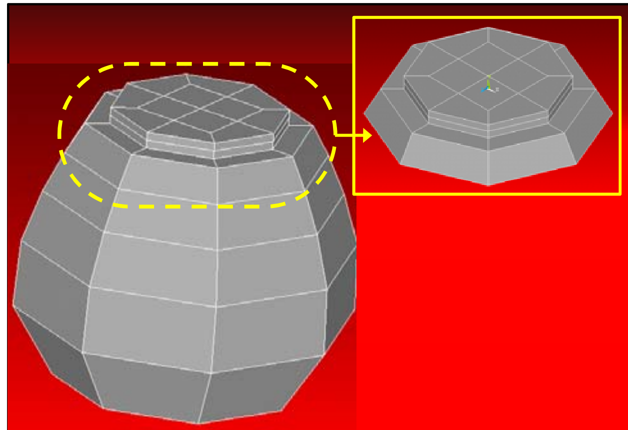

Figure 3-8: highlight of the element layers used for volume averaged work density calculations. The E-P model constants were calculated based on 10% of the solder volume. For this model, 10% of the solder volume is shown in the upper right-hand corner of the figure, and it had three out-of-plane layers and 44 elements.

The mechanistic damage prediction shows that solder joints at the package corner undergo the maximum cyclic damage. The next highest damage level occurred in Net 11, in a solder joint next to the package corner. As expected, the die shadow region, Nets 2-4, had the next highest damage levels. The maximum damage predictions for all 12 daisy-chain nets are shown in Table 3-5. A contour plot of the creep work densities, for the 10% volumetric slice, at the end of the hot dwell for the third temperature cycle for select package corner solder joints is shown in Figure 3-9.

Table 3-5: comparison of mechanistic predicted damage for the 12 daisy-chain test nets. The cycles to failure (N_f), and damage ratios for each net are also shown.

Net ID:	Cr Wrk Dens (mJ/mm^3)	Pl Wrk Dens (mJ/mm^3)	Nfc	Nfp	Damage	Cycles to Failure	Damage ratio
12	269.5E-3	41.1E-3	2,190	40,144	481.5E-6	2,080	1.00
11	89.8E-3	29.6E-3	4,801	60,385	224.9E-6	4,450	0.47
10	19.5E-3	7.6E-3	14,286	332,136	73.0E-6	13,700	0.15
9	9.4E-3	4.7E-3	24,107	595,927	43.2E-6	23,170	0.09
8	6.9E-3	4.2E-3	30,163	689,726	34.6E-6	28,900	0.07
7	6.1E-3	4.1E-3	32,595	716,554	32.1E-6	31,180	0.07
6	7.9E-3	4.5E-3	27,221	630,075	38.3E-6	26,090	0.08
5	18.7E-3	8.7E-3	14,748	278,093	71.4E-6	14,010	0.15
4	18.9E-3	8.5E-3	14,597	289,053	72.0E-6	13,900	0.15
3	19.0E-3	7.1E-3	14,574	361,843	71.4E-6	14,010	0.15
2	42.4E-3	13.8E-3	8,204	156,859	128.3E-6	7,800	0.27
1	26.8E-3	10.8E-3	11,377	214,148	92.6E-6	10,800	0.19

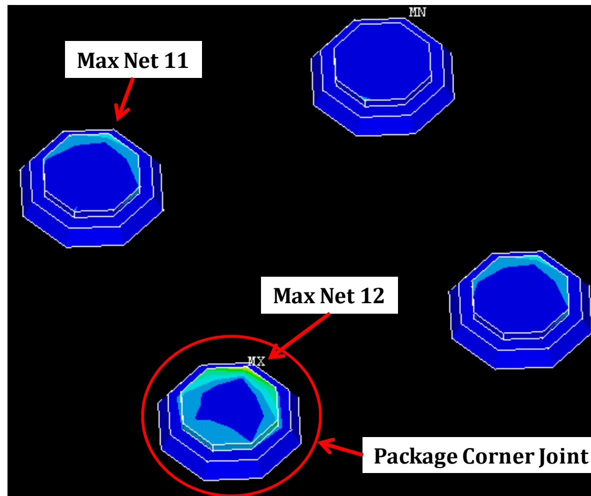

Figure 3-9: contour plots of creep work density for 10% volumetric slices of four solder joints located at the package corner. The joints with the maximum creep work densities for Nets 12 and 11 are highlighted.

A sensitivity study was conducted to determine the relative change in damage ratios with varying energy-partitioning constants. The parameter W_{co} was chosen, as this is the most influential in constant for SAC solders. W_{co} varied by three orders of magnitude. It can be seen in Figure 3-10 that damage ratio predictions are insensitive to the choice of energy portioning constant.

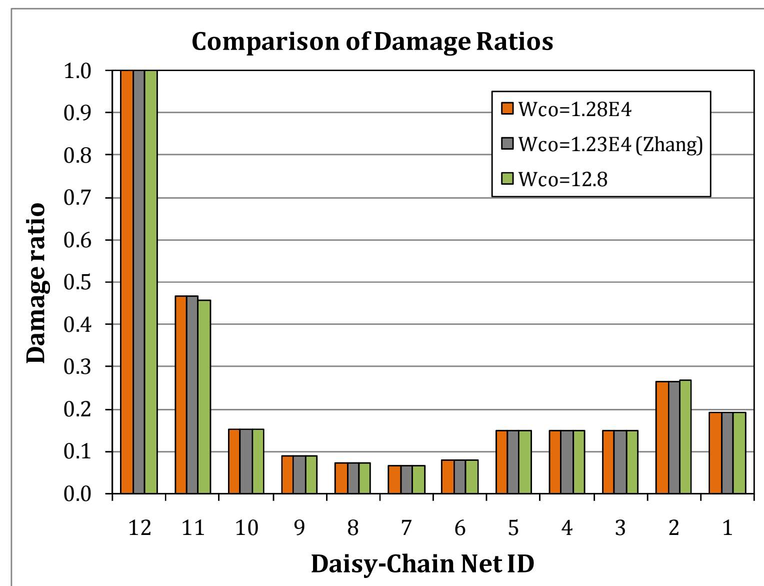

Figure 3-10: comparsion of damage ratios for various values of W_{co}. Damage ratios are relatively insensitive to the value of the energy-partitioning constant.

3.2.3 Mechanistically Scaled Test Data

Damage ratios for all test nets were calculated using the net with the greatest mechanistic predicted damage, Net 12. Mechanistic scaling factors for each daisy-chain net for the maximum damage values are shown in Figure 3-11. The damage ratios are used to scale the test data of each net to be at equivalent loading and damage levels. For mechanistic scaling, the redistribution of load sharing among the surviving joints after each failure was ignored for simplicity.

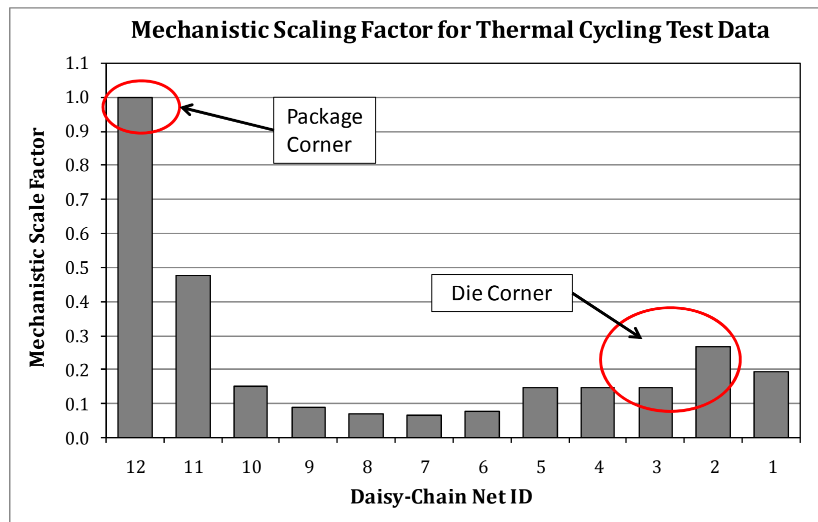

Figure 3-11: comparison of mechanistic scaling factors for thermal cycling test data. Mechanistic scaling factors were calculated using 3-D FEA and energy-partitioning. Scaling factors are the damage ratios for each net based on the maximum damage levels found in all 12 daisy-chain nets.

Rank regression methods (RRX) were used to estimate the Weibull parameters for the 3-P distribution. The parameter estimates for the mechanistically scaled test data are shown in Table 3-6. As expected, the shape parameter estimates for the mechanistically scaled data are the same as the unscaled data, indicating that the scatter in the test data does not change. Also, location and scale parameters per net shifted by their respective mechanistic scaling factor, as expected, since all cycles to failure shifted equally.

Table 3-6: rank regression estimated Weibull parameters for mechanistically scaled test data. Mechanistic scaling factors were applied to the cycles to failure from test data. Scaling of test data was done to simulate equivalent damage levels for all 12 daisy-chain nets. As expected, the shape parameter (β) does not scale with damage level, but the location (γ) and scale (η) parameters have shifted by the mechanistic scaling factor.

D-C Net ID	I/O Count	Number of Solder Failures	Number of Survivors	Number of Wire Failures	Parameters Scaled for Maximum Damage				
					β	η	γ	θ	ρ
12	8	51	1	1	2.5	1,570	10	1,580	0.992
11	24	51	0	2	2.3	530	50	580	0.980
10	96	53	0	0	2.0	110	10	130	0.989
9	144	51	0	2	1.8	90	10	100	0.989
8	128	46	4	3	1.5	80	40	120	0.992
7	112	25	15	13	1.5	140	40	180	0.997
6	72	33	9	11	1.9	140	30	170	0.994
5	48	32	9	12	2.1	260	70	330	0.991
4	16	40	6	7	1.7	210	70	280	0.996
3	8	37	10	6	1.2	260	90	350	0.990
2	24	34	10	9	1.1	410	160	580	0.997
1	24	35	11	7	2.5	440	10	450	0.993

3.3 Effect of Number of Joints

In the previous section, mechanistically scaled Weibull parameters were calculated for the durability test results for individual daisy-chains (D-Cs). However, Weibull parameters of different D-C nets cannot be directly compared since not all nets have the same numbers of solder joints. As was shown in (8)-(10), the Weibull scale parameter and therefore the characteristic life for joints in series is always less than a single solder joint in the set. Thus, the test data for each net must be scaled for the probabilistic effect introduced by the number of joints in the net. Assuming per net that all joints have the same probability of failure, then the probabilistic scaling factor for the number of joints present in a daisy-chain is simply:

$$Probabilistic\ Scaling\ Factor\ per\ net = (I/O\ Count_{net})^{\frac{1}{\beta_{net}}}. \tag{17}$$

The probabilistic scaling factor to account for the number of joints in a daisy-chain is presented in Figure 3-12. The daisy-chain nets in the middle of the package (Nets 7-9) require large probabilistic corrections due to the large I/O counts (>100) in these nets. Net 2 has a large probabilistic scaling factor due to the very low shape parameter, 1.1, estimated for the data. The probabilistic scaling for the number of solder joints found in a daisy-chain net is applied to the scale parameter only. The location parameter is theoretically not affected by the number of joints because essentially a "weakest link" theory implies that the first joint to fail is the failure of the group. Additionally, the shape parameter is also not affected by the number of joints in the group, if the manufacturing quality is assumed to be uniform within a net. Figure 3-13 shows the characteristic life estimates of a single solder joint for each of the 12 nets. These estimates assume that each joint in the net have identical Weibull parameters.

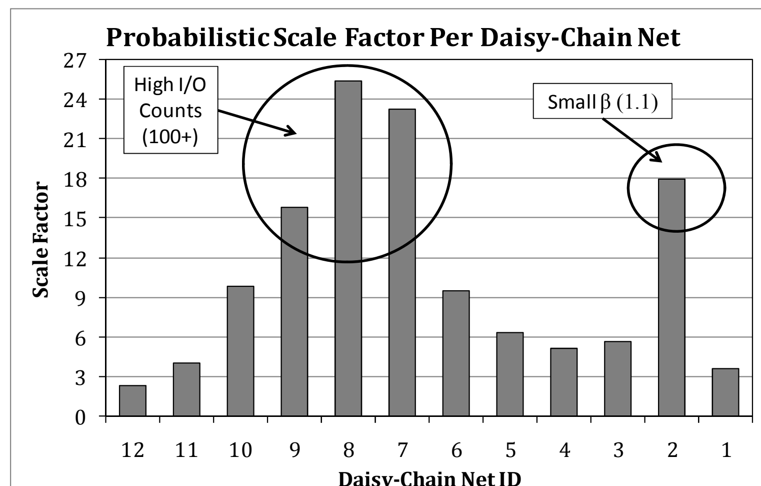

Figure 3-12: comparison of probabilistic scaling factors per daisy-chain net. Large scale factors for Nets 9-7 are attributed to the high-I/O counts (>100) found in these nets; while in Net 2 the scale factor is large because of the extremely low shape factor (1.1). The probabilistic scaling factor adjusts the Weibull scale parameter of a group of identically loaded joints to provide the scale parameter of a single solder joint in the set. Theoretically, neither the location parameter, nor the shape parameter is affected by the number of joints in the daisy-chain.

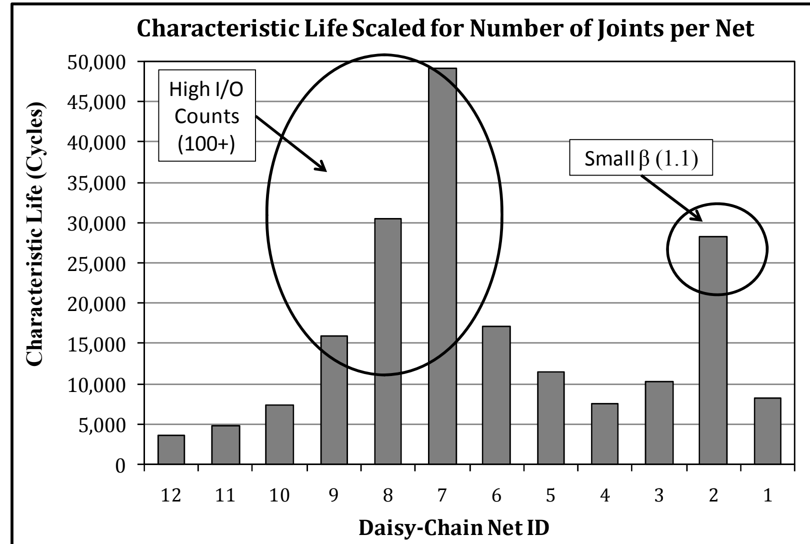

Figure 3-13: comparsion of characteristic life estimates scaled to account for the number of solder joints per daisy-chain net. Essentially, these estimates imply that each solder joint per net has the given characteristic life.

3.3.1 Scaled Weibull Parameters

Theoretically, mechanistic and probabilistic (effect of number of joints) scaling of the thermal cycling test results for all 12 daisy-chain nets should result in identical characteristic life estimates (θ_j) per solder joint per net. In essence, mechanistic scaling ensures that all test nets are at the same damage level. Probabilistic scaling accounts for varying probability of failure due to the number of joints per net. Thus, the fully scaled Weibull parameters are representative of the Weibull distributions found in each solder joint per daisy-chain net. The mechanistically and probabilistically scaled Weibull parameters are presented in Table 3-7. The characteristic life estimates for each solder joint in a net (θ_j) are presented in Figure 3-14. It is evident that there are large differences in predicted θ_j values per net. These difference can be explained by a) the mechanistic scaling factor does not adequately capture the thermomechanical cycling damage equally well for all the nets, and/or b) additional probabilistic effects (due to manufacturing

variabilities such as varying microstructures, joint geometries and void densities) are not uniform across all the nets in the package.

Table 3-7: comparison of mechanistically and probabilistically scaled Weibull parameters for the 12 daisy-chain test nets. The parameter values represent the characteristics of a single solder joint per net.

D-C Net ID	I/O Count	Parameters Scaled for I/O Count & Maximum Damage			
		β	η	γ	θ
12	8	2.5	3,610	10	3,620
11	24	2.3	2,110	50	2,160
10	96	2.0	1,080	10	1,090
9	144	1.8	1,420	10	1,430
8	128	1.5	2,030	40	2,070
7	112	1.5	3,250	40	3,290
6	72	1.9	1,330	30	1,360
5	48	2.1	1,640	70	1,710
4	16	1.7	1,070	70	1,140
3	8	1.2	1,470	90	1,560
2	24	1.1	7,370	160	7,530
1	24	2.5	1,570	10	1,580

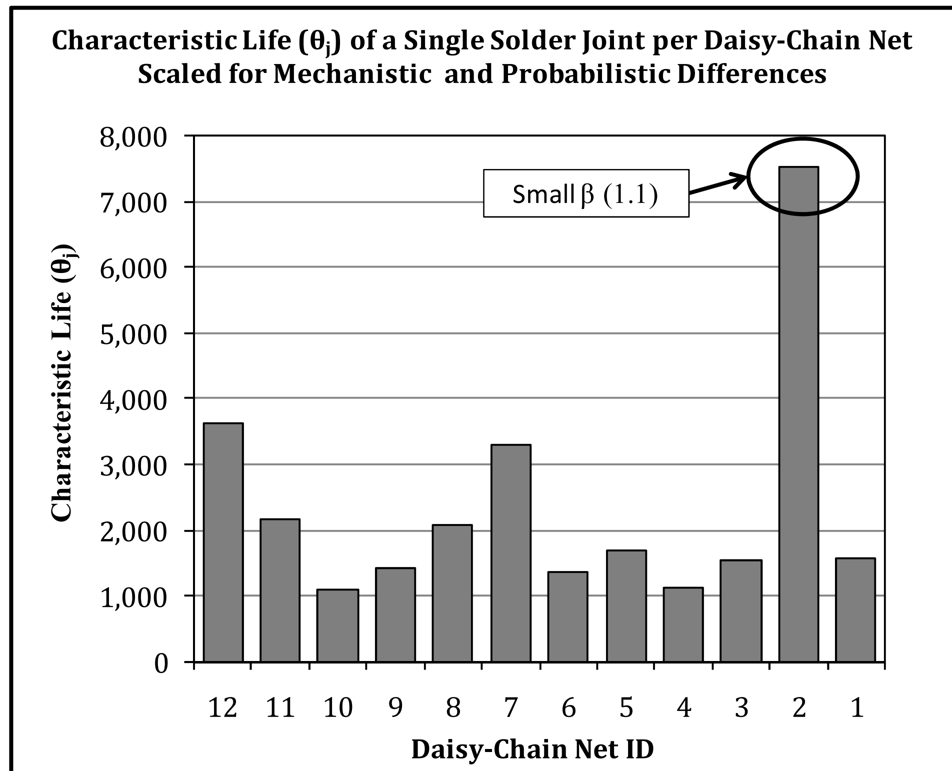

Figure 3-14: comparison of characteristic life (θ_j) estimates for a each solder joint per daisy-chain net, scaled for mechanistic and probabilistic differences per net.

Based on strictly probabilistic effects (varying number of joints per net) an implied mechanistic correction factor can be calculated. This implied mechanistic correction factor is simply the inverse of the ratio of each net's probabilistically scaled characteristic life (θ_{jnet}) divided by that for Net 12 (θ_{j12}); i.e. $\theta_{j12}/\ \theta_{jnet}$. Essentially, this ratio accounts for sample size differences only between each of the test nets. Thus, the difference between these nets should only be mechanistic after scaling. A comparison of E-P predicted and probabilistically implied mechanistic scaling is shown in Figure 3-15; there are large differences between the two factors.

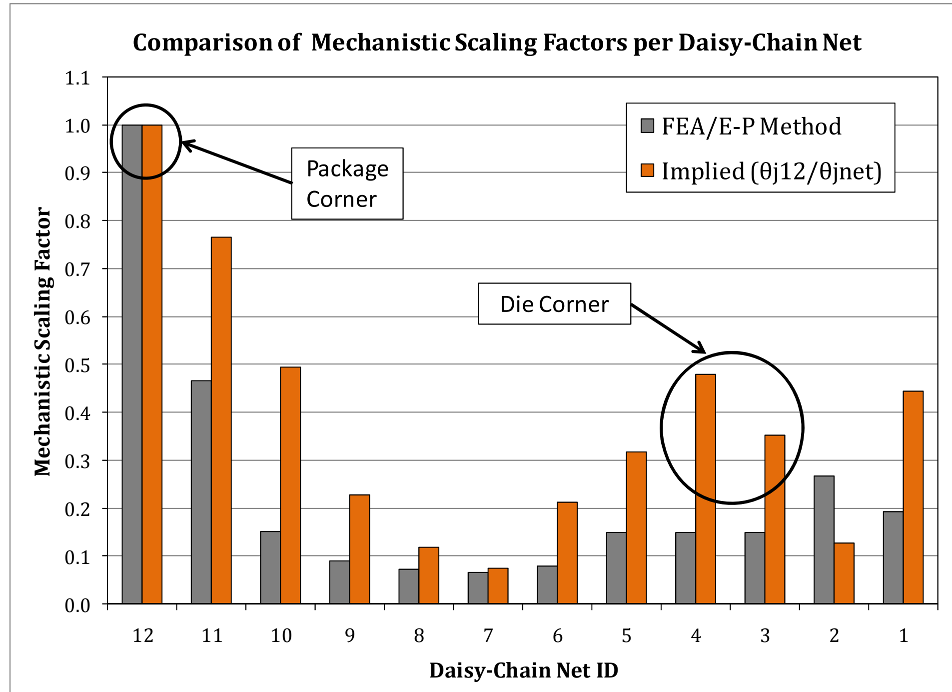

Figure 3-15: comparison of mechanistic scaling factors. The FEA/energy-partitioning (E-P) method is shown based on maximum damage ratios. The probabilistically implied mechanistic scaling factor ($\theta_{j12}/\ \theta_{jnet}$), shown in orange, is the result of subtracting probabilistic effects (difference in number joints per net) from the unscaled test data. The package corner is located in Net 12, and the die-corner shadow is located in Net 3.

3.4 Grouping of Daisy-chain Nets: Simulation of Increasing Critical Region

The goal of this study was to quantify the effect that probabilistic factors have on durability predictions for high-I/O PBGAs. This was done by grouping mechanistically scaled daisy-chain test results in order of decreasing DNP to investigate trends as the number of joints in the critical region increases in components of increasing size. The grouped results were then compared with a series reliability model to assess the validity of the approach.

3.4.1 Grouping of Mechanistically Scaled Thermal Cycling Test Data

The grouping of test results in order of decreasing DNP is only valid for solder joints that experience a common loading (or damage) level. Therefore, the test results were first mechanistically scaled to a common reference damage level; as described in Section 3.2. The scaled failure data for each component were then grouped as follows: As each new net was progressively added to a group, the first failure in the group of nets was treated as the N_f for the group. This grouping technique was applied to all 53 components and all 12 distinct nets. In the event that the first failure for the grouped set was a censored data point (either a known survivor or a known wire failure), the grouped data set N_f was used as a censor data point. Weibull parameters for the 12 distinct grouped sets were performed using rank regression. The Weibull parameters, as well as their correlation coefficients, for the grouped sets are shown in Table 3-8.

Table 3-8: comparison of Weibull parameter estimates for mechanistically scaled and grouped test net data. The thermal cycling test results for each daisy-chain net were grouped in order of decreasing DNP to simulate increasing component size as the number of equivalently loaded joints in the critical region increases.

D-C Group ID	D-C Grp I/O Count	Number of Survivors	Parameters for Mechanistically Scaled and Grouped Test Data				
			β	η	γ	θ	ρ
Net:12	8	2	2.5	1,570	10	1,580	0.992
Nets:12 -11	32	2	2.2	520	50	570	0.979
Nets:12 -10	128	0	2.0	110	10	120	0.989
Nets:12 - 9	272	0	1.7	70	10	80	0.988
Nets:12 - 8	400	0	2.0	60	10	70	0.989
Nets:12 - 7	512	0	2.0	60	10	70	0.989
Nets:12 - 6	584	0	1.7	50	20	70	0.992
Nets:12 - 5	632	0	1.7	50	20	70	0.992
Nets:12 - 4	648	0	1.9	50	20	70	0.990
Nets:12 - 3	656	0	1.9	50	20	70	0.990
Nets:12 - 2	680	1	1.9	50	20	70	0.990
Nets:12 - 1	704	0	1.9	50	20	70	0.990

3.4.2 Series Reliability Model

To verify the accuracy of such an approach, series reliability modeling was used to compare experimental results to reliability theory. For each group, the daisy-chains were modeled as independent units in series; i.e. the failure of one net resulted in the failure of the group. Thus, calculation of the reliability of each distinct group entailed taking the product of the reliability of the mechanistically scaled Weibull distributions of all the nets in the group. For the 3-parameter distribution, the failure-free period of a group set is equal to the minimum γ of the constituent nets. The ensemble scale and shape parameters of the group are easily calculated using graphical methods. Essentially, taking the natural log of Equation (1) twice and rearranging terms generates the simple relationship:

$$\ln\left(-\ln(R(N))\right) = \beta\ln(N - \gamma) - \beta\ln(\eta) \tag{18}$$

Thus, if ln(-ln(R(N)) is plotted on the ordinate and ln(N-γ) on the abscissa, the shape parameter is simply the slope, and the scale parameter is related to the y-intercept by the relationship:

$$\eta = Exp\left(-\frac{b}{\beta}\right);\ \{b = y\ intercept\}. \tag{19}$$

The results of the series model Weibull parameter estimates are shown in Table 3-9. The Weibull parameters for the grouped test data fit the series reliability model quite well.

Table 3-9: comparison of series reliability estimated Weibull parameters for grouped daisy-chain Weibull reliability distributions. The grouped Weibull parameter estimates were calculated using graphical methods. The correlation coefficients (ρ) for the fitted data are also presented.

D-C Group ID	D-C Grp I/O Count	Scaled and Grouped Test Data					Series Reliability Model				
		β	η	γ	θ	ρ	β	η	γ	θ	ρ
Net:12	8	2.5	1,570	10	1,580	0.992	2.5	1,570	10	1,580	1.000
Nets:12 -11	32	2.2	520	50	570	0.979	2.9	560	10	570	0.984
Nets:12 -10	128	2.0	110	10	120	0.989	2.0	110	10	120	1.000
Nets:12 - 9	272	1.7	70	10	80	0.988	1.9	70	10	80	1.000
Nets:12 - 8	400	2.0	60	10	70	0.989	1.9	60	10	70	0.999
Nets:12 - 7	512	2.0	60	10	70	0.989	1.9	50	10	60	0.999
Nets:12 - 6	584	1.7	50	20	70	0.992	1.9	50	10	60	0.998
Nets:12 - 5	632	1.7	50	20	70	0.992	1.9	50	10	60	0.999
Nets:12 - 4	648	1.9	50	20	70	0.990	1.9	50	10	60	0.998
Nets:12 - 3	656	1.9	50	20	70	0.990	1.9	50	10	60	0.998
Nets:12 - 2	680	1.9	50	20	70	0.990	1.9	50	10	60	0.998
Nets:12 - 1	704	1.9	50	20	70	0.990	2.0	50	10	60	0.998

3.4.3 Results: PPoF Correction Factor for Mechanistic Durability Predictions

A plot of Weibull shape parameters estimated for the grouped test data and the series model mechanistically scaled for maximum damage ratios is shown in Figure 3-16. This data set was chosen because the differences between the series model and the test data had the greatest variance. The grouped test data shows that there was a large spread in the CTFs for the grouping of data sets 12-9 and 12-8. However, the spread in β values for the test data, 1.5 to 2.5, is relatively small.

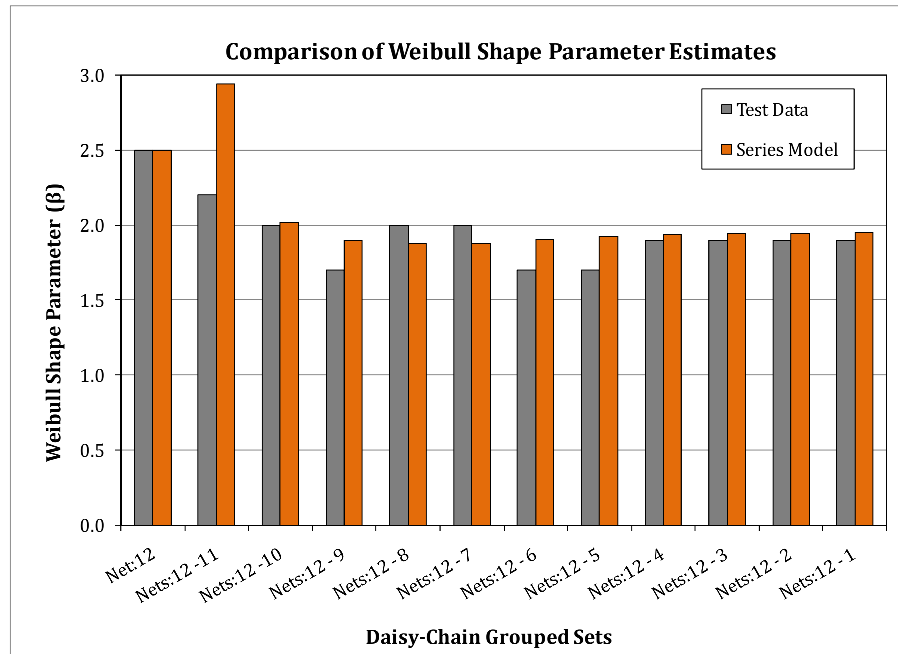

Figure 3-16: comparison of Weibull shape parameter estimates for grouped nets mechanistically scaled to the maximum damage ratios. This data set had the greatest difference in parameter values between the test data and the series model. The grouped test data shows that was a large spread in the CTFs for the grouping of data sets 12-9 and 12-8. However, the spread in β values for the test data, 1.5 to 2.5, is relatively small.

A comparison of characteristic life estimates for the mechanistically scaled grouped (to maximum damage ratios) daisy-chains shows excellent agreement. The characteristic life for each grouped set is shown in Figure 3-17. The test data (grey) and the series reliability model (orange) both show a characteristic life saturation as the number of I/O count increase in the package critical region due to increasing package size.

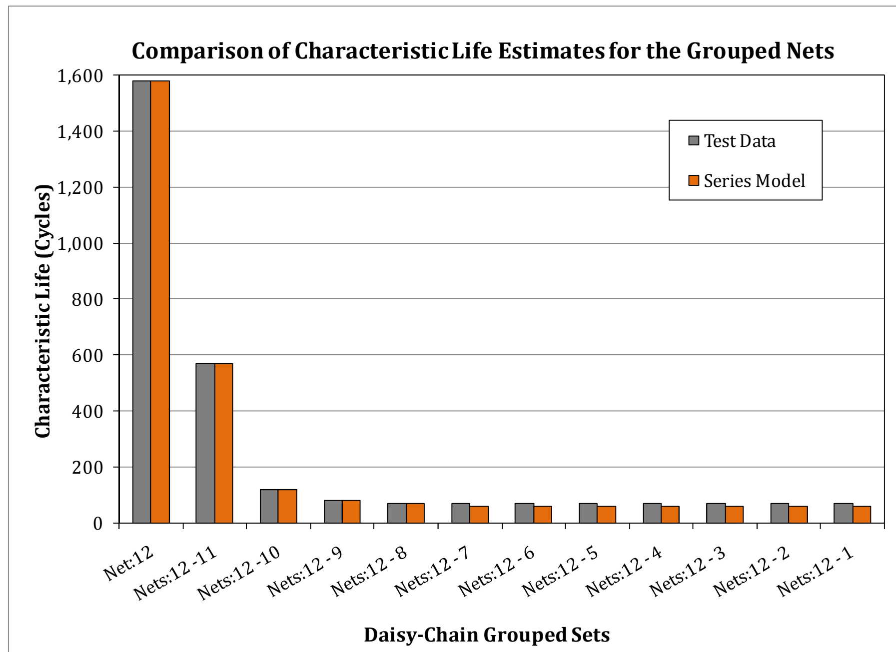

Figure 3-17: comparsion of characteristic life estimates for the mechanistically scaled, to the maximum damage ratio, grouped daisy-chain nets. The grouped test data agrees well with the series reliability model. Additionally, the characteristic life is seen to saturate as the number of I/O in the critical region increases due to increasing size of the component.

The characteristic life estimates of the mechanistically scaled and grouped test data are shown in Figure 3-18 plotted against the number of joints in the package critical region. Estimates for characteristic life are shown for test data scaled to maximum damage ratios. Power laws were fitted to the parameter estimates, and are shown in dashed lines. The scale parameter is seen to drop dramatically as the critical region I/O count increases. A saturation value of approximately 90 is reached when the critical region I/O count reaches approximately 250 (62 joints per quadrant).

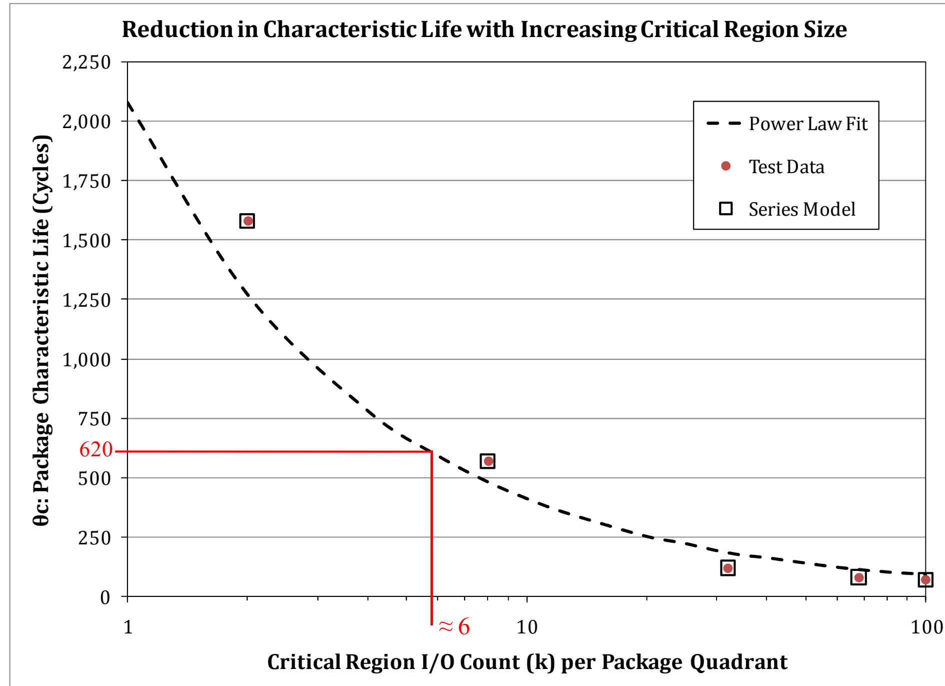

Figure 3-18: comparison of Weibull scale parameter estimates for the mechanistically scaled and grouped test data sets. The data scaled to maximum damage ratios are shown in red circles, the series reliability model estimates are shown in open-face black squares. A power-law was fitted to the test data, and is shown by a black dashed line. Combination of this result with the durability test results of this study (620 thermal cycles to failure) suggest that the manufacturing quality of the tested PBGA1156 is such that it has approx 24 joints in the critical region (6 per quadrant)

A probabilistic de-rating factor was calculated to correct the mechanistic prediction of thermomechanical durability of the solder. The correction factor (θ_c/θ_j) was based on maximum damage ratios for mechanistic scaled and grouped daisy-chain test data, and is shown in Figure 3-19.

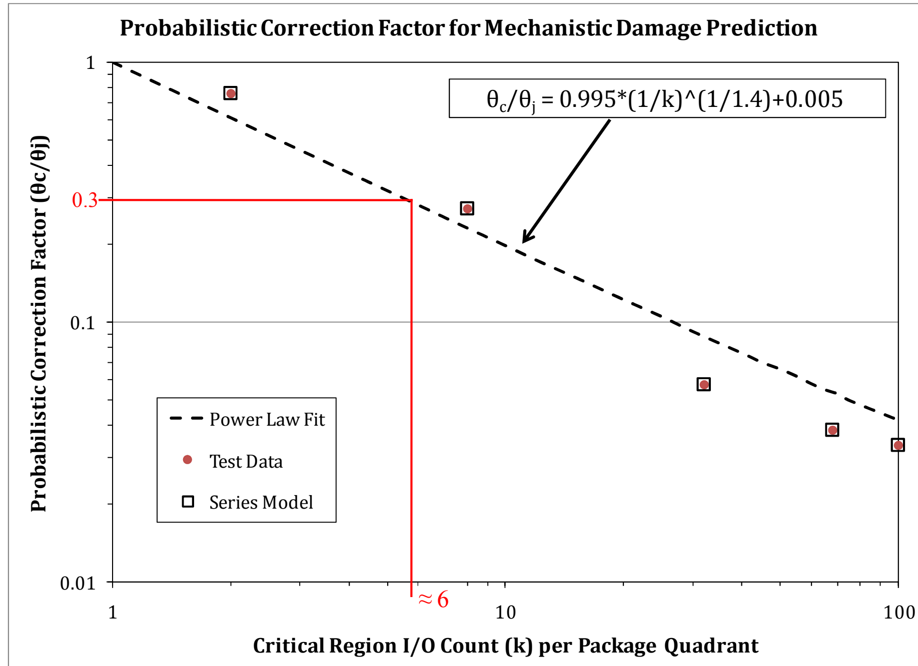

Figure 3-19: probabilistic correction factor for mechanistic predictions of solder characteristic life. Correction factors based on maximum damage ratios for mechanistic scaling of the grouped daisy-chain test data are presented. For large critical region I/O counts in a quadrant of the package (>30) the results suggest that mechanistic predictions could over-predict characteristic life by as much as an order of magnitude. The critical region I/O count per quadrant is the number of highest stressed solder joints at identical load levels for one quadrant of the package.

The correction factor (20) represents the necessary de-rating of the mechanistic prediction of characteristic life based on the worst case solder joint, θ_j, to account for probabilistic effects. The parameter θ_c represents the expected characteristic life of the package.

$$\frac{\theta_c}{\theta_j} = 0.995\left(\frac{1}{\mathrm{k}}\right)^{\frac{1}{1.4}} + 0.005 \tag{20}$$

For large critical region I/O counts (>24 per quadrant) the results suggest that mechanistic predictions could over-predict characteristic life by as much as an order of magnitude. When applying the probabilistic correction factor, the critical region I/O count refers to the number of highest stressed solder joints at identical load levels for one

quadrant of the package. As an example, for the PBGA1156 examined in this study, the number of joints in the critical region is approximately 6, and the corresponding probabilistic correction factor of 0.3 should be applied to the mechanistic predicted characteristic life of the joint with the highest damage (package corner).

The probabilistic correction factor (20) is similar to the modified de-rating factor (12) proposed by Darveaux [12]. A simple series reliability modeling was used to derive (12), assuming that the all solder joints had identical Weibull parameters equal to that of the worst case solder joint. However, the data used to develop Equation (20) in this study, was series summation of dissimilar Weibull distributions with varying shape and scale parameters. Thus, the power-law degradation is greater than that proposed by Darveaux. This is evident in Figure 3-20 where Equation (12) is plotted using a β of 2.1 (average of all grouped test nets) for various values of α. For comparison, the probabilistic correction factor of Equation (20) is also presented in Figure 3-20.

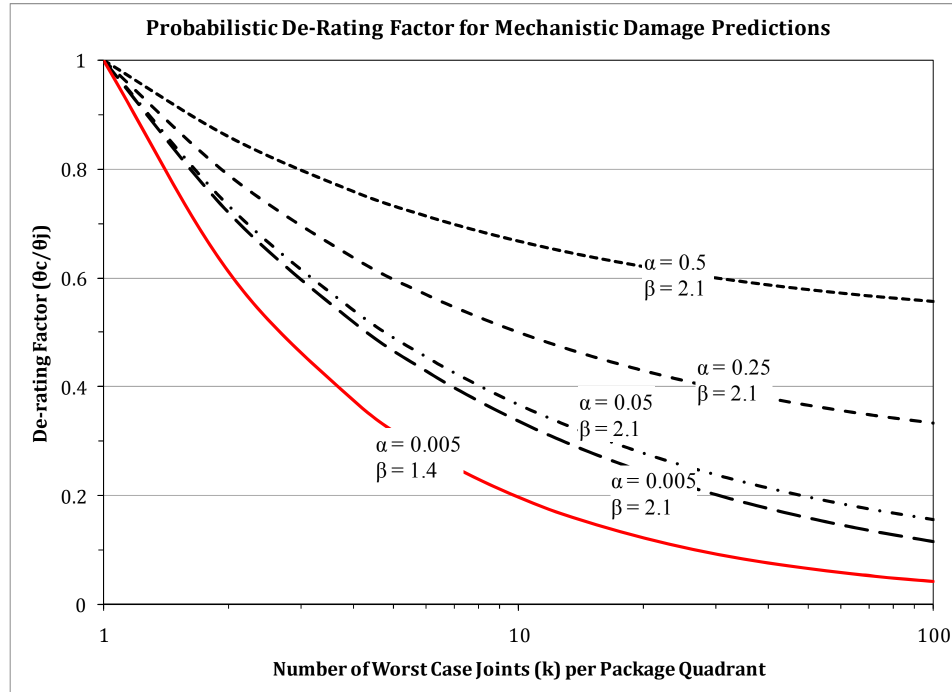

Figure 3-20: comparison of probabilistic de-rating factors for mechanistic predictions of solder damage. The family of curves shown in black dashed lines represents series summations of equivalently stressed solder joints having identical Weibull distributions, with shape parameters β. The parameter α is the ratio of failure-free period to the characteristic life of a single solder joint in each series. The red solid line represents the probabilistic correction factor obtained from mechanistically scaled and grouped test data. The grouped solder joints had equivalent load levels, but dissimilar Weibull parameters.

3.5 Summary and Conclusions

This chapter presented mechanistic and probabilistic scaling of the CTF test data from Chapter 2. The test data were mechanistically scaled to ensure that the failure data for all test nets were scaled to the same reference damage levels, for comparison purposes. Mechanistic scaling factors for the test data were calculated using a combination of 3-D nonlinear FEA and an energy-partitioning fatigue damage model to calculate the average damage in the solder. The damage ratios used for scaling were the maximum damage values found in each of the 12 daisy-chain nets. Wiebull 3-parameter distributions were fitted to the mechanistically scaled daisy-chain net data.

The mechanistically scaled test results were then grouped for all 12 nets in order of decreasing DNP. The 1st net failure of each grouped set in the population was therefore the component N_f for that grouped set Weibull parameters for the grouped sets were estimated using rank regression methods. A series reliability model was used to compare the grouped test data to theory. The series reliability model was the cumulative product of the mechanistically scaled Weibull parameters for each daisy-chain net. The test data parameters were found to fit the series model parameters well.

The Weibull characteristic life asymptotically decreased according to a power-law, as the number of solder joints in the package critical region increased with increasing component size according . For large critical region sizes containing approximately 250 joints (62 joints per quadrant), the characteristic life was found to saturate. Results showed that when the I/O count in the critical region exceeded 24 joints per quadrant, mechanistic (deterministic) predictions could over-predict characteristic life by as much as an order of magnitude.

4 Summary

This chapter presents a summary of the salient features of this thesis, as well as the contributions of this work. Finally, the limitations of this thesis and suggestions for future work are offered.

4.1 Conclusions & Discussions

This thesis quantifies the effect that probabilistic factors have on the durability of high-I/O PBGAs under thermal cycling, through a combination of experimentation and mechanistic modeling. Statistically significant sample lots of 1156 I/O PBGAs were thermally cycled. An innovative daisy-chain design was devised for the test specimens, by partitioning the I/O into 12 independent test nets. The daisy-chain design was instrumental in tracking the progress of interconnect failures in the test population. Weibull statistics were collected for each net and statistics were also collected to identify the location of the first failure in each component. Results showed that the first interconnect failure in each package of the population was predominantly (for almost 72% of all reported failures) located in the middle region of the package, in Nets 10 and 9; rather than at the package corner (Net 12) or die corner (Net 3). Although the solder joints in these nets were not predicted to be the ones with the highest stress levels, these nets happen to be the ones with maximum number of I/O in the net, thus further illustrating the severity of the probabilistic effects.

The test data from these partitioned daisy-chains was then hierarchically grouped in order of increasing DNP, to virtually simulate packages of increasing size and increasing number of solder joints in the critical region. In order to correctly perform this grouping, the failure results were first scaled to a common reference damage level using mrthods

summarized below. Weibull parameters were estimated for the grouped test results. The results provide insight into the change in durability and in the Weibull statistics of the failure data, as I/O count increases in the critical region with increasing package size.

Mechanistic scaling factors, for normalizing the test data to a common damage level, were calculated using a combination of 3-D nonlinear FEA and an energy-partitioning fatigue damage model to calculate the damage density in the critical region of the critical solder joint in each net. Wiebull 3-parameter distributions were fitted to the mechanistically scaled data for each net. A series reliability model was used to account for the effect of the number of joints in each net, and to estimate the change in durability statistics as the number of critical joints grew with increasing package size. This statistical estimate was then compared with the mechanistically scaled and grouped test data. The series reliability model was found to agree well with the grouped test data.

The stochastic degradation in Weibull characteristic life for the grouped data sets was found to have a power-law dependence on the number of critical I/O. The drop in characteristic life for statistical reasons was found to saturate, for approximately 250 joints (62 joints per quadrant) in the critical region of the package. This drop is expressed with a probabilistic de-rating factor that can be used in conjunction with mechanistic durability estimates, to estimate the true durability of large PBGAs. Results showed that for large critical regions with over 200 joints, mechanistic predictions may overpredict the package characteristic life by as much as an order of magnitude. Other similar series models in the literature are shown to under-predict the severity of this probabilistic derating, possibly because the simple models failed to account for the fact that the

process quality is not uniform across all joints possibly worsens as the distance from the package edge increases, in large packages.

4.2 Contributions of Thesis

The major contributions of this thesis are outlined in this section.

- To the authors' knowledge, this is the most systematic and detailed quantitative example in the literature of the relative effects that mechanistic factors and probabilistic factors have on interconnect failures for large I/O PBGAs.

- The randomness of the location of the 1st failure for PBGA interconnects is quantified in detail for the first time, demonstrating that dominant daisy-chain failure sites are half-way between the die corner and the package corner; rather than at the corners, as predicted by mechanistic criteria. The partitioned daisy-chain design used in this study provides the resolution necessary to pinpoint interconnect failure locations in the package.

- This study provided the most quantitative insight to date, into the severity of probabilistic effects on the durability of high-I/O PBGAs. Test data clearly indicate that the Weibull characteristic life reduces by almost an order of magnitude as the number of critical I/O increases to 250.

- A systematic methodology and a comprehensive example are presented for the first time, for developing probabilistic de-rating factors that can be used to correct mechanistic predictions of the characteristic life of large PBGAs under thermal cycling.

4.3 Limitations and Suggestion for Future Work

The following limitations of the current thesis are outlined below, along with suggestions for future work.

4.3.1 Effect of Assembly Quality

The methodology presented in this thesis is applicable to any area-array component. However, the specific mechanistic correction factors presented here are relevant to the PBGA1156 and the probabilistic correction factors presented are applicable to the fabrication quality encountered in this study. The solder defect density is predominantly affected by the process control at the fabrication/assembly house. Therefore, extrapolation of the same probabilistic correction to different assembly lines should be done with care. Future work should include testing PBGAs of different sizes from multiple assembly lines in order to obtain insights about the range for probabilistic correction factors, and their dependence on package size.

4.3.2 Daisy-Chain Design

Great care was taken in selection of the test vehicle daisy-chain design. The design intent was to have all solder joints in a net at approximately the same DNP. However, the design was limited by the package itself. The test component had internal, substrate level, daisy-chains as shown in Figure 2-2. These were laid out in a concentric rectangular pattern. Thus, it was not possible to have all the joints in a net at the same DNP. Additionally, the rectangular die presented a design challenge as it was not known to what effect this asymmetry would affect the joints around the die-shadow. At the time of the daisy-chain design phase there was not a functional FEA model to determine

qualitatively the magnitude of the solder damage levels. Thus, there was no *a priori* knowledge of the large damage gradient between Nets 12, 11 and 10 that was revealed by subsequent FEA. Additionally, not all the solder joints in the package were monitored. It is entirely likely that unmonitored solder joints may have failed before the joints in any test net, thus introducing some uncertainty and approximation in the results of this study. For future studies, it would be ideal to use mechanistic modeling to design and develop a test vehicle without substrate level daisy-chains, as this would allow test designers to better control the grouping of the interconnects, based on better knowledge of which interconnects are at approximately equivalent damage levels. Also, all solder joints in the package should be monitored, as it was observed that the joints at the highest load levels were not necessarily the first to fail in the package.

4.3.3 Thermal Cycling Test Limitations

The thermal cycling testing of the sample population was conducted in unison with a separate study. Due to space limitations in the thermal chamber, access to the test boards for this study was limited. Thus, it was not possible to regularly check the boards for wire failures; introducing uncertainty in the test data. Detailed analysis of the failure data was performed in Section 2.4, and results showed that Nets two and seven had probable wire failures affecting their Weibull parameter estimates. These failures were easy to detect because they were clustered. However, there is also some possibility of other undetected wire failures in other daisy-chains. Therefore, in future work it is essential that the test specimens be checked for wire failures on a regular basis to improve the accuracy of the Weibull parameter estimates of interconnect failure.

4.3.4 FEA Approximations

Mechanistic scaling of the test results could not have been performed without the use of finite elements. The results of these simulations can be dependent upon the mesh density when large gradients are present in the results. Due to the large size of the component that was modeled (289 solder joints in the quarter model), there had to be compromises in the mesh density. The energy-partitioning fatigue damage constants were therefore calibrated based on 10% of the critical solder volume (44 elements) in order to reduce the influence of mesh density on damage calculations. Therefore, the damage calculations for this study are assumed to be representative of the package response. One suggestion for future work would be to perform a study of the sensitivity of the damage estimates on the mesh density.

An additional approximation in the FEA simulations is that the package was unwarped and planar to the board. In reality, during the reflow process PBGA packages may warp. This warpage causes varying pre-stress states in the solder joints which are dependent on the degree of warpage and the DNP of the solder joint. Thus, depending on the degree of warpage the solder joints in the middle of the package may experience greater damage levels and not the joints at the package corner or the die corner.

4.3.5 Determination of Package Critical Region

As mentioned previously, the probabilistic correction factors presented in this study are valid for the fabrication quality of the particular board assemblies used in this study. The piece-to-piece variation in solder defects is clearly going to be a function of the amount of process control. Thus, the package critical region for the same size/type of component could vary depending on the quality of the assembly house. Therefore, in

order to properly use a probabilistic correction factor, it is important for the design engineer to have some working knowledge of the quality capability of the assembly house. For the particular example reported in this study, the data indicated that for this quality and package geometry, the critical region was large enough to contain approximately 6 joints per quadrant. Worst-case assumptions must be used when such quantitative information is not available.

5 Appendices

Appendix A: Thermal Cycling Test Data

The thermal cycling test data is presented in tabular form. State refers to the daisy-chain net status at the end of testing; either F (failure) or S (suspended). The number of cycles to either F or S is located in the second column. The subset identification column indicates the daisy-chain net number, where there is a total of 53 entries per net.

State (F or S)	Cycle to F or S	Subset ID
F	2224	Net:1
F	1627	Net:1
S	2415	Net:1
F	1842	Net:1
S	1209	Net:1
S	2415	Net:1
S	2415	Net:1
F	501	Net:1
F	745	Net:1
S	2415	Net:1
F	1399	Net:1
F	906	Net:1
S	2098	Net:1
F	2141	Net:1
F	1411	Net:1
S	2070	Net:1
F	2208	Net:1
F	2376	Net:1
F	1976	Net:1
S	2415	Net:1
F	1173	Net:1
S	2415	Net:1
F	1726	Net:1
F	2171	Net:1
F	2196	Net:1
S	2415	Net:1
S	2415	Net:1
S	2415	Net:1
S	1407	Net:1
S	2415	Net:1
F	1635	Net:1
F	729	Net:1
F	1586	Net:1
S	2415	Net:1
F	1231	Net:1
F	2209	Net:1
F	1424	Net:1
F	1916	Net:1
S	938	Net:1
F	2071	Net:1
F	562	Net:1
F	1143	Net:1
S	2398	Net:1
S	2392	Net:1
F	1123	Net:1
F	2162	Net:1
F	1574	Net:1
F	2312	Net:1
F	1269	Net:1
F	1740	Net:1
F	2034	Net:1
F	1171	Net:1
F	1786	Net:1
F	1394	Net:2
F	2099	Net:2
F	1239	Net:2
F	1248	Net:2
S	1209	Net:2
F	707	Net:2
F	983	Net:2
S	512	Net:2
S	512	Net:2
F	1188	Net:2
F	1627	Net:2
F	1154	Net:2
F	766	Net:2
S	2415	Net:2
F	793	Net:2
F	1110	Net:2
S	2415	Net:2
F	900	Net:2
S	2415	Net:2
F	2216	Net:2
S	1181	Net:2
S	2415	Net:2
F	680	Net:2
F	2185	Net:2
S	2415	Net:2
F	1039	Net:2
S	501	Net:2
S	2415	Net:2
S	1407	Net:2
F	1742	Net:2
F	1976	Net:2
F	2051	Net:2
F	1981	Net:2
S	2415	Net:2
F	1608	Net:2
S	501	Net:2

F	647	Net:2
F	1526	Net:2
S	938	Net:2
F	2199	Net:2
F	2265	Net:2
S	1199	Net:2
F	2397	Net:2
F	2346	Net:2
F	990	Net:2
S	2415	Net:2
S	2415	Net:2
S	2415	Net:2
F	1405	Net:2
F	759	Net:2
F	1011	Net:2
F	1531	Net:2
F	1161	Net:2
S	2415	Net:3
F	1457	Net:3
S	2415	Net:3
F	2311	Net:3
S	1209	Net:3
S	2415	Net:3
F	1322	Net:3
F	706	Net:3
F	938	Net:3
F	1455	Net:3
F	1063	Net:3
S	1155	Net:3
F	1778	Net:3
F	1639	Net:3
F	2113	Net:3
S	2070	Net:3
S	2415	Net:3
F	1194	Net:3
S	2415	Net:3
F	2054	Net:3
S	1181	Net:3

S	2415	Net:3
S	2415	Net:3
F	1844	Net:3
S	2415	Net:3
F	813	Net:3
F	877	Net:3
F	951	Net:3
S	1407	Net:3
F	1810	Net:3
F	1953	Net:3
F	2151	Net:3
S	2415	Net:3
S	2415	Net:3
F	2090	Net:3
F	1851	Net:3
F	1974	Net:3
F	2196	Net:3
F	646	Net:3
F	2211	Net:3
F	783	Net:3
F	937	Net:3
F	1766	Net:3
F	2352	Net:3
F	1154	Net:3
F	2396	Net:3
F	2210	Net:3
F	1509	Net:3
S	1572	Net:3
F	838	Net:3
F	1816	Net:3
F	1470	Net:3
F	796	Net:3
F	1319	Net:4
F	1251	Net:4
S	2415	Net:4
F	1509	Net:4
F	1016	Net:4
F	875	Net:4

F	605	Net:4
F	758	Net:4
F	647	Net:4
F	981	Net:4
F	1632	Net:4
S	1155	Net:4
S	2098	Net:4
F	2166	Net:4
F	1021	Net:4
F	1425	Net:4
F	1792	Net:4
F	1100	Net:4
S	2415	Net:4
F	1263	Net:4
S	1181	Net:4
S	2415	Net:4
F	823	Net:4
F	2154	Net:4
S	2415	Net:4
F	1995	Net:4
F	1142	Net:4
F	1926	Net:4
S	1407	Net:4
F	1461	Net:4
F	1993	Net:4
F	1035	Net:4
F	1959	Net:4
F	1801	Net:4
F	812	Net:4
F	1714	Net:4
F	1982	Net:4
F	1204	Net:4
S	938	Net:4
F	1171	Net:4
F	2147	Net:4
F	1144	Net:4
S	2398	Net:4
S	2392	Net:4

F	1697	Net:4
F	2091	Net:4
S	2415	Net:4
F	2068	Net:4
F	1213	Net:4
F	1621	Net:4
S	2094	Net:4
F	1531	Net:4
F	1244	Net:4
F	1921	Net:5
S	2415	Net:5
F	1258	Net:5
F	2223	Net:5
S	1209	Net:5
F	1151	Net:5
F	1438	Net:5
S	800	Net:5
F	1017	Net:5
F	1241	Net:5
F	1554	Net:5
S	1155	Net:5
S	2098	Net:5
F	2214	Net:5
F	2048	Net:5
S	2070	Net:5
F	1324	Net:5
F	1518	Net:5
S	2415	Net:5
F	2085	Net:5
S	1181	Net:5
S	2415	Net:5
F	681	Net:5
S	2184	Net:5
S	2415	Net:5
S	2415	Net:5
F	2351	Net:5
S	2415	Net:5
S	1407	Net:5

F	1448	Net:5
F	977	Net:5
F	1537	Net:5
S	2415	Net:5
F	1944	Net:5
F	904	Net:5
F	1989	Net:5
F	1721	Net:5
F	1319	Net:5
S	938	Net:5
F	2183	Net:5
F	2378	Net:5
S	1199	Net:5
S	2398	Net:5
S	2392	Net:5
F	1144	Net:5
S	2415	Net:5
F	1608	Net:5
S	2415	Net:5
F	1522	Net:5
F	2000	Net:5
F	1873	Net:5
F	1329	Net:5
F	1424	Net:5
S	2415	Net:6
F	710	Net:6
F	1225	Net:6
F	1821	Net:6
S	1209	Net:6
F	1998	Net:6
S	2415	Net:6
S	800	Net:6
F	1023	Net:6
F	1472	Net:6
F	1225	Net:6
F	1112	Net:6
S	2098	Net:6
F	2309	Net:6

F	1135	Net:6
F	1755	Net:6
F	1976	Net:6
F	887	Net:6
S	2415	Net:6
F	2163	Net:6
S	1181	Net:6
S	2415	Net:6
F	2323	Net:6
S	2184	Net:6
S	2415	Net:6
F	951	Net:6
F	1512	Net:6
S	2415	Net:6
S	1407	Net:6
F	1348	Net:6
F	1990	Net:6
F	1509	Net:6
S	2415	Net:6
F	1080	Net:6
F	1445	Net:6
F	2191	Net:6
F	647	Net:6
F	608	Net:6
S	938	Net:6
F	1829	Net:6
F	1231	Net:6
S	1199	Net:6
S	2398	Net:6
S	2392	Net:6
S	2415	Net:6
F	1474	Net:6
F	1041	Net:6
S	2415	Net:6
S	1572	Net:6
F	1752	Net:6
F	2052	Net:6
F	1530	Net:6

F	1735	Net:6
S	2415	Net:7
S	2415	Net:7
F	1509	Net:7
S	2415	Net:7
S	1209	Net:7
S	2415	Net:7
F	1969	Net:7
S	800	Net:7
S	1035	Net:7
F	2353	Net:7
F	851	Net:7
F	780	Net:7
F	2087	Net:7
F	2169	Net:7
S	1077	Net:7
S	1071	Net:7
S	2415	Net:7
F	1319	Net:7
F	1593	Net:7
S	2415	Net:7
S	1181	Net:7
S	2415	Net:7
S	2415	Net:7
S	2184	Net:7
F	2113	Net:7
S	1046	Net:7
F	1492	Net:7
F	1099	Net:7
S	1407	Net:7
F	1800	Net:7
S	1032	Net:7
S	2415	Net:7
F	2085	Net:7
S	2415	Net:7
F	2157	Net:7
F	938	Net:7
F	2001	Net:7

F	975	Net:7
S	938	Net:7
F	1426	Net:7
S	1046	Net:7
S	1199	Net:7
F	1238	Net:7
F	2255	Net:7
S	2415	Net:7
S	2415	Net:7
S	2415	Net:7
S	2415	Net:7
S	1572	Net:7
F	1655	Net:7
S	2094	Net:7
F	1088	Net:7
S	1048	Net:7
F	1249	Net:8
F	2327	Net:8
F	1186	Net:8
F	1524	Net:8
S	1209	Net:8
F	2208	Net:8
S	2415	Net:8
S	800	Net:8
F	1034	Net:8
F	2020	Net:8
F	1068	Net:8
F	1685	Net:8
F	2053	Net:8
F	2327	Net:8
F	1898	Net:8
F	619	Net:8
F	1802	Net:8
F	1000	Net:8
S	2415	Net:8
F	1673	Net:8
F	1138	Net:8
F	857	Net:8

F	1146	Net:8
F	2173	Net:8
F	1945	Net:8
F	1779	Net:8
F	1628	Net:8
F	1046	Net:8
F	1013	Net:8
F	1329	Net:8
F	1815	Net:8
F	707	Net:8
F	2171	Net:8
F	1319	Net:8
F	1262	Net:8
F	2171	Net:8
F	1083	Net:8
F	1405	Net:8
S	938	Net:8
F	652	Net:8
F	849	Net:8
F	855	Net:8
S	2415	Net:8
S	2415	Net:8
F	2256	Net:8
F	639	Net:8
F	1336	Net:8
F	1098	Net:8
F	1584	Net:8
F	1043	Net:8
F	1324	Net:8
F	1470	Net:8
F	718	Net:8
F	1511	Net:9
F	1704	Net:9
F	1580	Net:9
F	1685	Net:9
F	782	Net:9
F	783	Net:9
F	1740	Net:9

S	800	Net:9
F	1153	Net:9
F	1520	Net:9
F	671	Net:9
F	614	Net:9
F	1111	Net:9
F	1339	Net:9
F	1386	Net:9
F	1207	Net:9
F	983	Net:9
F	899	Net:9
F	275	Net:9
F	1156	Net:9
F	888	Net:9
F	1690	Net:9
F	262	Net:9
F	1008	Net:9
F	1752	Net:9
F	1011	Net:9
F	334	Net:9
F	346	Net:9
F	1057	Net:9
F	662	Net:9
F	653	Net:9
F	531	Net:9
F	1263	Net:9
F	504	Net:9
F	929	Net:9
F	353	Net:9
F	1364	Net:9
F	951	Net:9
F	510	Net:9
F	710	Net:9
F	976	Net:9
S	1199	Net:9
F	1469	Net:9
F	520	Net:9
F	775	Net:9

F	1009	Net:9
F	976	Net:9
F	472	Net:9
F	322	Net:9
F	461	Net:9
F	1783	Net:9
F	1341	Net:9
F	1087	Net:9
F	911	Net:10
F	650	Net:10
F	1007	Net:10
F	1400	Net:10
F	1117	Net:10
F	840	Net:10
F	1394	Net:10
F	680	Net:10
F	500	Net:10
F	553	Net:10
F	404	Net:10
F	697	Net:10
F	371	Net:10
F	1166	Net:10
F	529	Net:10
F	511	Net:10
F	809	Net:10
F	802	Net:10
F	1835	Net:10
F	758	Net:10
F	999	Net:10
F	1013	Net:10
F	505	Net:10
F	397	Net:10
F	521	Net:10
F	661	Net:10
F	361	Net:10
F	1013	Net:10
F	900	Net:10
F	616	Net:10

F	822	Net:10
F	444	Net:10
F	745	Net:10
F	800	Net:10
F	797	Net:10
F	681	Net:10
F	706	Net:10
F	445	Net:10
F	507	Net:10
F	786	Net:10
F	172	Net:10
F	687	Net:10
F	1345	Net:10
F	421	Net:10
F	604	Net:10
F	244	Net:10
F	528	Net:10
F	421	Net:10
F	1115	Net:10
F	1519	Net:10
F	187	Net:10
F	943	Net:10
F	423	Net:10
F	1579	Net:11
F	2287	Net:11
F	1098	Net:11
F	1387	Net:11
S	1209	Net:11
F	735	Net:11
F	905	Net:11
F	940	Net:11
F	636	Net:11
F	1951	Net:11
F	1177	Net:11
F	1432	Net:11
F	824	Net:11
F	615	Net:11
F	1885	Net:11

F	925	Net:11
F	682	Net:11
F	858	Net:11
F	1618	Net:11
F	1334	Net:11
F	1723	Net:11
F	1723	Net:11
F	1789	Net:11
F	858	Net:11
F	1718	Net:11
F	836	Net:11
F	911	Net:11
F	1158	Net:11
S	1407	Net:11
F	650	Net:11
F	1586	Net:11
F	1448	Net:11
F	1617	Net:11
F	847	Net:11
F	1679	Net:11
F	728	Net:11
F	737	Net:11
F	820	Net:11
F	749	Net:11
F	1211	Net:11
F	501	Net:11
F	233	Net:11
F	938	Net:11
F	444	Net:11
F	736	Net:11
F	1237	Net:11

F	740	Net:11
F	529	Net:11
F	1016	Net:11
F	998	Net:11
F	1013	Net:11
F	1509	Net:11
F	851	Net:11
F	1384	Net:12
F	1514	Net:12
F	1194	Net:12
F	597	Net:12
S	2415	Net:12
F	1857	Net:12
F	1236	Net:12
F	1403	Net:12
F	1249	Net:12
F	1698	Net:12
F	542	Net:12
F	913	Net:12
F	1907	Net:12
F	1378	Net:12
F	2159	Net:12
F	971	Net:12
F	1139	Net:12
F	788	Net:12
F	950	Net:12
F	1763	Net:12
F	2116	Net:12
F	1061	Net:12
F	859	Net:12
F	558	Net:12

F	2351	Net:12
F	900	Net:12
F	1940	Net:12
F	1440	Net:12
S	1407	Net:12
F	2131	Net:12
F	1587	Net:12
F	820	Net:12
F	1613	Net:12
F	1876	Net:12
F	983	Net:12
F	2032	Net:12
F	1198	Net:12
F	821	Net:12
F	712	Net:12
F	1624	Net:12
F	667	Net:12
F	822	Net:12
F	1663	Net:12
F	1757	Net:12
F	2104	Net:12
F	2322	Net:12
F	2229	Net:12
F	602	Net:12
F	268	Net:12
F	1901	Net:12
F	1331	Net:12
F	1531	Net:12
F	1202	Net:12

Appendix B: Failure Monitoring Program

The MATLAB code used to extract the failure times and state for each daisy-chain net of each component is listed below. The program was run approximately daily for the datalogger output files. The program reads in the csv files and finds whether any channels have a 20% increase in resistance value occurring for at least 10 consecutive cycles. If this happens, the channel is recorded as a failure. All failures and suspensions are recorded in a new excel output file.

```
“'C08-28 Test Results”.
clear all
close all
%---- Daily Failure Log Import -----
dname = uigetdir('C:\'); %set directory base to C drive
cd(dname) %change direct to C drive
%File Selection Box for obtaining Daily Failure Record XL file
[xlfilename, xlpathname] = uigetfile({'*.xls','Excel File
(*.xls)'},...
  'Pick Daily Failure Log',...
  'C08-28 Test Data Summary.xls');
%Create Message Box to Alert User that Program is Working
h = msgbox({'Please Wait Reading File...',...
  char({[xlpathname,xlfilename]})},'Reading Failure Summary
File',...
  'help');
%Read in Summary sheet from Failure Log
[Data, Text] = xlsread(char({[xlpathname,xlfilename]}),...
  'Summary Data');
%Find total cycle count
TotCycleCt = Data(1,2);
%Obtain Failures (0 or 1)
Fail_Y_N = Data(4:end,7);
%Obtain Cycles to Failure
FailureInfo = Data(4:end,8);
%Get date of failure
FailDate = Text(6:end,9);
%Find Date of Last Data entry
TestDate = Text(2,2);
close(h) %closes Alert message box
%---- END: Daily Failure Log Import -----
%---- Compilation of Test Data Nets ----
%Finds # of Channels
Channel = length(FailureInfo);
%Find # of Components (# channels/# Nets)
CompTot = Channel/12;
%vector of # joints/net (nets are 1-12)
jointct = [24 24 8 16 48 72 112 128 144 96 24 8];
jointct = transpose(jointct);
%Damage ratios Dnet/D12 (nets 1-12)
%-max values-
dratio = [1 0.460 0.153 0.091 0.072 0.067 0.080 0.148 ...
  0.150 0.150 0.267 0.192];
dratio = fliplr(dratio);
%Sort failure data by component and net
%create empty matrix (12nets, #comps)
Net_Raw_Nf = zeros(12,CompTot);
Net_censor = zeros(12,CompTot);
Net_Raw_Nf_date = cell(12,CompTot);
censor_type = zeros(12,2);
for j = 1:12
  for i = 1:CompTot
  %Unscaled failure data cycle count per comp per net
  Net_Raw_Nf(j,i) = FailureInfo(j+(i-1)*12);
  %Location of censored data per comp per net (survivor & wire
fail)
  Net_censor(j,i) = Fail_Y_N(j+(i-1)*12);
  %Unscaled failure data date and time per comp per net
  Net_Raw_Nf_date(j,i) = FailDate(j+(i-1)*12);
  end
  %# of surviving components per net
  censor_type(j,1) = size(find(Net_Raw_Nf(j,:) == 0),2);
  %# of Wire failures per net
  censor_type(j,2) = size(find(Net_censor(j,:) == 0),2)-
censor_type(j,1);
end
%transpose sorted data
Net_Raw_Nf = transpose(Net_Raw_Nf);
Net_censor = transpose(Net_censor);
Net_Raw_Nf_date = transpose(Net_Raw_Nf_date);
%Create cell array for raw net data export
NetRawExport = cell(CompTot,3,12);
for i = 1:12
  %Make default state for failure = F
  NetRawExport(:,1,i) = {'F'};
  %Add net addition IDs to cell array
  NetRawExport(:,3,i) = {['Net:',num2str(i)]};
end
%Find any non-failed channels & make cycle count = max
%find nonfailed data indices
if any(any(Net_Raw_Nf == 0))
  %find nonfailed data indices
  [rows,cols] = find(Net_Raw_Nf == 0);
  for i = 1:length(rows)
    %Replace cycle ct of 0 w/ total # cycles
    Net_Raw_Nf(rows(i),cols(i)) = TotCycleCt;
  end
end
%Create data censoring matrix for right censored data
Net_censor = 1 - Net_censor;
%Find any non-failed channels
if any(any(Net_censor == 1))
  %find nonfailed data indices
  [rows,cols] = find(Net_censor == 1);
  for i = 1:length(rows)
    %Make failure state = to S
    NetRawExport(rows(i),1,cols(i)) = {'S'};
  end
end
%_______________________________________________
%Mechanistically Normalized Nf
Net_Mech_Nf = ones(CompTot,1)*(dratio).*Net_Raw_Nf;
%Compute Weibull 2-parameters for net data
Wbl_net_raw = zeros(12,2);
Wbl_net_mech = Wbl_net_raw;
CI_net_raw = zeros(2,2,12);
CI_net_mech = CI_net_raw;
for i = 1:12
  %Calculate Weibull params & 95% CI for net data
  [Wbl_net_raw(i,:),CI_net_raw(:,:,i)] =
wblfit(Net_Raw_Nf(:,i),[],...
    Net_censor(:,i));
  [Wbl_net_mech(i,:),CI_net_mech(:,:,i)] =
wblfit(Net_Mech_Nf(:,i),...
```

```
    [],Net_censor(:,i));
end
%Create matrices for CI export
for i=1:12
  CI_eta_net_raw(i,:) = transpose(CI_net_raw(:,1,i));
  CI_eta_net_mech(i,:) = transpose(CI_net_mech(:,1,i));
  CI_beta_net_raw(i,:) = transpose(CI_net_raw(:,2,i));
  CI_beta_net_mech(i,:) = transpose(CI_net_mech(:,2,i));
end

%Create cell array for mech normalized data export
NetMechExport = NetRawExport;
%Insert censored raw Nf into net data
NetRawExport(:,2,:) = num2cell(Net_Raw_Nf);
%Insert censored mech Nf into net data
NetMechExport(:,2,:) = num2cell(Net_Mech_Nf);
%___________________________________________
%Find which nets have 1st failure
Fail1st = cell(CompTot,3);
for i = 1:CompTot
  %find uncensored data
  col = find(Net_censor(i,:)==0);
  if length(col) > 0
    for j = 1:length(col)
      uncensored_Nf = (min(Net_Raw_Nf(i,col)));
      loc = (find(Net_Raw_Nf(i,:) == uncensored_Nf));
      Fail1st(i,2) = {uncensored_Nf};
      Fail1st(i,1) = {loc(1)};
      Fail1st(i,3) = Net_Raw_Nf_date(i,loc(1));
    end
  %If no uncensored data exists for component then NaN
  else
    Fail1st(i,:) = {NaN, NaN, NaN};
  end
end
%________________________________________________
%Create DNP grouped data
GrpOrder = [12 11 10 9 8 7 6 5 4 3 2 1];
%# of grouped Nets
GrpCombos = length(GrpOrder);
%Create empty arrays and matrices
NetRaw = zeros(CompTot,GrpCombos);
NetMech = zeros(CompTot,GrpCombos);
GrpIO = zeros(size(1:GrpCombos));
Censor_sort = zeros(CompTot,GrpCombos);
Grp_Raw_censor = Censor_sort;
Grp_Mech_censor = Censor_sort;
for i = 1:GrpCombos
  %sort raw failure data to match order
  NetRaw(:,i) = Net_Raw_Nf(:,GrpOrder(i));
  %sort mech norm failure data to match order
  NetMech(:,i) = Net_Mech_Nf(:,GrpOrder(i));
  %sort # of joints to match order
  GrpIO(i) = jointct(GrpOrder(i));
  %sort right censored data to match order
  Censor_sort(:,i) = Net_censor(:,GrpOrder(i));
end
%make joint count cum sum
GrpIO = cumsum(GrpIO);
%create empty matrix (#components, #combo-nets)
Grp_Raw_Nf = zeros(CompTot,GrpCombos);
Grp_Mech_Nf = Grp_Raw_Nf;
%Create compiled net IDs
GrpTags = cell(1,GrpCombos);
%Create cell array for net addition export
GrpRawExport = cell(CompTot,3,GrpCombos);

%Compile net failure data by grouping failures
%--Group1: Net 12--
Grp_Raw_Nf(:,1) = NetRaw(:,1);
Grp_Mech_Nf(:,1) = NetMech(:,1);
Grp_Raw_censor(:,1) = Censor_sort(:,1);
Grp_Mech_censor(:,1) = Censor_sort(:,1);
%Make default state for failure = F
GrpRawExport(:,1,1) = {'F'};
%Tag Nf data w/ grouped net IDs
GrpRawExport(:,3,1) = {['Net:',int2str(GrpOrder(1))]};
%--Groups 2-12--
for j = 2:GrpCombos
  %change grouped data values to have NaN for surviving
channels
  for i = 1:CompTot
    Grp_Raw_Nf(i,j) = transpose(min(transpose(NetRaw(i,1:j))));
    col = find(NetRaw(i,1:j) == Grp_Raw_Nf(i,j));
    Grp_Raw_censor(i,j) = Censor_sort(i,col(1,1));
    Grp_Mech_Nf(i,j) =
transpose(min(transpose(NetMech(i,1:j))));
    col = find(NetMech(i,1:j) == Grp_Mech_Nf(i,j));
    Grp_Mech_censor(i,j) = Censor_sort(i,col(1,1));
  end
  %Make default state for failure = F
  GrpRawExport(:,1,j) = {'F'};
  %Tag Nf data w/ grouped net IDs
  GrpTags(j) = {['Nets:',int2str(GrpOrder(1)),'-
',int2str(GrpOrder(j))]};
  GrpRawExport(:,3,j) = GrpTags(j);
end
%Create cell array for normalized data
GrpMechExport = GrpRawExport;
%Insert Failure cycle count into net addition cells
GrpRawExport(:,2,:) = num2cell(Grp_Raw_Nf);
GrpMechExport(:,2,:) = num2cell(Grp_Mech_Nf);

%Check to see if any raw grouped channels not failed
if any(any(Grp_Raw_censor==1))
  %find location of non-Failures (rows,cols)
  [rows,cols] = find(Grp_Raw_censor==1);
  for i = 1:length(rows)
    %Make failure state = to S
    GrpRawExport(rows(i),1,cols(i)) = {'S'};
  end
end
%Check to see if any mech normalized grouped channels not
failed
if any(any(Grp_Mech_censor==1))
  %find location of non-Failures (rows,cols)
  [rows,cols] = find(Grp_Mech_censor==1);
  for i = 1:length(rows)
    %Make failure state = to S
    GrpMechExport(rows(i),1,cols(i)) = {'S'};
  end
end

%Compute Weibull 2-parameters for grouped data
Wbl_Grp_raw = zeros(GrpCombos,2);
Wbl_Grp_mech = Wbl_Grp_raw;
CI_Grp_raw = zeros(2,2,GrpCombos);
CI_Grp_mech = CI_Grp_raw;
for i = 1:GrpCombos
  %Calculate Weibull params & 95% CI for net data
  [Wbl_Grp_raw(i,:),CI_Grp_raw(:,:,i)] =
wblfit(Grp_Raw_Nf(:,i),[],...
    Grp_Raw_censor(:,i));
  [Wbl_Grp_mech(i,:),CI_Grp_mech(:,:,i)] =
wblfit(Grp_Mech_Nf(:,i),...
    [],Grp_Mech_censor(:,i));
end
%Create matrices for CI export
for i=1:GrpCombos
  CI_eta_grp_raw(i,:) = transpose(CI_Grp_raw(:,1,i));
```

```
  CI_eta_grp_mech(i,:) = transpose(CI_Grp_mech(:,1,i));
  CI_beta_grp_raw(i,:) = transpose(CI_Grp_raw(:,2,i));
  CI_beta_grp_mech(i,:) = transpose(CI_Grp_mech(:,2,i));
end
%_____________________________________________________
%--Write Summary Data to "CO8-28 Test Results.xls"--
%create header row for net counts
nethead = {'State (F or S)','Cycle to F or S','Subset ID'};

%EXCEL file name for DATA
xlname = 'C08-28 Test Results';

% %Create Excel worksheet for single net data
Giant = [TestDate,{'',''}; nethead; NetRawExport(:,:,1)];
for i = 2:12
  Giant = [Giant; NetRawExport(:,:,i)];
end
xlswrite(char({[xlpathname,xlname]}),Giant,'Net Raw','A1')

%Create Excel worksheet for Mech normalized single net data
Giant = [TestDate,{'',''}; nethead; NetMechExport(:,:,1)];
for i = 2:12
  Giant = [Giant; NetMechExport(:,:,i)];
end
xlswrite(char({[xlpathname,xlname]}),Giant,'Net Mech','A1')

%Create Excel worksheet for DNP compiled net data
Giant = [TestDate,{'',''}; nethead; GrpRawExport(:,:,1)];
for i = 2:GrpCombos
  Giant = [Giant; GrpRawExport(:,:,i)];
end
xlswrite(char({[xlpathname,xlname]}),Giant,'Grp Raw','A1')

%Create Excel worksheet for Normalized DNP compiled net
data
Giant = [TestDate,{'',''}; nethead; GrpMechExport(:,:,1)];
for i = 2:GrpCombos
  Giant = [Giant; GrpMechExport(:,:,i)];
end
xlswrite(char({[xlpathname,xlname]}),Giant,'Grp Mech','A1')
```

```
%Create 1st failure sheet
xlswrite(char({[xlpathname,xlname]}),...
  [[{'Summary of 1st Component Failure',''},TestDate];...
  {'Net #','Cycle #','Fail Date'}; Fail1st],...
  '1st Failure','A1')

%Create single net data summary sheet
xlswrite(char({[xlpathname,xlname]}),...
  [TestDate,{'','','','','','','','','','','','','','',''};...
  {'','','','','Net Raw','','','','','','Net Mech','','','','',''};...
  {'Net #','I/O Count','Survivors','Wire Failures',...
  'eta Raw','eta lo CI','eta up CI',...
  'beta Raw','beta lo CI','beta up CI',...
  'eta Mech','eta lo CI','eta up CI',...
  'beta Mech','beta lo CI','beta up CI',};...
  flipud(num2cell([transpose(1:1:12),jointct,censor_type,...
  Wbl_net_raw(:,1),CI_eta_net_raw,...
  Wbl_net_raw(:,2),CI_beta_net_raw,...
  Wbl_net_mech(:,1),CI_eta_net_mech,...
  Wbl_net_mech(:,2),CI_beta_net_mech]))],...
  'Net Summary','A1')

%Create grouped net data summary sheet
xlswrite(char({[xlpathname,xlname]}),...
  [TestDate,{'','','','','','','','','','','','',''};...
  {'','','Grp Raw','','','','','','Grp Mech','','','','',''};...
  {'Grp #','I/O Count',...
  'eta Raw','eta lo CI','eta up CI',...
  'beta Raw','beta lo CI','beta up CI',...
  'eta Mech','eta lo CI','eta up CI',...
  'beta Mech','beta lo CI','beta up CI',};...
  transpose(GrpTags),num2cell([transpose(GrpIO),...
  Wbl_Grp_raw(:,1),CI_eta_grp_raw,...
  Wbl_Grp_raw(:,2),CI_beta_grp_raw,...
  Wbl_Grp_mech(:,1),CI_eta_grp_mech,...
  Wbl_Grp_mech(:,2),CI_beta_grp_mech])],...
  'Grp Summary','A1')

h = helpdlg('Run Has Completed','Process Status');
```

Appendix C: FEA Preprocessing and Solution Input File

```
/PREP7    !preprocessor
/TITLE,     PBGA1156

!___Element Types & Keyopts___
ET,         1,          solid45 !--- Non-solder Vol
ET,         2,          solid185 !--- Solder Vol
KEYOPT, 2,          2,          2


!___MATERIAL Property Definitions___
sac                         =           1
die                         =           2
die_att                     =           3
substr                      =           4
overmold  =         5
pad                         =           6
pwb                         =           7

!_____Sn3.9Ag0.6Cu {Includes Hardening & Creep}____
! --- Elastic Properties ---
MP,         ALPX,       sac,        2.60E-05
MP,         PRXY,       sac,        0.35

!Young's Modulus of Soldr (MPa): From CALCE testing
!TMM testing by Qian Zhang for EUTECTIC SAC387
!Temperature for Young's Modulus
MPTEMP, 1,          198,        248,        298,        348,        403
MPDATA,EX,          sac,        1,          20.48E+3, 19.43E+3, 18.38E+3, 17.33E+3, 16.28E+3
! Plastic Properties (MULTI-LINEAR ISOTROPIC HARDENING)
! Yield stress calculated at 0.2% offset
!total strain to match the input modulus = offset yield stress/temp depend E modulus
TB,         MISO,       sac,        5
TBTEMP, 198
!____________________________________________
TBPT,       defi,       0.0008285,              16.968
TBPT,       defi,       0.00238     ,           18.700
TBPT,       defi,       0.006236,  27.360
TBPT,       defi,       0.013331,  36.020
TBPT,       defi,       0.024783,  44.681
TBPT,       defi,       0.041736,  53.341
TBPT,       defi,       0.065352,  62.001
TBPT,       defi,       0.096806,  70.661
TBPT,       defi,       0.137291,  79.322
TBPT,       defi,       0.188008,  87.982
TBPT,       defi,       0.250172,  96.642
TBPT,       defi,       0.325004,  105.302

TBTEMP, 248
!____________________________________________
TBPT,       defi,       0.000884262,            17.181
TBPT,       defi,       0.002464,  18.913
TBPT,       defi,       0.006822,  27.574
TBPT,       defi,       0.015397,  36.234
TBPT,       defi,       0.030006,  44.894
TBPT,       defi,       0.05261,    53.554
TBPT,       defi,       0.085295,  62.215
TBPT,       defi,       0.13026,    70.875
TBPT,       defi,       0.1898,                 79.535
TBPT,       defi,       0.266303,  88.195
TBPT,       defi,       0.36224,    96.856
TBPT,       defi,       0.480162,  105.516

TBTEMP, 298
!____________________________________________
TBPT,       defi,       0.000928168,            17.060
TBPT,       defi,       0.002554,  18.792
TBPT,       defi,       0.007717,  27.452
```

```
TBPT,    defi,    0.018825,  36.112
TBPT,    defi,    0.039099,  44.773
TBPT,    defi,    0.072256,  53.433
TBPT,    defi,    0.122464,  62.093
TBPT,    defi,    0.194315,  70.753
TBPT,    defi,    0.292794,  79.414
TBPT,    defi,    0.423264,  88.074
TBPT,    defi,    0.591443,  96.734
TBPT,    defi,    0.803392,  105.394

TBTEMP, 348
!________________________________________
TBPT,    defi,    0.000951834,       16.495
TBPT,    defi,    0.002654,  18.227
TBPT,    defi,    0.009212,  26.888
TBPT,    defi,    0.025158,  35.548
TBPT,    defi,    0.05702   ,        44.208
TBPT,    defi,    0.112966,  52.868
TBPT,    defi,    0.202773,  61.529
TBPT,    defi,    0.337803,  70.189
TBPT,    defi,    0.530979,  78.849
TBPT,    defi,    0.796771,  87.509
TBPT,    defi,    1.151176,  96.170
TBPT,    defi,    1.61171   ,        104.830

TBTEMP, 403
!________________________________________
TBPT,    defi,    0.000943156,       15.355
TBPT,    defi,    0.002773,  17.087
TBPT,    defi,    0.01209,           25.747
TBPT,    defi,    0.039023,  34.407
TBPT,    defi,    0.099873,  43.067
TBPT,    defi,    0.217259,  51.728
TBPT,    defi,    0.420564,  60.388
TBPT,    defi,    0.746328,  69.048
TBPT,    defi,    1.238584,  77.708
TBPT,    defi,    1.949171,  86.369


!--- IMPLICIT CREEP LAW (steady-state) ---
!g-hyposac creep prop - From Gayatri's creep testing of Sn3.0Ag0.5Cu
TB,      CREE,    sac,      1,        4,        8
TBDATA, 1,        0.02710,  0.369,    1.05,     5.08E+03
!_____End: Sn3.9Ag0.6Cu____

!___FR4 {Transversely Isotropic} ref: Vandervalve___
MP,      EX       ,         pwb       ,         17685
MP,      EY       ,         pwb       ,         7709.3
MP,      EZ       ,         pwb       ,         17685

MP,      PRXY     ,         pwb       ,         0.28
MP,      PRXZ     ,         pwb       ,         0.11
MP,      PRYZ     ,         pwb       ,         0.28

MP,      GXY      ,         pwb       ,         3472
MP,      GXZ      ,         pwb       ,         6908
MP,      GYZ      ,         pwb       ,         3472

MP,      alpx     ,         pwb       ,         1.80E-05
MP,      alpz     ,         pwb       ,         1.80E-05
MP,      alpy     ,         pwb       ,         6.00E-05
!___End: FR4____

!___Electrical Cu {matweb}___
MP,      EX       ,         pad       ,         1.29E+05
MP,      PRXY     ,         pad       ,         0.35
MP,      alpx     ,         pad       ,         1.85E-05
!___End: Electrical Cu_____

!____Substrate: BT, ref: Lall___
```

```
MP,     EX      ,   substr  ,   20000
MP,     EY      ,   substr  ,   4000
MP,     EZ      ,   substr  ,   20000

MP,     PRXY    ,   substr  ,   0.39
MP,     PRXZ    ,   substr  ,   0.11
MP,     PRYZ    ,   substr  ,   0.39

MP,     GXY     ,   substr  ,   7194
MP,     GXZ     ,   substr  ,   1801
MP,     GYZ     ,   substr  ,   7194

MP,     alpx    ,   substr  ,   1.50E-05
MP,     alpz    ,   substr  ,   1.50E-05
MP,     alpy    ,   substr  ,   6.00E-05
!___End: Substrate___

!___Si die ___
MP,     EX      ,   die     ,   1.91E+05
MP,     PRXY    ,   die     ,   0.278
MP,     alpx    ,   die     ,   2.10E-06
!___End: Si die__

!___Die Attach___
MP,     EX,     die_att,    1.20E+3
MP,     PRXY,   die_att,    0.42
MP,     ALPX,   die_att,    110.00E-6
!___End: Die Attach___

!___Overmold___
MP,     EX,     overmold,   23.6E+3
MP,     PRXY,   overmold,   0.3
MP,     ALPX,   overmold,   9.00E-6
!___End: Overmold__

!--- Add color to different materials-------
/NUMBER, 1
/PNUM, MAT, 1

/COLOR, NUM,    DGRA,   sac
/COLOR, NUM,    ORAN,   pad
/COLOR, NUM,    GCYA,   substr
/COLOR, NUM,    GREE,   pwb
/COLOR, NUM,    BMAG,   die
/COLOR, NUM,    YELL,   die_att
/COLOR, NUM,    RED,    overmold

/UDOC,  1,      DATE,   OFF     !turn off date plot

!======GEOMETRY PARAMETERS====
!--- Math ---
pi              =       4*atan(1)

!--- Package Dimensions ---
I_O     =       1156            !I/O Count
array_count_X   =       17              !# balls in package-array X direc
array_count_Z   =       17              !# balls in package-array Z direc
pitch   =       1               !1mm
die_count_X     =       4               !# balls in die-array
die_count_Z     =       5

!--- Cu pad parameters ---
pad_top_r =     0.254
pad_top_h =     0.032
pad_bot_r =     0.225
pad_bot_h =     0.019
pad_top_div     =       1
pad_bot_div     =       1

!--- Solder Mask parameters ---
```

```
soldermask_h		=		0.030
soldermask_r		=		0.160
mask_div	=		2

!--- Solder Ball parameters ---
ball_h1		=		0.479
ball_h2		=		0.163
ball_r1		=		0.204
ball_r2		=		0.310
ball_div	=		5

!--- Die parameters ---
die_l		=		8*pitch
die_w		=		10*pitch
die_h		=		0.505
die_div		=		2

!--- Die-attach parameters ---
die_att_h	=		0.072
die_att_div=		2

!--- substrate parameters ---
substr_h	=		0.513
substr_div =		2
substr_spc =		1.75

!--- Overmold parameters ---
overmold_h		=		0.595
overmold_div		=		2

!--- PWB parameters ---
pwb_h		=		1.47
pwb_l_X		=		4.5*array_count_X*pitch
pwb_l_Z		=		4.5*array_count_Z*pitch
pwb_div		=		3
pwb_spc		=		2
pwb_l_div_X		=		14
pwb_l_div_Z		=		14
pwb_l_spc_X		=		2.5
pwb_l_spc_Z		=		2.5

!====GEOMETRY======
!------Create Unit Cell-------
!__quarter of solder ball__
CLOCAL, 11,		CART,	1/2*pitch,  0,		1/2*pitch
K, 1, , pad_bot_h,
K, 2, , pad_bot_h+ball_h1,
K, 3, ball_r1, pad_bot_h+ball_h1
K, 4, ball_r2, pad_bot_h+ball_h2
K, 5, pad_bot_r, pad_bot_h
L, 1, 2		!Line 1
FLST, 3, 3, 3
FITEM, 3, 3
FITEM, 3, 4
FITEM, 3, 5
BSPLIN, , P51X		!Line 2
LGEN, 2, 2, , , -ball_r1+soldermask_r		!Line 3
L, 2, 6		!Line 4
L, 1, 7		!Line 5
L, 6, 3		!Line 6
L, 7, 5		!Line 7
AL,	1,	4,	3,	5 !Area 1
AL,	3,	6,	2,	7 !Area 2
K,	8,	1/2*soldermask_r,	pad_bot_h
K,	9,	,	pad_bot_h,-1/2*soldermask_r
k,	10,	1/2*soldermask_r,	pad_bot_h,-1/2*soldermask_r
A,	1,	8,	10,	9
VROTAT, 1,2 , , , , ,	1,	2,	90,	2	!Vol 2: rot A1 90°->Vol
VEXT,	3,	,	,	,	ball_h1
VSEL,	S,	VOLU,	,	1,	3,	2
```

```
CM,       Ball_Vol,  VOLU
ALLS,     ALL
VSBV,     Ball_vol,  5,,,      KEEP
LSEL,     S,         LOC,      Y,        pad_bot_h, pad_bot_h+1/2*ball_h1
LSEL,     U,         LOC,      Y,        pad_bot_h+ball_h1
LSEL,     U,         LOC,      Y,        pad_bot_h
LSEL,     U,         LENGTH, ,           ball_h1
LESIZE,   ALL,       ,         ,         ball_div,   2.4, 1
LSEL,     S,         LENGTH, ,           ball_h1
LESIZE,   ALL,       ,         ,         ball_div,   0.45, 1
LSEL,     S,         LOC,      Y,        pad_bot_h+ball_h1
LSEL,     A,         LOC,      Y,        pad_bot_h
LESIZE,   ALL,       ,,        1, , 1    !partition for 1 Elems

!__ Create solder mask ___
ASEL,     S,         LOC,      Y,        pad_bot_h+ball_h1
CLOCAL, 12,          CYLIN,    0, 0, 0,  0,
ASEL,     R,         LOC,      X,        0,          soldermask_r
CSYS,     11
VEXT,     ALL, , , , soldermask_h
LSEL,     S,         LOC,      Y,        pad_bot_h+ball_h1+1/2*soldermask_h
LESIZE,   ALL,,,     mask_div, , 1       !partition for 1 Elems
ALLSEL,   ALL
VATT,     sac,,      2,

!__top pad__
ASEL,     S,         LOC,      Y,        pad_bot_h+ball_h1+soldermask_h
VEXT,     ALL, , , , pad_top_h
ASEL,     S,         LOC,      Y,        pad_bot_h+ball_h1+soldermask_h+1/2*pad_top_h
CLOCAL, 12,          CYLIN,    0, 0, 0,  0,          90,
ASEL,     R,         LOC,      X,        soldermask_r
VEXT,     ALL, , ,   pad_top_r-soldermask_r
topper    =          soldermask_r + 1/2*(pad_top_r-soldermask_r)
zstart    =          -(pad_bot_h+ball_h1+soldermask_h+pad_top_h)
zend      =          -(pad_bot_h+ball_h1+soldermask_h)
LSEL,     S,         LOC,      Z,        zstart,     zend
LSEL,     R,         LOC,      X,        topper
LESIZE,   ALL,       ,         ,         1
CSYS,     11
ALLS,

!__bottom pad__
ASEL, S, LOC, Y, pad_bot_h
VEXT, ALL, , , , -pad_bot_h
LSEL, S, LOC, Y, pad_bot_h+ball_h1+soldermask_h+1/2*pad_top_h
LESIZE, ALL,,,       pad_top_div             , , 1
LSEL, S, LOC, Y, 1/2*pad_bot_h
LESIZE,   ALL, , , pad_bot_div,, 1
VSEL, S, LOC, Y, 1/2*pad_bot_h
VSEL, A, LOC, Y, pad_bot_h+ball_h1+soldermask_h+1/2*pad_top_h          VATT, pad, , 1

!__Create substrate __
ASEL, S, LOC, Y, pad_bot_h+ball_h1+soldermask_h+pad_top_h
CM, pad_top_area, area
NUMSTR, KP, 201
NUMSTR, LINE, 201
NUMSTR, AREA, 201
K, 201,   0, pad_bot_h+ball_h1+soldermask_h+pad_top_h, 0
K, 202,   1/2*pitch, pad_bot_h+ball_h1+soldermask_h+pad_top_h, 0
K, 203,   1/2*pitch, pad_bot_h+ball_h1+soldermask_h+pad_top_h, -1/2*pitch
K, 204,   0, pad_bot_h+ball_h1+soldermask_h+pad_top_h, -1/2*pitch
A, 201,   202, 203                                    !Area #    201
A, 201,   204, 203                                    !Area #    202
ASEL, S, AREA, , 201, 202
CM, sub_area, area
ALLSEL,  ALL
ASBA, sub_area, pad_top_area,
ASEL, S, LOC, Y, pad_bot_h+ball_h1+soldermask_h+pad_top_hLSLA, S,
LESIZE,   ALL, , , 1
ASEL, S, LOC, Y, pad_bot_h+ball_h1+soldermask_h+pad_top_h
```

```
VEXT, ALL, , , , substr_h
LSEL, S, LOC, Y, pad_bot_h+ball_h1+soldermask_h+pad_top_h+1/2*substr_h
LESIZE, ALL,,,          substr_div, substr_spc
VSEL, S, LOC, Y, pad_bot_h+ball_h1+soldermask_h+pad_top_h+1/2*substr_h
VATT, substr, ,          1

!__ Create PWB __
ASEL,     S,          LOC,        Y,          0
CM,       pad_bot_area,           area
NUMSTR,KP,            301
NUMSTR,LINE,          301
NUMSTR,AREA,          301
K,        301,        0,          0,          0
K,        302,        1/2*pitch,  0,          0
K,        303,        1/2*pitch,  0,          -1/2*pitch
K,        304,        0,          0,          -1/2*pitch
A,        301,        302,        303         !Area #    301
A,        301,        304,        303         !Area #    302
ASEL,     S,          AREA,       ,           301,       302
CM,       pwb_area,   area
ALLSEL,   ALL
ASBA,     pwb_area,   pad_bot_area,
ASEL,     S,          LOC,        Y,          0
LSLA,     S,
LESIZE,   ALL,        ,           ,           1
ASEL,     S,          LOC,        Y,          0
VEXT,     ALL, , , ,  -pwb_h
LSEL,     S,          LOC,        Y,          -1/2*pwb_h
LESIZE,   ALL,        ,           ,           pwb_div,   pwb_spc
VSEL,     S,          LOC,        Y,          -1/2*pwb_h
VATT,     pwb,        ,           1
ALLSEL,   ALL
CMDELE,ALL
ALLSEL,   ALL

!___ Mesh Solder, Substrate & PWB ___
ALLS,     ALL
VMESH,    ALL

!___Create Die Attach __
ASEL,     S,          LOC,        Y,          pad_bot_h+ball_h1+soldermask_h+pad_top_h+substr_h
EXTOPT,   ESIZE,      die_att_div
EXTOPT,   ACLEAR,     0
EXTOPT,   ATTR,       0,          0,          0
MAT,      die_att
TYPE,     1
VEXT,     ALL, , ,    0,          die_att_h

!__ Create Die -___
ASEL,     S,          LOC,        Y,          pad_bot_h+ball_h1+soldermask_h+pad_top_h+substr_h+die_att_h
EXTOPT,   ESIZE,      die_div
EXTOPT,   ACLEAR,     0
EXTOPT,   ATTR,       0,          0,          0
MAT,      die
TYPE,     1
VEXT,     ALL, , ,    0,          die_h

!__ Create Top of Overmold __
ASEL,     S,          LOC,        Y, pad_bot_h+ball_h1+soldermask_h+pad_top_h+substr_h+die_att_h+die_h
EXTOPT,   ESIZE,      overmold_div
EXTOPT,   ACLEAR,     0
EXTOPT,   ATTR,       0,          0,          0
MAT,      overmold
TYPE,     1
VEXT,     ALL, , ,    0,          overmold_h

!__ Make full Unit Cell & Components-___
ALLSEL,   ALL
VSYMM,    -X,         ALL
VSYMM,    Z,          ALL
```

```
ALLSEL,  ALL
NUMMRG,          ALL
NUMCMP,          ALL
CM,       UnitCell_E,       ELEM
CM,       UnitCell_N,       NODE
CSYS, 0
ALLS,

!___Create Full model___
!---------------------------------------------------------
!--- Create UnitCells in Row 1 (Z=0) ---
*DO,      i,        2,        array_count_X
          CSYS,     0
          CLOCAL, 14,         CART,     i*pitch-1/2*pitch, 0, 1/2*pitch,
          CSYS,     11
          *GET,     MaxN,     NODE,     ,NUM,     MAX
          TRANSFER,           14,       MaxN+1,   UnitCell_N
          EGEN,     2,        MaxN+1,   UnitCell_E
          ALLS,     ALL
*ENDDO


!--- Create UnitCells in Remaining Rows ---
*DO,      i,        2,        array_count_Z
          CSYS,     0
          CLOCAL, 14,         CART,     1/2*pitch, 0, i*pitch-1/2*pitch
          CSYS,     11
          *GET,     MaxN,     NODE,     ,NUM,     MAX
          TRANSFER,           14,       MaxN+1,   UnitCell_N
          EGEN,     2,        MaxN+1,   UnitCell_E
          ALLS,     ALL
          *DO,      j,        2,        array_count_X
                    CSYS,     14
                    CLOCAL, 15,         CART,     (j-1)*pitch, 0, 0,
                    CSYS,     11
                    *GET,     MaxN,     NODE,     ,NUM,     MAX
                    TRANSFER,           15,       MaxN+1,   UnitCell_N
                    EGEN,     2,        MaxN+1,   UnitCell_E
                    ALLS,     ALL
          *ENDDO
*ENDDO
ALLS,     ALL
NUMMRG,             ALL

!--- Change Die & Die att to overmold outside of die region ---
CSYS,     0
ystart    =         pad_bot_h+ball_h1+soldermask_h+pad_top_h+substr_h
yend      =         ystart+die_h
NSEL,     S,        LOC,      X,        0,        die_count_X*pitch
NSEL,     R,        LOC,      Z,        0,        die_count_Z*pitch
NSEL,     INVE
NSEL,     R,        LOC,      Y,        ystart,   yend
ESLN,     S,        0
ESEL,     U,        MAT,,     substr
MPCHG,  overmold,   ALL
allsel

!--- Create Chamfer1 ---
CSYS,     0
chacha=pad_bot_h+ball_h1+soldermask_h+pad_top_h+substr_h
NSEL,S,LOC,Y,chacha,chacha+die_att_h+die_h+overmold_h
NSEL,R,LOC,X,array_count_X-1/2*pitch,array_count_X
ESLN,S,1
EDELE,ALL
NDELE,ALL
NSEL,S,LOC,Y,chacha,chacha+die_att_h+die_h+overmold_h
NSEL,R,LOC,Z,array_count_Z-1/2*pitch,array_count_Z
ESLN,S,1
EDELE,ALL
NDELE,ALL
```

```
ALLS
!--- Create Chamfer2 ---
CSYS,     0
CLOCAL, 17,CART,array_count_X-1,chacha,array_count_Z-1,,,-45
NSEL,     S,        LOC,      X,        0,        2*pitch
NSEL,     R,        LOC,      Y,        0,die_att_h+die_h+overmold_h
ESLN,     S,        1
EDELE,    ALL
NDELE,    ALL
CSYS,     0
ALLS

!--- Create Remaining package ---
NUMCMP,             ALL
*GET,     MaxK,     KP,       ,NUM,     MAX       !determine the max number of nodes
*GET,     MaxL,     LINE,     ,NUM,     MAX       !determine the max number of lines
*GET,     MaxA,     AREA,     ,NUM,     MAX       !determine the max number of areas
*GET,     MaxV,     VOLU,     ,NUM,     MAX       !determine the max number of Vols
*GET,     MaxN,     NODE,     ,NUM,     MAX       !determine the max number of nodes
NUMSTR,KP,          MaxK
NUMSTR,LINE,        MaxL
NUMSTR,AREA,        MaxA
NUMSTR,VOLU,        MaxV
NUMSTR,NODE,        MaxN
K, MaxK+1,          array_count_X,      pad_bot_h+ball_h1+soldermask_h+pad_top_h,        0
K, MaxK+2,          array_count_X+1/2*pitch,pad_bot_h+ball_h1+soldermask_h+pad_top_h,    0
K,        MaxK+3,   array_count_X,      pad_bot_h+ball_h1+soldermask_h+pad_top_h,        1/2*pitch
K,        MaxK+4,   array_count_X+1/2*pitch,pad_bot_h+ball_h1+soldermask_h+pad_top_h,    1/2*pitch
L,        MaxK+1,   MaxK+2                        !Line# MaxL+1
L,        MaxK+3,   MaxK+4                        !Line# MaxL+2
L,        MaxK+1,   MaxK+3                        !Line# MaxL+3
L,        MaxK+2,   MaxK+4                        !Line# MaxL+4
LSEL,     S,        LINE,     ,         MaxL+1, MaxL+4
LESIZE,   ALL,      ,         ,         1
AL,       MaxL+1, MaxL+4, MaxL+2, MaxL+3
ASEL,     S,        AREA,     ,         MaxA+1
EXTOPT,   ATTR,     0,        0,        0
MAT,      substr
TYPE,     1
VEXT,     ALL, , ,  0,        substr_h
LSEL,     S,        LOC,      X,        array_count_X,      array_count_X+1/2*pitch
LSEL,     R,        LOC,      Y,        pad_bot_h+ball_h1+soldermask_h+pad_top_h+1/2*substr_h
LESIZE,   ALL,      ,         ,         substr_div,substr_spc
VMESH,    MaxV+1
!--- copy the elements to make 3-D slice ---
*DO,      i,        1,        2*array_count_X
          VGEN,     2,        MaxV+1, , , , , i*1/2*pitch
*ENDDO
VSEL,     S,        LOC,      X,        array_count_X, array_count_X+1/2*pitch
VSEL,     R,        LOC,      Z,        array_count_Z, array_count_Z+1/2*pitch
VSEL,     R,        LOC,      Y,        pad_bot_h+ball_h1+soldermask_h+pad_top_h+1/2*substr_h
CM,       substr_end, VOLU
*DO,      i,        1,        2*array_count_X
          VGEN,     2,        substr_end, , , -i*1/2*pitch
*ENDDO
ALLS

!--- Create Remaining PWB ---
*GET,     MaxK,     KP,       ,NUM,     MAX       !determine the max number of nodes
*GET,     MaxL,     LINE,     ,NUM,     MAX       !determine the max number of lines
*GET,     MaxA,     AREA,     ,NUM,     MAX       !determine the max number of areas
*GET,     MaxV,     VOLU,     ,NUM,     MAX       !determine the max number of Vols
*GET,     MaxN,     NODE,     ,NUM,     MAX       !determine the max number of nodes
NUMSTR,KP,          MaxK
NUMSTR,LINE,        MaxL
NUMSTR,AREA,        MaxA
NUMSTR,VOLU,        MaxV
NUMSTR,NODE,        MaxN
K,        MaxK+1,   array_count_X,      0,        0
K,        MaxK+2,   pwb_l_X,  0,        0
```

```
K,        MaxK+3,  array_count_X,        0,          array_count_Z
K,        MaxK+4,  pwb_l_X,  0,          array_count_Z
K,        MaxK+5,  0,        0,          array_count_Z
K,        MaxK+6,  0,        0,          pwb_l_Z
K,        MaxK+7,  array_count_X,        0,          pwb_l_Z
K,        MaxK+8,  pwb_l_X,  0,          pwb_l_Z
L,        MaxK+1,  MaxK+2                            !Line# MaxL+1 (pwb_l_div_X)
L,        MaxK+3,  MaxK+4                            !Line# MaxL+2 (pwb_l_div_X)
L,        MaxK+1,  MaxK+3                            !Line# MaxL+3 (2*array_count_Z)
L,        MaxK+2,  MaxK+4                            !Line# MaxL+4 (2*array_count_Z)
L,        MaxK+5,  MaxK+6                            !Line# MaxL+5 (pwb_l_div_Z)
L,        MaxK+3,  MaxK+7                            !Line# MaxL+6 (pwb_l_div_Z)
L,        MaxK+5,  MaxK+3                            !Line# MaxL+7 (2*array_count_X)
L,        MaxK+6,  MaxK+7                            !Line# MaxL+8 (2*array_count_X)
L,        MaxK+7,  MaxK+8                            !Line# MaxL+9 (pwb_l_div_X)
L,        MaxK+4,  MaxK+8                            !Line# MaxL+10 (pwb_l_div_Z)
LSEL,     S,       LINE,     ,           MaxL+1,   MaxL+2
LSEL,     A,       LINE,     ,           MaxL+9
LESIZE,   ALL,     ,         ,           pwb_l_div_X,        pwb_l_spc_X,        1
LSEL,     S,       LINE,     ,           MaxL+5,   MaxL+6
LSEL,     A,       LINE,     ,           MaxL+10
LESIZE,   ALL,     ,         ,           pwb_l_div_Z,        pwb_l_spc_Z,        1
LSEL,     S,       LINE,     ,           MaxL+3,   MaxL+4
LESIZE,   ALL,     ,         ,           2*array_count_Z
LSEL,     S,       LINE,     ,           MaxL+7,   MaxL+8
LESIZE,   ALL,     ,         ,           2*array_count_X
ALLS
AL,       MaxL+1,  MaxL+4,   MaxL+2,     MaxL+3    !Area# MaxA+1
AL,       MaxL+6,  MaxL+8,   MaxL+5,     MaxL+7    !Area# MaxA+2
AL,       MaxL+2,  MaxL+10,  MaxL+9,     MaxL+6    !Area# MaxA+3
ASEL,     S,       AREA,     ,           MaxA+1,   MaxA+3
EXTOPT,   ATTR,    0,        0,          0
MAT,      pwb
TYPE,     1
VEXT,     ALL, , , 0,        -pwb_h
LSEL,     S,       LOC,      Y,          -1/2*pwb_h
LESIZE,   ALL,     ,         ,           pwb_div,  pwb_spc
VMESH,    MaxV+1,  MaxV+3
ALLSEL,   ALL
NUMMRG,            ALL
NUMCMP,            ALL

!======Boundary Condititons========
!--- Constrain Rigid Body Motion ---
NSEL,     S,       LOC,      X,          0
NSEL,     R,       LOC,      Y,          0
NSEL,     R,       LOC,      Z,          0
D,        ALL,     UY,       0
ALLSEL
!--- SYMMETRY ABOUT X AXIS ---
NSEL,     S,       LOC,      X,          0
D,        ALL,     UX,       0
!--- SYMMETRY ABOUT Z AXIS ---
NSEL,     S,       LOC,      Z,          0
D,        ALL,     UZ,       0
allsel

!===== Solution Settings========
!------- Create Solder Components for Solu DATA----------
ESEL,     S,       MAT,      ,           SAC
CM,       Solder_elems,      ELEM
ALLS,

/SOLU
ANTYPE, STATIC, NEW

solcontrol, on                           !turn on the optimized nonlinear solver
nlgeom, on                     !turn on the large deformation effect
lnsrch, auto                             !Auto line search
autots, on
```

```
TOFFST, 0                              !Temp in K (K-K=0)
RATE, ON                                              !Turn on creep strain criteria
cutcontrol, crplimit, 0.25, 1          !specifies cutcontrol of creep

OUTRES, ALL,        NONE
OUTRES, ESOL, LAST, solder_elems

!=====Accel Temp Cycle======
ALLSEL,  ALL
starttemp = 298                        !25°C
TREF,       starttemp
minute = 60

DELTIM,  0.1,          1e-5,        1

!Step 1
TIME,      1          $          TUNIF,    298.16     $          SOLVE    $          SAVE
DELTIM,  1/8*minute,             1,          1/2*minute,          ON
!Step 2
TIME,      150        $          TUNIF,    321.75     $          SOLVE    $          SAVE
!Step 3
TIME,      300        $          TUNIF,    345.50     $          SOLVE    $          SAVE
!Step 4
TIME,      450        $          TUNIF,    369.25     $          SOLVE    $          SAVE
!Step 5
TIME,      600        $          TUNIF,    393.00     $          SOLVE    $          SAVE
!Step 6
TIME,      840        $          TUNIF,    401.00     $          SOLVE    $          SAVE
!Step 7
TIME,      960        $          TUNIF,    398.00     $          SOLVE    $          SAVE
!Step 8
TIME,      1120       $          TUNIF,    398.00     $          SOLVE    $          SAVE
!Step 9
TIME,      1280       $          TUNIF,    398.00     $          SOLVE    $          SAVE
OUTRES, ALL,        LAST
!Step 10
TIME,      1440       $          TUNIF,    398.00     $          SOLVE    $          SAVE
OUTRES, ALL,        NONE
OUTRES, ESOL, LAST, solder_elems
!Step 12
TIME,      1620       $          TUNIF,    374.95     $          SOLVE    $          SAVE
!Step 13
TIME,      1800       $          TUNIF,    351.91     $          SOLVE    $          SAVE
!Step 14
TIME,      1980       $          TUNIF,    328.86     $          SOLVE    $          SAVE
!Step 15
TIME,      2160       $          TUNIF,    305.82     $          SOLVE    $          SAVE
!Step 16
TIME,      2340       $          TUNIF,    282.77     $          SOLVE    $          SAVE
!Step 17
TIME,      2520       $          TUNIF,    259.73     $          SOLVE    $          SAVE
!Step 18
TIME,      2760       $          TUNIF,    229.00     $          SOLVE    $          SAVE
!Step 19
DELTIM,  1/4*minute,             1,          1*minute,  ON
TIME,      3000       $          TUNIF,    216.00     $          SOLVE    $          SAVE
!Step 20
TIME,      3240       $          TUNIF,    216.00     $          SOLVE    $          SAVE
!Step 21
TIME,      3480       $          TUNIF,    216.00     $          SOLVE    $          SAVE
OUTRES, ALL,        LAST
!Step 22
TIME,      3720       $          TUNIF,    216.00     $          SOLVE    $          SAVE
OUTRES, ALL,        NONE
OUTRES, ESOL, LAST, solder_elems
DELTIM,  1/8*minute,             1,          1/2*minute,          ON
!Step 23
TIME,      3840       $          TUNIF,    222.00     $          SOLVE    $          SAVE
!Step 24
```

```
TIME,     4080     $     TUNIF,   260.00   $      SOLVE   $      SAVE
OUTRES, ALL,       LAST
!Step 25
TIME,     4320     $     TUNIF,   298.00   $      SOLVE   $      SAVE
OUTRES, ALL,       NONE
OUTRES, ESOL, LAST, solder_elems

FINISH
/EXIT,    ALL
```

Appendix C: FEA Postprocessing Input file

A sample ANSYS postprocessing file used to calculate plastic and creep work density for critical solder joints in the model is given below. The postprocessing file requires a csv file located in the working directory of critical solder joint element numbers. The csv file was a m x n matrix, where the m rows were the element numbers of each critical solder joint, and the n columns were each critical solder joint of interest.

```
/POST26
ALLS
RESET
NUMVAR,          200

!-- Create Variable for # of Elems in ea Jt
NumElems = 44

!-- Create Variable for # of Jts in Solu
NumJts = 44 !total of 44 solder balls

!-- Find # of time substeps in solution
*GET, NumSets, ACTIVE, , SET, NSET

!-- Create List of Elements (44 per Jt) for solder joints
*DIM, Elem_list, TABLE, NumElems, NumJts

!-- Read csv file of element values
*TREAD, Elem_list, SolderElems, csv

!-- Create Work Density Arrays --
*DIM, WrkD_Cr, ARRAY, NumSets, NumJts+2
*DIM, WrkD_Pl, ARRAY, NumSets, NumJts+2

!---Calculate Vol ave Work Density for all Joints---
*DO, j, 1, NumJts
 !---Variable increment #s---
 SumVol = 0
 SumWKCr = 0
 SumWKPl = 0

 !--- Calc vol tot and wrk tot for all elems in joint --
 *DO, i, 1, NumElems

  !---make variable num > 1 (reserved for time)---
  b = i+1
  bb = 2*NumElems+b
  bbb = 3*NumElems+b
  EE = Elem_list(i,j)

  !--- Find Vol for Elems ---
  ESOL, b, Elem_list(i,j), , VOLU, , Vol%EE%
  STORE, MERGE

  !--- Find Work Dens for Elems ---
  ESOL, bb, Elem_list(i,j), , SEND, CREEP, WKCR%EE%
  STORE, MERGE
  ESOL, bbb, Elem_list(i,j), , SEND, PLASTIC, WKPL%EE%
  STORE, MERGE

  !--- Calc Work ---
  PROD, bb, bb, b, , WKCR%EE%
  PROD, bbb, bbb, b, , WKPL%EE%
 *ENDDO

 *DO, i, 1, NumElems
  !---make variable num > 1 (reserved for time)---
  b = i+1
```

```
  bb = 2*NumElems+b
  bbb = 3*NumElems+b

  !--- Sum Work and Vol --
  ADD, b, b, SumVol, , Vol%b%
  ADD, bb, bb, SumWKCr, , WKCR%bb%
  ADD, bbb, bbb, SumWKPl, , WKPL%bbb%

  !---set increment #s = to current varaible #---
  SumVol = b
  SumWKCr = bb
  SumWKPl = bbb
 *ENDDO

  !--- vol Ave Wrk Density --
  QUOT, bb, bb, b
  QUOT, bbb, bbb, b
  ADD,      bbb, bb, bbb, , , , , -1

  !--- Fill WrkD with Vol Ave Wrk D for all solder joints---
  VGET, WrkD_Cr(1,j+2), bb
  VGET, WrkD_Pl(1,j+2), bbb
*ENDDO

!--- Get Elem Temp --
ESOL, 2, Elem_list(1,1), , BFE, TEMP, temp

!--- Create variable 200 fill with -273 (Kelvin to Celsius)---
FILLDATA, 200, , , , -273, 0

!--- ADD -273 to element Temp
ADD, 2, 2, 200, , Temp

!--- Fill WrkD with time & temp ---
VGET, WrkD_Cr(1,1), 1
VGET, WrkD_Cr(1,2), 2
VGET, WrkD_Pl(1,1), 1
VGET, WrkD_Pl(1,2), 2

!--- DATA Export ---
/NOPR

/OUTPUT, Work_D_Cr, csv
*MWRITE, WrkD_Cr(1,1)
(46(F12.6,','))

/OUTPUT, Work_D_Pl, csv
*MWRITE, WrkD_Pl(1,1)
(46(F12.6,','))
/OUTPUT
/GOPR

FINISH
```

Appendix D: FEA Model Reduction Strategies

Due to the size of the package being modeled for this study, model reduction strategies were explored to reduce computation time. The nonlinear material behavior of solder significantly increases the computation time in FEA. Therefore, model simplification strategies should focus on reducing the number of nonlinear elements in the model. Beam modeling was employed to replace noncritical solder joints with shear deformable beam elements. This strategy reduces a complex solder joint and copper pad assembly to a simple beam element. Thus, many brick elements (solid185) are replaced by a single beam element (beam189) for the non-critical solder joints in the model. For example, in the figure below a complex three-dimensional solder joint is replaced by a simple one-dimensional beam element.

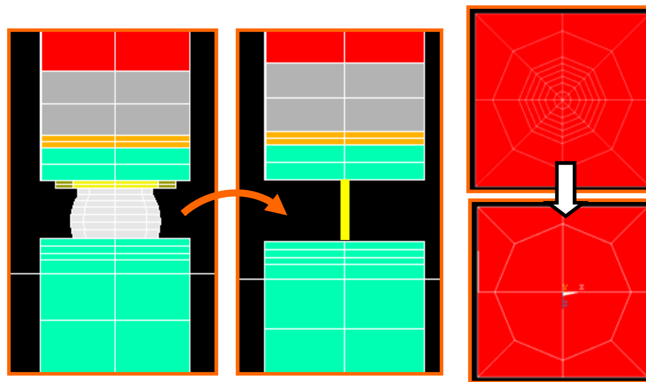

Example of a complex 3-D solder/copper pad assembly replaced with a simple 1-D beam element. The top-view on the right shows how the mesh density is reduced throughout the package "unit cell".

In order to accurately capture the complex 3-D response of the solder and pad, it is necessary to characterize the six DoFs possible in the structure. Thus, the stiffness in: tensile, shear, bending and torsion for multiple temp profiles (see figure below) must be quantified. This is accomplished by subjecting a 3-D model of the solder and pad geometry to stepped displacement loading in the four primary directions for various reference temperature conditions. The resulting force and moments produce "stress-strain" curves that fully describe the deformation response of a solder/pad unit.

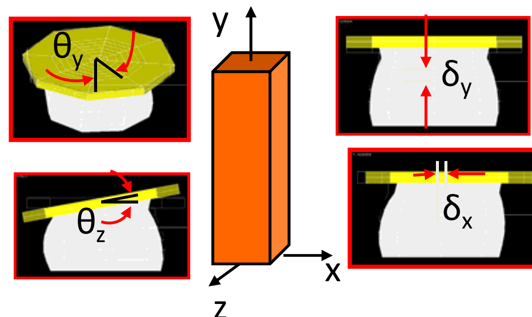

Representative 3-D solder joint and copper pad FEA model. This model is used to characterize the 6 DoFs possible in the structure.

For the geometry and material properties encountered in this study, the beam response was found to be a function of an abstract cross-section. This section was characterized by the diagonal terms in stiffness matrix of the beam. Essentially, the beam's displacement response was found to be correct parallel to element axes only. The beam was too stiff at an angle to element axes; non-isotropic in-plane bending and shear response. The beam's elastic properties are anisotropic but anisotropy of nonlinear behavior in bending and shear cannot be independently controlled. Thus, the non-linear generalized beam cross-section (NLGEOM) was chosen as most representative of the beam behavior.

Beam elements have six DoFs per node; translations and rotations in the three Cartesian coordinates. Therefore, to couple beam rotations to element to solid continuum element translations (3 DoFs per node) it is necessary to use constraint equations. Thus, per interfacial node, four constraint equations are required; three for rotational DoFs, one for out-of-plane translation to prevent concentrated loading.

A benchmark PBGA256 model based on the cross-sectional geometry of the PBGA1156 test specimen was used to quantify the computation time savings of replacing X percentage of 3-D solder/pad section with beam elements. In this study, four PBGA256 models were run for three temperature cycles. The baseline model was a PBGA256; for comparison purposes three reduced models were created. The reduced models had 10%, 25% and 50% of package non-critical solder joints replaced with elastic beam elements. These models had 6%, 16%, and 31% reductions in model DoFs, respectively.

Results indicated that it was not advantageous to use beam modeling when there was less than a 20% reduction in model DoFs. In fact, the full solder model had a faster solution time below 20% reduction. This can be explained by the addition of constraint equations to the model. Constraint equations cause the stiffness matrix to be asymmetrical, and thus require more solution time. However, as the percentage reduction in model DoFs increased above 20%, the penalty of using constraint equations was negated by the reduction in the size of the stiffness matrix.

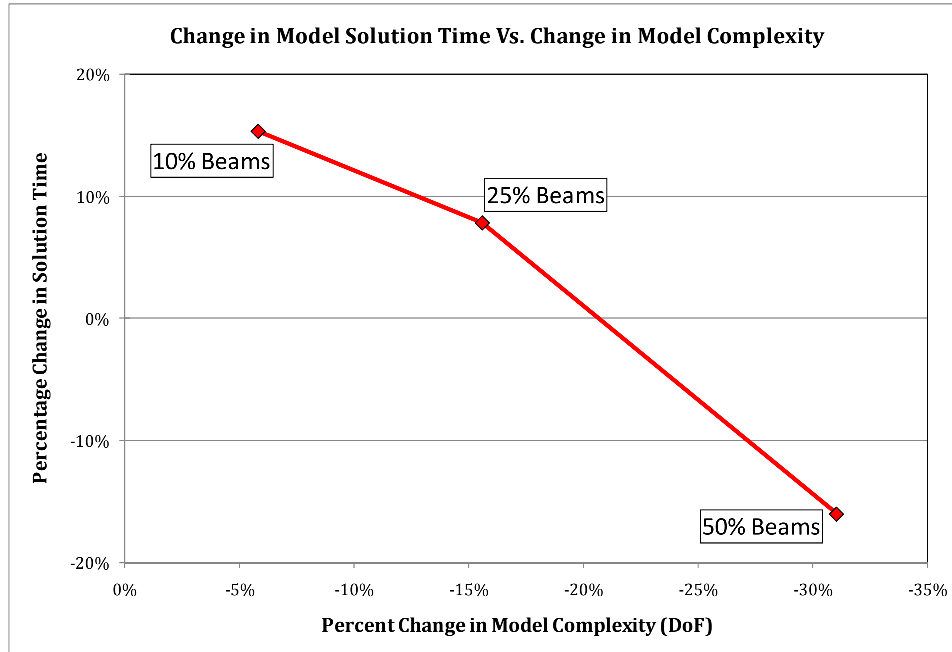

Percenatge change in solution time as the model complexity is reduced through the use of beam elements to replace non-critical solder joints. The FEA model was a PBGA256 quarter symmetry model. The results indicate that beam elements yield compututationl time savings when the percentage reduction in model DoFs is greater than 20%.

Appendix E: Damage Ratios Parametric Study

A parametric study was performed to ascertain the relative sensitivity of damage ratio calculations for the 12 daisy-chain test nets. The study consisted of comparing damage ratios of three separate FEA simulations. Simulations I and II used a partitioned constitutive model with separate rate-independent Ramberg-Osgood plasticity and steady-state (Garafalo) creep model, with properties defined for SAC solder, as described in Chapter 3; simulation III used a rate-dependent, unified Anand inelastic model for SAC solder response. Anand inelasticity incorporates creep and viscoplasticity into a single flow rule for the deformation response of the material.

In Anand's model the steady-state stress-strain-relation can be summarized in the following three equations:

$$\dot{\varepsilon} = A\left[sinh\left(\xi\frac{\sigma}{S}\right)\right]^{\frac{1}{m}} exp\left(-\frac{Q}{RT}\right)$$

$$\dot{S} = \dot{\varepsilon}h_0\left|1-\frac{S}{S^*}\right|^{a} sign\left(1-\frac{S}{S^*}\right) \tag{21}$$

$$S^* = \tilde{S}\left[\frac{\varepsilon}{A}exp\left(\frac{Q}{RT}\right)\right]^{n};$$

where A, ξ, and Q, m, h_0, a, $\tilde{S}$ *and* n are material properties, R is Boltzman's constant, s is an internal state variable, and T is the absolute temperature. Model constants were found in the literature (see Reinikainen et al. [16]).

Material constants for Anand plasticity model [16].

Anand Constants	A	m	ξ	Q/R	h_0	a	$\tilde{s}$	n	s_0
Sn3.38Ag0.84Cu	500	0.3	7.1	9000	5900	1.4	39.4	0.03	1.3

Damage calculations for Simulations I and II used the energy-partitioning approach presented in Chapter 3. In order to calculate damage for the Anand FEA model (Simulation III), a power-law, total-energy damage model was employed:

$$N = \left(\frac{\Delta W}{C}\right)^{\frac{1}{n}} \tag{22}$$

In (22), N is the characteristic life, ΔW is the inelastic work density, and C and n are material constants. Where C and n for SAC387 are 5.92E3 and -1.3 respectively, and are readily found in the literature (see Zhang [14]). Results for the parametric study indicate that the damage ratios are relatively insensitive to choice of solder constitutive model and damage model.

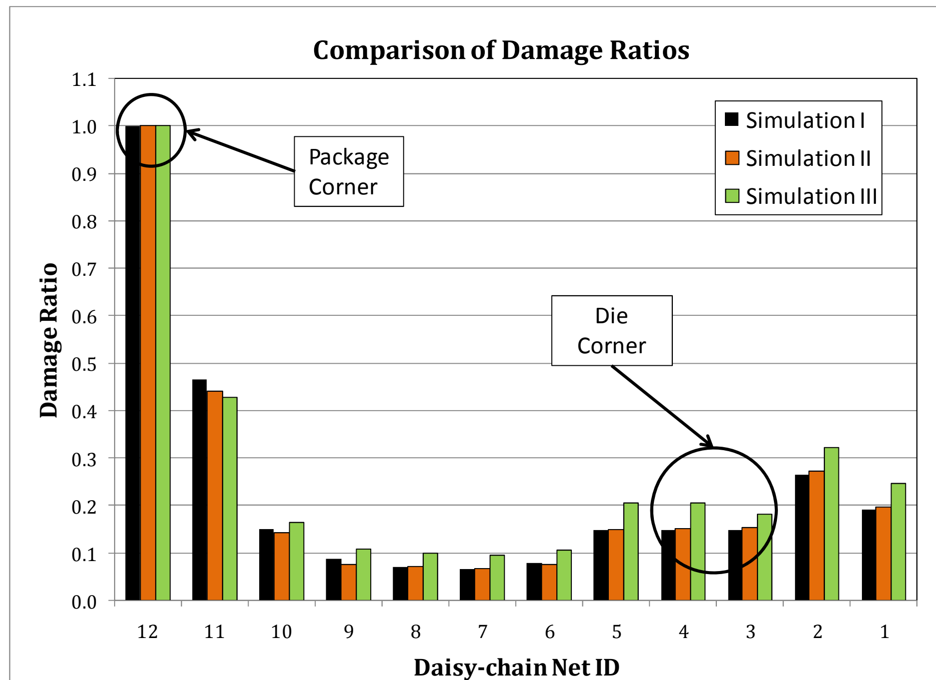

Comparison of damage ratios for the three temperature cycling simulations. The parametric study results indicate that the damage ratios are relatively insensitive to either the choice of solder constitutive model or the choice of damage model.

6 References

[1] Practical Components, Cross-section of PBGA architecture, http://www.practicalcomponents.com/catalog.htm#online_catalog

[2] R. Darveaux, K. Banerji, A. Mawer and G. Dody, "Reliability of Plastic Ball Grid Array Assembly," Ball Grid Array Technology, J. Lau Editor, McGraw-Hill, Inc., (New York, 1995).

[3] A. Dasgupta, C. Oyan, D. Barker, and M. Pecht, ''Solder Creep-Fatigue Analysis by an Energy Partitioning Approach,'' *ASME Journal of Electronic Packaging*, Vol. 114, (1992), pp. 152–160.

[4] J. P. Clech, D. M. Noctor, J. C. Manock, G. W. Lynott and F. E. Bader, "Surface Mount Assembly Failure Statistics And Failure-Free Times," *Proc 44th Electronic Components and Technology Conf*, Washington, DC, May 1994, pp. 487-497.

[5] A. Perkins and S. K. Sitaraman, "Analysis And Prediction of Vibration-Induced Solder Failure for a Ceramic Column Grid Array Package," *ASME Journal of Electronic Packaging*, Vol. 130, No. 1 (2008), pp. 011012-1

[6] M. Meilunas, A. Primavera, and S. O. Dunford, "Reliability and Failure Analysis of Lead-free Solder Joints," *Proc IPC Conf*, New-Orleans, LA, Nov 2002.

[7] J. C. Manock and P. C. Moy, "Solder Joint Reliability and Failure Analysis of the 244 I/O Pre-Molded PolyHIC Package," *Proc 43rd Electronic Components and Technology Conf*, Orlando, FL ,June 1993, pp. 1156-1160.

[8] K. C. Kapur and L. R. Lamberson, Reliability in Engineering Design, Wiley, (New York, 1977).

[9] Reliasoft Corporation, Weibull++6.

[10] W. Liu and R. Lewis, "A Comparison of Statistical Distribution Functions to Predict BGA Attach Reliability," *IEEE Transactions On Components And Packaging Technologies*, Vol 31, No. 3 (2008), pp. 726-733.

[11] J. L. Devore, Probability And Statistics For Engineering And The Sciences, C. Crockett Editor, Brooks/Cole, (Belmont 2004).

[12] R. Darveaux, "Effect of Simulation Methodology on Solder Joint Crack Growth Correlation," *Proc 50th Electronic Components and Technology Conf*, Las Vegas, NV, May 2000, pp. 1048-1058.

[13] Practical Components Onling BGA Catalog, http://www.practicalcomponents.com/drawings/pdf/PBGA/A-PBGA1156-2dwg.pdf

[14] Q. Zhang, A. Dasgupta, and P. Haswell, "Partitioned Viscoplastic-Constitutive Properties Of The Pb-Free Sn3.9Ag0.6Cu Solder," *TMS Journal of Electronic Materials*, Vol. 33, No. 11 (2004), 1338-1349.

[15] G. Cuddalorepatta and A. Dasgupta, "Viscoplastic Behavior of Hypo-Eutectic Sn3.0ag0.5cu Pb-Free Alloy Under Creep Loading Conditions", *ASME IMECE 2007*, Seattle, WA, Nov 2007.

[16] T.O. Reinikainen, P. Marjamaki, and J.K. Kivilahti, "Deformation Characteristics and Microstructural Evolution of SnAgCu Solder Joints," *Proc. 6th IEEE Components, Packaging and Manufacturing Technology Society EuroSimE Conf.*, Berlin, Germany, April 2005, pp. 91-98.